T.R.

GEBZE TECHNICAL UNIVERSITY

GRADUATE SCHOOL OF NATURAL AND APPLIED SCIENCES

GENERATION OF PRECISE 3D MODEL WITH RGB UAV AND INTEGRATION TO THE GAME ENGINE: CASE STUDY GEBZE TECHNICAL UNIVERSITY

MERTCAN NAZAR

A THESIS SUBMITTED FOR THE DEGREE OF

MASTER OF SCIENCE

DEPARTMENT OF GEOMATICS ENGINEERING

GEODESY AND GEOGRAPHICAL INFORMATION TECHNOLOGIES PROGRAM

GEBZE

2022

T.R.

GEBZE TECHNICAL UNIVERSITY

GRADUATE SCHOOL OF NATURAL AND APPLIED SCIENCES

GENERATION OF PRECISE 3D MODEL WITH RGB UAV AND INTEGRATION TO THE GAME ENGINE: CASE STUDY GEBZE TECHNICAL UNIVERSITY

MERTCAN NAZAR

A THESIS SUBMITTED FOR THE DEGREE OF

MASTER OF SCIENCE

DEPARTMENT OF GEOMATICS ENGINEERING

GEODESY AND GEOGRAPHICAL INFORMATION TECHNOLOGIES PROGRAM

THESIS SUPERVISOR

PROF. DR. UMUT GÜNEŞ SEFERCİK

GEBZE

2022

T.C.
GEBZE TEKNİK ÜNİVERSİTESİ
FEN BİLİMLERİ ENSTİTÜSÜ

RGB İHA İLE HASSAS 3B MODEL ÜRETİMİ VE OYUN MOTORUNA ENTEGRASYONU: GEBZE TEKNİK ÜNİVERSİTESİ ÖRNEĞİ

MERTCAN NAZAR

YÜKSEK LİSANS TEZİ
HARİTA MÜHENDİSLİĞİ ANABİLİM DALI
JEODEZİ VE COĞRAFİ BİLGİ TEKNOLOJİLERİ PROGRAMI

DANIŞMANI
PROF. DR. UMUT GÜNEŞ SEFERCİK

GEBZE
2022

GEBZE TEKNİK ÜNİVERSİTESİ	**YÜKSEK LİSANS JÜRİ ONAY FORMU**

GTÜ Fen Bilimleri Enstitüsü Yönetim Kurulu'nun 16/06/2022 tarih ve 2022/29 sayılı kararıyla oluşturulan jüri tarafından 22/06/2022 tarihinde tez savunma sınavı yapılan Mertcan NAZAR'ın tez çalışması Harita Mühendisliği Anabilim Dalı, Jeodezi ve Coğrafi Bilgi Teknolojileri Programında YÜKSEK LİSANS tezi olarak kabul edilmiştir.

JÜRİ

ÜYE (TEZ DANIŞMANI)	: Prof. Dr. Umut Güneş SEFERCİK
ÜYE	: Prof. Dr. Fevzi KARSLI
ÜYE	: Doç. Dr. İsmail ÇÖLKESEN

ONAY

Gebze Teknik Üniversitesi Fen Bilimleri Enstitüsü Yönetim Kurulu'nun

..../...../…… tarih ve ……/…..... sayılı kararı.

İMZA/MÜHÜR

SUMMARY

Lately, concepts of both virtual reality (VR) and augmented reality (AR), gained increased attraction due to improvements in game engine technology. Also, due to the ongoing COVID-19 pandemic and requirements to stay at home, VR visits become more popular. In this study, the Gebze Technical University (GTU) Campus area was chosen to create a three-dimensional (3D) VR tour application by integrating data obtained from an unmanned aerial vehicle (UAV) into a virtual environment by utilizing the Unity game engine. For acquiring high-quality 3D textured mesh models of the Campus, various imaging geometries and flight altitudes were employed. With a ground sampling distance (GSD) of ≤2.2 cm, the aerial photos were obtained from 20 megapixels (MP) Sony Exmor RGB camera equipped DJI Phantom 4 Pro V2.0 UAV. Structure from motion (SfM) based image matching software Agisoft Metashape Professional was used for point cloud generation and 3D textured mesh model production. The geometric correction was carried out by utilizing 86 well-distributed ground control points (GCPs) with an accuracy of ±2 cm (~0.9 pixels) as root mean square error (RMSE). Produced 3D textured mesh models were imported into the Unity game engine and rendering optimization algorithms such as occlusion culling and space subdivision were applied for increasing performance. In addition, the visual capability of the application was enhanced by adding premade 3D models of singular objects such as trees, lighting poles, benches, and arbours. Interactive information panels with metadata of Campus buildings were placed over the environment for providing general knowledge about the Campus area. Finally, for a realistic VR tour, a first-person player was added.

Key Words: Unmanned Aerial Vehicle (UAV), Structure From Motion (SFM), 3D Textured Mesh Model, Virtual Reality (VR), Unity.

ÖZET

Son zamanlarda oyun motoru teknolojisinde yaşanan gelişmeler doğrultusunda sanal gerçeklik (VR) ve arttırılmış gerçeklik (AR) konseptleri birer ilgi odağı haline gelmektedir. Ayrıca devam eden COVID-19 salgını ve evde kalma zorunluluğu nedeniyle çeşitli müzeleri ve cazibe merkezlerini kapsayan VR uygulamalarına gerçekleştirilen ziyaretlerin arttığı gözlemlenmiştir. Bu çalışma kapsamında, Gebze Teknik Üniversitesi (GTÜ) Kampüs alanına ait bir üç boyutlu (3B) VR tur uygulaması oluşturmak amacıyla insansız hava aracından (İHA) elde edilen veriler Unity oyun motoru kullanılarak sanal bir ortama entegre edilmiştir. Kampüs alanına ait yüksek kaliteli doku giydirilmiş 3B katı modellerin elde edilmesi için farklı görüntüleme geometrilerinde ve yüksekliklerde uçuşlar gerçekleştirilmiştir. DJI Phantom 4 Pro V2.0 üzerine yerleştirilmiş 20 megapiksel (MP) Sony Exmor RGB kamera kullanılarak 2.2 cm'den küçük yer örnekleme aralığına (GSD) sahip hava fotoğrafları elde edilmiştir. Nokta bulutu ve doku giydirilmiş 3B katı model üretimi işlemleri için hareketten yapı tabanlı Agisoft Metashape Professional görüntü eşleme yazılımı kullanılmıştır. Geometrik düzeltme sırasında arazi üzerine yerleştirilmiş 86 adet yer kontrol noktası (YKN) kullanılmış ve karesel ortalama hata değeri ±2 cm (~0.9 piksel) olarak elde edilmiştir. Üretilen 3B doku giydirilmiş katı modeller Unity oyun motoruna aktarılmış ve büyük boyuttaki poligon verisinin uygulama performansına olan etkisinin azaltılması amacıyla oklüzyon ayırma ve uzay alt bölümü gibi görselleştirme optimizasyonu algoritmaları uygulanmıştır. Ek olarak, ağaç, aydınlatma direği, bank ve çardak gibi objelere ait hazır 3B obje modelleri eklenerek uygulamanın görselliği iyileştirilmiştir. Kampüs hakkında bilgi vermek amacıyla kampüs binalarına ait öznitelik bilgisi içeren interaktif bilgi panelleri yerleştirilmiştir. Son olarak, gerçekçi bir VR deneyimi için uygulamaya birinci şahıs bir oyuncu eklenmiştir.

Anahtar Kelimeler: İnsansız Hava Aracı (İHA), Hareketten Yapı, 3B Doku Giydirilmiş Katı Model, Sanal Gerçeklik, Unity.

ACKNOWLEDGEMENTS

I would like to express my deepest and most sincere gratitude and appreciation to my supervisor, Prof. Dr. Umut Güneş SEFERCİK for his endless support, and valiant encouragement, and for sharing all of his very valuable knowledge and treasured experience from the beginning of my thesis journey. His never-ending support, understanding, and pieces of advice he has given me since the beginning of my thesis work gave me the will, and strength to complete this effort.

I wish to express my most humble thanks and gratitude to Prof. Dr. Taşkın KAVZOĞLU for his valuable support and great encouragement, Prof. Dr. Fevzi Karslı, and Assoc. Prof. Dr. İsmail ÇÖLKESEN for their important pieces of advice and helpful suggestions. I want to thank and show my gratitude to all my co-workers and friends at Gebze Technical University for their support, and reassurance. The friendship they showed me shed light on my path and inspired me.

I would like to show my heartfelt thanks and most humble gratitude to my beloved family and loved ones for their continuous support, deepest understanding, and relentless reassurance they have given me during my thesis work. They are my biggest supporter in the journey of life and they are the reason who I became, and I would like to dedicate this thesis to them. Last but not least, I would like to express my deepest gratitude to Almighty Allah for granting me the opportunity to complete this thesis work.

This thesis is supported by Gebze Technical University with Scientific Research Project (SRP) number 2020-A-105-42.

TABLE of CONTENTS

LIST OF ABBREVIATIONS AND ACRONYMS

Abbreviations and Acronyms		**Explanations**
2D	:	Two-Dimensional
3D	:	Three-Dimensional
θ	:	Incidence Angle of the Laser Beam
λ	:	Wavelength
λ_{scale}	:	Scale Factor
ω, ϕ, κ	:	Rotations Between Image and Ground Coordinate Systems
$\overrightarrow{a_1}, \overrightarrow{a_2}$	:	Vectors Between Ground Point A and Corresponding Image Points
$\vec{b}$	:	Base Vector Between Two Perspective Centres
$\vec{V}$	:	The Vector Between C and Ground Point A
$\vec{v}$	:	The Vector Between C and Image Point a
μm	:	Micrometers
A_{11}, A_{12}, A_{13}	:	Components of Orthogonal Matrix
ADS-B	:	Automatic Dependent Surveillance-Broadcast
AGB	:	Above-Ground Biomass
AGL	:	Above Ground Level
AI	:	Artificial Intelligence
AIP	:	Aeronautical Information Publication
ALS	:	Airborne Laser Scanning
AR	:	Augmented Reality
ASPRS	:	The American Society for Photogrammetry and Remote Sensing
AV	:	Augmented Virtuality
B.C.	:	Before Christ
BIM	:	Building Information Modeling
BLOS	:	Beyond Line-of-Sight
c	:	The Speed of Light
C	:	Projection Centre
CAD	:	Computer-Aided Design
cm	:	Centimeters

CORS	:	Continuously Operating Reference Stations
DEM	:	Digital Elevation Model
DGCA	:	The Directorate General of Civil Aviation
DN	:	Digital Number
DSM	:	Digital Surface Model
E	:	The Energy of a Photon
ENR	:	En-Route
EO	:	Electro-Optic
ESC	:	Electronic Speed Controller
f	:	Focal Length
FOV	:	Field of View
ft	:	Feet
g	:	Grams
GB	:	Gigabyte
GCP	:	Ground Control Point
GIS	:	Geographic Information System
GLCM	:	Gray-Level Co-Occurrence Matrix
GNSS	:	Global Navigation Satellite Systems
GPS	:	Global Positioning System
GS Pro	:	Ground Station Pro
GSD	:	Ground Sampling Distance
GTU	:	Gebze Technical University
h	:	Planck's Constant
H	:	Flight Height
HALE	:	High-Altitude, Long Endurance
h_g	:	Height of the Projection Centre From the Ground
ICAO	:	International Civil Aviation Organization
IFOV	:	Instantaneous Field of View
IMU	:	Inertial Measurement Unit
INS	:	Inertial Navigation System
ISP	:	International Society for Photogrammetry
ISPRS	:	International Society for Photogrammetry and Remote Sensing
J	:	Joule

kg	:	Kilograms
kHz	:	Kilohertz
km	:	Kilometers
LADAR	:	Laser Detection and Ranging
LAI	:	Leaf Area Index
LED	:	Light-Emitting Diode
LiDAR	:	Light Detection and Ranging
LOS	:	Line-of-Sight
LRF	:	Laser Range Finder
LST	:	Land Surface Temperature
LULC	:	Land Use and Land Cover Classification
m	:	Meters
MALE	:	Medium-Altitude, Long Endurance
M_b	:	Mean Photo Scale
m_b	:	Mean Photo Scale Number
mm	:	Millimeters
MR	:	Mixed Reality
MSL	:	Mean Sea Level
MSS	:	The Multispectral Scanner System
NASA	:	The National Aeronautics and Space Administration
NDVI	:	Normalized Difference Vegetation Index
NIR	:	Near-Infrared
nm	:	Nanometers
NM	:	Nautical Miles
NSO	:	North Atlantic Treaty Organization Standardization Office
p	:	The Footprint of the Laser Beam
p_1, p_2	:	Principal Image Points
PPI	:	Plan Position Indicator
R	:	Slant Range
R&D	:	Research and Development
RADAR	:	Radio Detection and Ranging
RAR	:	Real Aperture Radar
RMSE	:	Root Mean Square Error

RPAS	:	Remotely Piloted Aircraft System
R^T	:	3D Rotation Matrix
RTK	:	Real-Time Kinematic
s	:	Second
SAR	:	Synthetic Aperture Radar
SD	:	Secure Digital
SfM	:	Structure from Motion
SLR	:	Side-Looking Radar
SVM	:	Support Vector Machine
TCAS	:	The Traffic Alert and Collision Avoidance System
TM	:	The Thematic Mapper
TR	:	Turkish Republic
U.S.	:	United States
UAS	:	Unmanned Aircraft Systems
UAV	:	Unmanned Aerial Vehicle
USA	:	United States Army
v	:	Frequency
VR	:	Virtual Reality
VRML	:	Virtual Reality Modeling Language
VTOL	:	Vertical Take-Off and Landing
x_a, y_a	:	Image Coordinates of Image Point a
X_A, Y_A, Z_A	:	Ground Coordinates of Ground Point A
x_c, y_c	:	Image Coordinates of the Principal Point
X_c, Y_c, Z_c	:	Ground Coordinates of C

LIST OF FIGURES

LIST OF TABLES

1. INTRODUCTION

1.1. Motivation

Remote sensing is a powerful tool for obtaining data about the environment and objects without requiring physical contact. Compared to traditional terrestrial methods which are generally laborious and ineffective in gathering information, the remote sensing technique is extremely advantageous in large area studies. Especially in the geomatics engineering discipline, remote sensing is frequently utilized for various purposes from simply deriving information about the Earth's surface to determining land use and land cover of an area using pixel-based or object-based classification algorithms. The main data source of remote sensing is optical satellite systems which operate based on capturing reflectance values of surfaces and objects on the ground in different intervals of the electromagnetic spectrum and assigning these values to image pixels for acquiring a satellite image. However, unmanned aerial vehicles (UAVs), remotely controlled aerial platforms, are becoming a prominent alternative to optical satellite platforms due to their advantages such as high-resolution rapid data acquisition from different flight altitudes. Compared to some high-resolution optical satellite systems including WorldView-4 (31 cm resolution), WorldView-3 (31 cm resolution), GeoEye-1 (41 cm resolution), WorldView-2 (46 cm resolution), WorldView-1 (50 cm resolution), and Quickbird (60 cm resolution), UAV systems offer resolution in mm to cm according to operating flight altitude. Satellites pass over an area in certain time intervals limiting the potential of data reachability whereas a UAV can collect data in rapid succession between small intervals. However, due to being an aerial system UAVs do not have the large coverage ability of optical spaceborne systems. So, for large-scale studies, optical UAV platforms are not ideal systems but on the local scale, they overshine optical satellite systems regarding their higher resolution and data acquisition capability in short intervals. Moreover, in photogrammetric studies, optical UAVs are increasingly used due to low-cost flights in contrast to conventional aircraft with high operational costs. Also, changeable flight altitude and easy maneuverability offer more flexibility in UAV flight missions than in aircraft flights.

High-resolution UAV data is employed in different engineering applications processes and analyses, from orthomosaic map production to realistic three-dimensional (3D) model generation. UAV data is processed in the different photogrammetric evaluation software; lately, point cloud-based ones are frequently utilized. In a cloud-based photogrammetric evaluation or image matching software, aerial photos are orientated based on the structure from motion (SfM) algorithm which reconstructs 3D geometry from two-dimensional (2D) data, and a point cloud which displays geometry in noncontinuous vector data format is obtained as a result of this procedure. Then using the point cloud, 3D mesh models, digital surface models (DSMs), and orthomosaic maps are generated for various purposes. A 3D mesh model depicts a surface or an object in continuous vector data format and it is generally generated by applying a triangulation method on obtained point clouds in SfM based software. Real-like 3D meshes are acquired by applying a high-resolution texture to the surface of the mesh by utilizing image pixels. Also, by applying texture spectral information can be gathered apart from spatial information. Moreover, metadata about objects such as buildings and roads can be added to 3D textured mesh models for geographic information system (GIS) studies or building information modeling (BIM) applications. Integration of 3D models into a virtual domain is also an interesting topic with an ever-growing demand for making digital twins of real structures in an artificial environment. Also, digital twin applications are utilized for educational purposes such as introducing equipment to employees in a facility.

Humans are in constant interaction with the concept of physical reality, and they also have deep knowledge about it. Humans learn to predict aspects of the physical environment and the consequences of particular occurrences by being in continuous connection with their surroundings. To have a perception of unfamiliar events, digital computers which enable the user to have a glimpse of a “mathematical wonderland” are utilized [Sutherland, 1965]. Using computers, users can get in contact with the digital environment and immerse themselves inside an artificial world through virtual reality (VR) technology, a particular branch of computer graphics [Brooks, 1999]. In other words, the computer system becomes a virtually generated atmosphere for users to interact and behave as a participant in a digital environment [Pantelidis, 1993]. The phrase “virtual reality” is generalized by Jaron Lanier, a computer scientist and founder of the Virtual Programming Languages Research company [Zheng et al., 1998]. In VR systems, users interact with the virtual world and immerse themselves in

a synthetic environment through computers and other special equipment such as a virtual headset system with the visual and audio transmission. As an indispensable component of VR applications, game engines generally differentiate largely in several aspects of their architectural composition and implementation, however, from the virtual concept they contain a common array of core elements such as engines for rendering, collision, and physics, systems for animation and audio contents, the game environment object model, a system for artificial intelligence (AI) infrastructure, and so forth [Gregory, 2018]. Improvements in game engine technology resulted in an elevated interest in VR technology, including several applications both in scientific and commercial areas. Also, the increasing number of free game engine software in the market including Unity, Unreal Engine, CryEngine, Armory, and Godot provides a heightened potential for VR applications. Utilizing game engines, VR applications for various platforms such as computers, mobile phones, and game consoles can be created for entertainment and educational purposes. With the ever-growing demand for innovation in the game development industry, modern versions of game engines are emerging, and the way for further expansion is widening. In addition, VR technology is progressively applied in different applications, studies, and research. Moreover, with the rise of the metaverse concept, which is basically the Internet of the future, the potential of VR technology is highly expanded. VR will have an important role in the structure of metaverse, fueling the interest for different applications and software in the process. In addition, Web 3.0, the future phase of the evolutionary cycle of the internet, will further increase the implementation of VR technology, especially for websites and web-based applications.

The main aims of this thesis can be summarized as; generating high-quality 3D textured mesh model of the GTU Campus area and integrating generated 3D textured mesh models into a virtual environment for creating a 3D VR tour of the Campus. For this purpose, the entire area was flown with DJI Phantom 4 Pro V2.0 UAV with 20 megapixel RGB camera, and utilizing the captured aerial photos 3D textured mesh models were generated. Additionally, generated 3D models were integrated into the Unity game engine for the creation of the 3D VR tour. By creating a 3D VR tour for GTU Campus candidate students, academicians and other visitors can gather information about the university, faculty, and administrative buildings in an interactive environment.

1.2. State of the Art

Considering their advantages UAVs are frequently operated platforms besides conventional satellite platforms and airplanes. Moreover, UAVs are utilized for different purposes in both civilian applications for the industry and scientific studies for differentiating disciplines. Some examples of the UAV applications include cultural heritage documentation, land use and land cover classification, natural disaster monitoring (earthquake, landslide, land subsidence, flood, volcanic eruption), digital agriculture, forestry research, 3D mesh model generation, and creation of VR applications. UAVs are generally equipped with two different sensors including an optical camera or a light detection and ranging (LiDAR) sensor according to their purposes. In optical UAV photogrammetry reflectance values of the objects and surfaces are captured and stored as digital numbers of corresponding pixels in the form of high-resolution aerial photos. However, in the LiDAR UAV technique, the distance between sensor and object is measured using the electromagnetic waves traveling through a medium such as air. So, the LiDAR UAV method offers point cloud data without a secondary process through direct measurements. In contrast, the optical UAV method provides the point cloud data through specific sub-processes including image orientation and densification of the point cloud.

3D textured mesh models of objects and surfaces are generated mainly using point cloud data obtained using varying methods which differ from each other via utilized sensor platforms. These methods can be divided into two main branches spaceborne remote sensing and airborne remote sensing technology. Optical satellites are used in large-scale modeling studies in spaceborne remote sensing with their large coverage advantage. However, due to lower spatial resolution compared to airborne platforms objects are captured in lower detail thus resulting in poor 3D mesh generation. On the other hand, airborne remote sensing platforms including aircraft, optical UAV, and LiDAR UAV offer high spatial resolution data which can be used to produce more detailed 3D mesh models and higher resolution textures. Also, due to changeable flight height and increased flexibility objects especially buildings with varying shapes can be captured in more detail. Additionally, the land cover and topography of the area affect the modeling performance of the UAV sensor. In areas

with dense vegetation such as forests, LiDAR UAVs have an advantage over optical ones due to their ability to scan forest understory.

Geospatial data visualization is an important concept in VR technology with 3D textured object models and high-resolution images being an important tool for this purpose. Some examples of VR applications for geospatial data visualization are 3D VR tours and 2D panoramic VR tours. For creating realistic and interactive 3D VR tours 3D textured mesh models are utilized for offering users visual and textual information about buildings and other areas. The optical UAV technique is an indispensable instrument for generating 3D textured meshes and integration of these models can be conveniently carried out in a game development environment including a game engine. As one of the most popular free game engines Unity is frequently utilized in VR integration of geospatial data. Unity offers a user-friendly interface and handy tools for creating a VR application with built-in components for game development.

1.3. Structure of the Study

The main aims of this study can be grouped under two main sections. The first one is the generation of 3D textured mesh models using high-resolution UAV data. The second one is the integration of 3D meshes into a virtual environment using a game development engine. The structure of the study is divided into six main sections.

In the first chapter *Introduction*, general information was given. It has subparts including motivation (chapter 1.1.), state of the art (chapter 1.2.), and the structure of the study (chapter 1.3.).

The second chapter is presented as *Literature Review*. This chapter gives fundamental knowledge about the concepts, technologies, and methods used in this thesis. The first subchapter is remote sensing (chapter 2.1.) in which basic information about remote sensing science such as electromagnetic energy transmission (chapter 2.1.1.), and remote imaging principle (chapter 2.1.2.) is given. The second subchapter is airborne remote sensing technologies (chapter 2.2.) in this chapter information about aerial remote sensing systems is given including the principle of photogrammetry (chapter 2.2.1.) and airborne laser scanning (chapter 2.2.2.). The third subchapter is optical unmanned aerial vehicle technology (chapter 2.3.) in this chapter classification

of optical UAVs (chapter 2.3.1.), legislation (chapter 2.3.2.), instruments of optical UAVs (chapter 2.3.3.), optical UAV utilization areas (chapter 2.3.4.) and fundamentals of optical UAVs (chapter 2.3.5.) are explained in detail. The fourth and last subchapter is VR and augmented reality (AR) (chapter 2.4.) in this chapter concepts of VR (chapter 2.4.1.), and AR (chapter 2.4.2.) are identified, and the integration of UAV data and virtual reality (chapter 2.4.3.) is presented with some example studies and research.

The third chapter is *Study Area and Utilized Materials*. In this chapter, the study area (chapter 3.1.) and utilized materials (chapter 3.2.), and software (chapter 3.3.) are introduced with specifications.

The fourth chapter is *Methodology* in which methods and techniques utilized in this thesis are explained thoroughly. The first subchapter is optical UAV data acquisition (chapter 4.1.) including pre-flight stages (chapter 4.1.1.), flight stages (chapter 4.1.2.), and post-flight stages (chapter 4.1.3.) of the UAV survey. The second subchapter is orthomosaic generation using optical UAV data (chapter 4.2.) which consists of geometric orientation steps (chapter 4.2.1.), dense point cloud generation (chapter 4.2.2.), 3D mesh model generation (chapter 4.2.3.), 3D textured mesh model generation (chapter 4.2.4.), digital surface model generation (chapter 4.2.5.) and orthomosaic generation (chapter 4.2.6.). The third and the last subchapter is the 3D virtual reality tour creation (chapter 4.3.) which involves steps of 3D textured mesh model importation (chapter 4.3.1.), setting up the environment (chapter 4.3.2.), rendering optimization algorithm application (chapter 4.3.3.), first-person player implementation (chapter 4.3.4.) and building an executable (chapter 4.3.5.).

The fifth chapter is *Results* which displays the results of this thesis study with statistics and visual materials. In the first subchapter orthomosaic generation using optical UAV data (chapter 5.1.), results of the orthomosaic generation process including geometric orientation results (chapter 5.1.1.), dense point cloud (chapter 5.1.2.), 3D mesh model (chapter 5.1.3.), 3D textured mesh model (chapter 5.1.4.), digital surface model (chapter 5.1.5.) and orthomosaic (chapter 5.1.6) are displayed. In the second subchapter 3D virtual reality tour creation (chapter 5.2.), the results of 3D textured mesh model importation (chapter 5.2.1.), setting up the environment (chapter 5.2.2.), rendering optimization algorithm (chapter 5.2.3.), first-person player implementation (chapter 5.2.4) and building an executable (chapter 5.2.5.) are given.

The sixth and last chapter is *Conclusion and Discussion* which concludes the thesis and also future remarks are presented in this chapter.

2. LITERATURE REVIEW

2.1. Remote Sensing

Earth's surface and objects emit and reflect sunlight according to their physicochemical characteristics. Thanks to this natural phenomenon humans can gather visual information using their optical receptors which are their eyes. In other words, human eyes perceive objects by detecting reflected sunlight remotely and interpreting the acquired signal without physical contact. Remote sensing is the science and art of acquiring information about the phenomena, surfaces, or objects via a sensor device without physical contact [Lillesand et al., 2015]. Remote sensing technology is utilized in various fields, including agriculture, forestry, disaster monitoring, geology, hydrology, and security [Mather and Koch, 2011]. In remote sensing science, acquired electromagnetic energy is captured and interpreted to derive information using spaceborne, airborne, and terrestrial systems or techniques, including optical satellites, side-looking radar platforms such as real aperture radar (RAR), and synthetic aperture radar (SAR), doppler, plan position indicator (PPI), traditional photogrammetry, optical UAV, traditional LiDAR, UAV LiDAR, and bathymetric systems. Also, remote sensing systems differ from each other according to the principle of active and passive remote sensing.

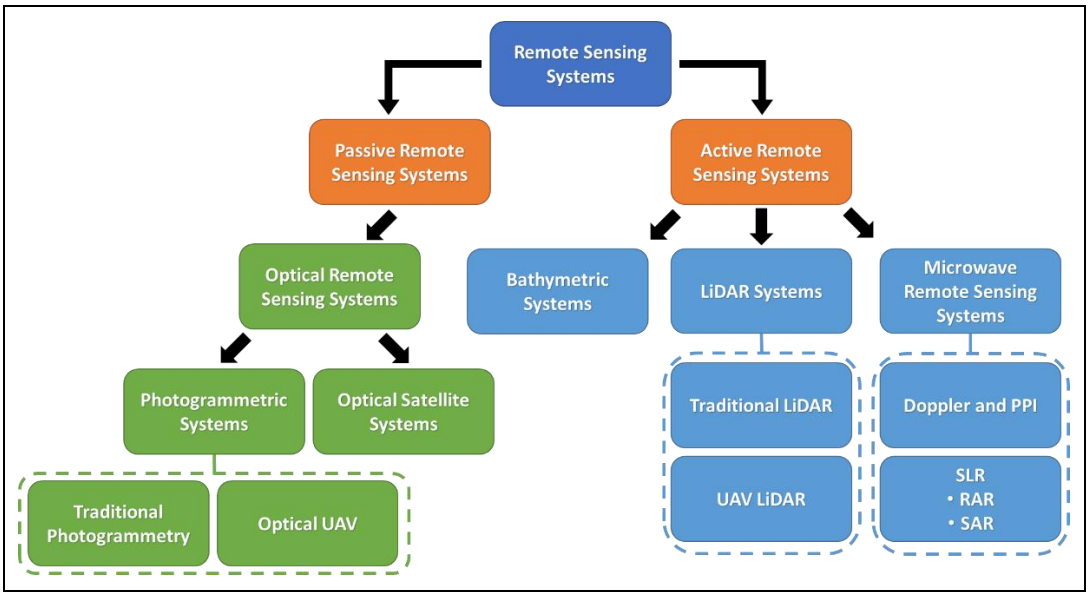

Figure 2.1: Passive and active remote sensing systems.

2.1.1. Electromagnetic Energy and Electromagnetic Spectrum

Sun is one of the most powerful natural illumination sources for Earth and it has utmost significance in human life whether doing everyday tasks or gathering information from the environment. In remote sensing, the passive sensor detects electromagnetic energy in the form of sunlight to distinguish objects from each other. Sunlight as an electromagnetic wave interacts with the atmosphere before reaching the Earth's surface. After this interaction, electromagnetic energy is emitted or reflected by objects by solar radiation. In addition, some of the energy is transmitted through the objects. The interaction of objects and electromagnetic energy can be presented by identifying the total incident energy using reflected, emitted, and transmitted energy (Equation 2.1).

$$E_I(\lambda) = E_R(\lambda) + E_A(\lambda) + E_T(\lambda) \tag{2.1}$$

In the Equation 2.1, $E_I(\lambda)$ represents the total amount of incident energy which is coming from the sun through electromagnetic radiation, $E_R(\lambda)$ displays the total amount of reflected energy from objects, $E_A(\lambda)$ is the total amount of energy absorbed by objects, and the total amount of transmitted energy through objects is defined by $E_T(\lambda)$. Components of remote sensing can be expressed as the Sun as the source of energy, the satellite system as the remote sensing platform, and the investigated object.

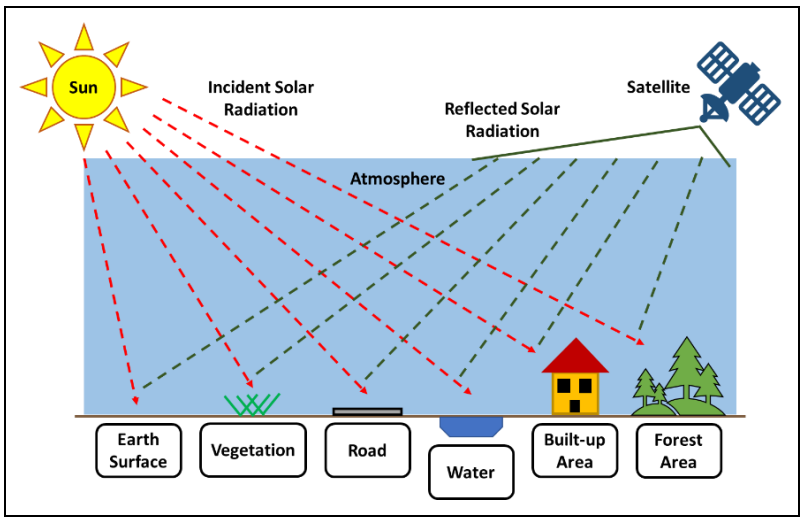

Figure 2.2: Detection of solar radiation by an optical remote sensing system.

While the Sun is the main energy source for passive remote sensing systems there are other systems that do not rely on natural sources for detection. Active remote sensing systems which transmit directed waves of energy to illuminate Earth and objects, then collect a fraction of backscattered energy, have fewer constraints than passive remote sensing sensors because sensitivity to differences in solar radiance limits the utilization capacity by daytime and weather conditions [Campbell and Wynne, 2011]. Passive sensors' dependency on natural illumination sources constrains their usage whereas active sensors have the ability to view an area without the dependency of daylight and thus they are utilized in military operations and border security. Depending on the features of the material including structural and physicochemical, objects return varying amounts of energy in differentiating wavelengths or bands of the electromagnetic spectrum [Aggarwal, 2004]. Optical sensors including spaceborne and airborne passive remote sensing systems generally operate between visible light which has a wavelength between 0,4 µm (micrometers) and 0,7 µm and near-infrared (NIR) which is between 0,7 µm and 1,3 µm, bands of the electromagnetic spectrum. Figure 2.3 represents electromagnetic spectrum with spectral regions [Sublime, 2021].

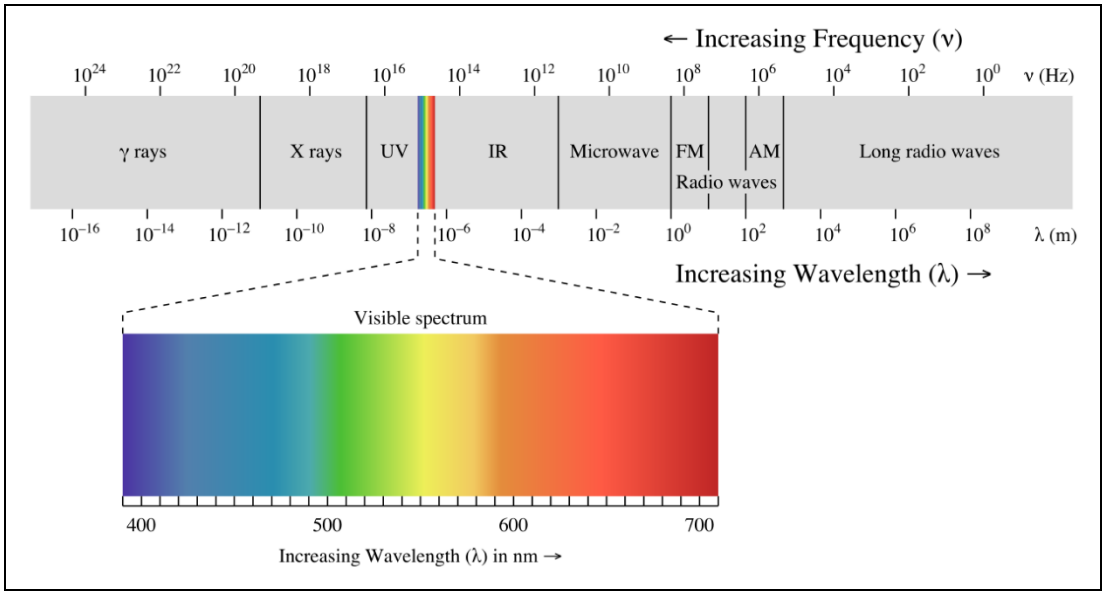

Figure 2.3: Electromagnetic spectrum.

In the visible spectrum, there are three bands with different wavelength intervals including blue (0,4 – 0,5 µm), green (0,5 – 0,6 µm) and red (0,4 – 0,5 µm). After the visible spectrum region, there is the red edge band (0,68 – 0,75 µm) which is

characterized by the sudden change in the leaf reflectance values and thus utilized in different vegetation indices [Horler et al., 1982]. In the infrared region, there are three main bands such as NIR, mid-infrared (1,3 – 3 μm), and thermal infrared (3 – 14 μm). While the NIR band of the infrared region is used in different studies such as the detection of water vapor [Kaufman and Gao, 1992], determination of leaf water content [Tucker, 1980], and monitoring of plant biomass using vegetation indices like normalized difference vegetation index (NDVI) [Le Maire et al., 2011], thermal infrared is utilized in various types of research including urban thermal analysis through detecting land surface temperature (LST) [Weng, 2009], crop water stress detection [Gerhards et al., 2019] and monitoring of geothermal resources [Seward et al., 2018]. The microwave region of the electromagnetic spectrum includes longer wavelengths than the visible spectrum and infrared zone, between 1 mm to 1 m. Passive microwave sensors including radiometers measure electromagnetic energy in the microwave region which is radiated through thermal emission or reflected via the surface of the Earth or the atmosphere, whereas active microwave sensors such as radar illuminate an area by sending waves of electromagnetic energy and then measure the backscattered signal from the region [Woodhouse, 2017]. In the microwave region, wavelengths are longer than previous ones including infrared and visible spectrum but gathered energy is limited in contrast. Longer wavelengths tend to be less likely to get in interference with atmospheric particles and other molecules. But as the wavelength gets longer the frequency of the electromagnetic wave becomes lower as an opposite reaction. From the fundamentals of basic physics, electromagnetic radiation waves travel at the same speed as defined by Equation 2.2.

$$c = v\lambda \tag{2.2}$$

In Equation 2.2, c is the speed of electromagnetic radiation in the vacuum which is 299,793 kilometers (km) s^{-1} (approx. 3 x 10^8 m s^{-1}), v is the frequency of the wave in hertz, and λ is the wavelength which is the distance between two successive wave crest which generally given in nm (10^{-6} m) or μm (10^{-9} m). Particles of electromagnetic radiation are firstly described by Max Planck, and according to the equation defining the energy of a photon (Equation 2.3), photons of wavelength shorter than others or

photons of a wave with higher frequency carry more energy than those of bigger wavelength or lesser frequency [Gupta, 2006].

$$E = hv = \frac{h.c}{\lambda} \tag{2.3}$$

In Equation 2.3, E symbolizes the photon energy (Joule) and h is the Planck's constant (6.62×10^{-34} J s), v is the frequency of the electromagnetic wave, c and λ are the same as the Equation 2.2. The wavelength of the electromagnetic radiation affects the penetration capacity of the signal. For example, microwave remote sensing systems such as SAR operate on a longer wavelength than optical satellite systems, so the penetration capacity is higher which is especially beneficial for sensing dense vegetation and forest areas [Sinha et al., 2015]. In other words, as the wavelength gets longer the amount of backscattered signal received by the sensor is decreased but the penetration capability of the remote sensing system is increased. Also, in the microwave region active and passive sensors seems to be sensitive to different features of the objects. While active remote sensing sensors are prone to be more sensitive to roughness and the physical structure of objects, passive microwave sensors are likely to be more feasible in sensing soil moisture and surface temperature [Li et al., 2011]. Waves with wavelengths longer than microwaves are called radiowaves (> 1 m) which have the largest wavelengths but carry the lowest electromagnetic energy.

2.1.2. Remote Imaging Principles

A digital image consists of smaller components called picture elements or pixels which are the most basic element of imagery. After a physical image is captured by a remote sensing system the brightness or reflectance values of the corresponding points are recorded and converted through the digitalization process by sampling and quantizing the brightness of the image for each pixel location [Castleman, 1996]. After this process, each pixel is assigned with an address showing the row and column number, and a digital number (DN) value called the gray level displaying the captured brightness amount. Properties of the remote sensing data including satellite imagery and aerial photos differentiate according to the characteristics of the utilized sensor. So, the effectivity or suitability of the data varies due to the resolution parameters of

the utilized sensor. These parameters include spatial resolution, spectral resolution, radiometric resolution, and spatial resolution [Mather and Koch, 2011]. Overall, there is a fundamental relationship between the resolution concept and the characteristics of image pixels.

The spatial resolution of a remote sensing sensor is defined as the minimum size of objects on the surface of the Earth that can be individually distinguished or detected and the most basic measure of spatial resolution is the instantaneous field of view (IFOV) which defines the total area of a single-pixel covered by the sensor during the sensing process [Townshend, 1981]. Different remote sensing systems including spaceborne and aerial have varying spatial resolutions. Sensor flight height is one of the biggest factors affecting the IFOV and spatial resolution. As the flight height increases, IFOV becomes larger thus decreasing the spatial resolution because the area covered by a single pixel becomes larger. A large pixel area corresponds to less detailed imagery meaning objects smaller than the IFOV become indistinguishable. Basically, high spatial resolution corresponds to more detailed images but smaller area coverage due to low flight height. In general, photogrammetric systems such as aircraft and optical UAVs have a higher spatial resolution (mm to cm) than conventional optical remote sensing systems including satellites (cm to m). Figure 2.4 shows images with different spatial resolutions [Liang et al., 2012].

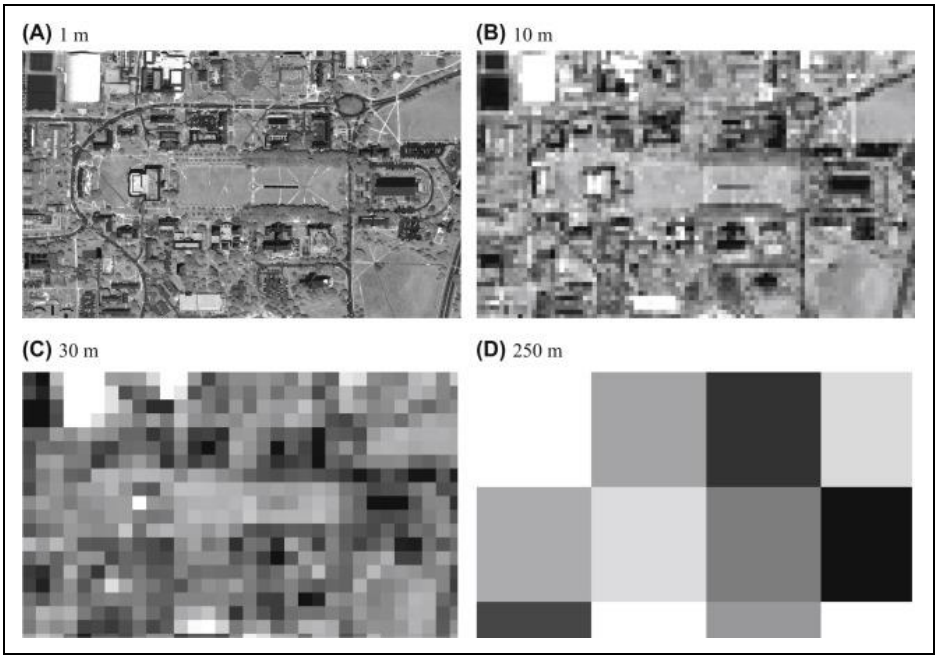

Figure 2.4: Images of the same area with spatial resolutions of a) 1 m, b) 10 m, c) 30 m, and d) 250 m.

The spectral resolution is defined as the wavelength interval and number of sensing bands that a remote sensing sensor can record the acquired electromagnetic energy. Therefore, larger wavelength intervals and greater electromagnetic spectrum coverage through more sensing bands mean higher spectral resolution. Generally, when the spatial resolution of a multispectral satellite system with multiple imaging bands including red, green, blue, and NIR increases, spectral resolution decreases [Dalponte et al., 2009]. Spatial resolution is an essential factor for detecting details of objects but the high spectral resolution is an essential aspect for object classification studies including land use and land cover classification (LULC). Apart from multispectral sensors, hyperspectral remote sensing systems can simultaneously obtain electromagnetic energy in hundreds of imaging bands for each pixel [Fauvel et al., 2012].

The radiometric resolution of the remote sensing system describes the data depth sensitivity of the sensor to acquired electromagnetic energy in bit depth format, including 8-bit (DN range of 0-255) and 16-bit (DN range of 0-65535) [Thenkabail, 2015]. Sensitivity to electromagnetic radiation and thus display capability of image pixel increases as the bit depth of the imagery increases. For example, 8-bit data describes grayness values in a wider spectrum than 6-bit. Moreover, when the impact of radiometric resolution on the image classification is investigated, the classification accuracy is increased for the data with higher radiometric resolution compared to the data with lower radiometric resolution [Verde et al., 2018]. However, the increased bit depth also results in a bigger file size which can elevate hardware requirements and data process time.

Apart from the spatial, spectral, and radiometric resolutions, temporal resolution is an essential feature of a remote sensing system. Temporal resolution defines the revisit time between two successive acquisition dates by a remote sensing sensor [Mather and Koch, 2011]. Moreover, it specifies the visit count and the number of images for a remote sensing system over the same area. For a multitemporal analysis that covers time intervals between predefined dates, the temporal resolution concept has an important role because of revisit frequency. Spaceborne and airborne remote sensing systems have different temporal resolutions. While satellite systems have predesignated revisit dates over an area, airborne systems with manual or autonomous operational capability can be used to acquire data on selected dates, offering more flexibility compared to spaceborne systems.

2.2. Airborne Remote Sensing Technologies

Remote sensing technology is utilized in various domains of physical reality, including Earth's ground, water, space, and air. Different techniques and sensors are used in various environments, such as spaceborne satellites, bathymetric systems, aircraft, and UAV platforms. Before the invention of airplanes, remote sensing of Earth was firstly carried out based on the concept of photography by capturing terrestrial photos of ground and objects. It was 1909 which saw the invention of the first powered aircraft by the Wright Brothers and capturing of aerial photos from an airplane which was operated by Wilbur Wright over the Italian landscape close to Centocelli [Campbell and Wynne, 2011]. After this great milestone for airborne remote sensing technologies, incidents of World War I (1914-1918) and World War II (1939-1945) further expanded the use of aerial systems for data acquisition, especially in reconnaissance and wartime operations. So, in the beginning, airborne systems are generally utilized in the military field. After the World War II era, optical aircraft systems are increasingly beginning to be used for civilian applications, including scientific and commercial ones.

Aerial systems dominated remote sensing technology till the beginning of the 1960s when electronic sensor equipment progressively started to be utilized for both image acquisition and data storage, and optical satellite systems emerged as an alternative source for remote sensing studies [Klemas, 2013]. As the pioneer of spaceborne optical systems, the launch of Sputnik 1, the first artificial satellite system, in 1957 by the former Soviet Union introduced a new era in remote sensing systems [Tatem et al., 2008]. With the heraldry of the satellite remote sensing era, countries worldwide started various initiatives for earth observation satellite missions. Among the first initiatives, the first multispectral satellite remote sensing system Landsat 1 was launched on July 23, 1972, by the United States National Aeronautics and Space Administration (NASA) in the scope of the Landsat Program, which is the longest-running operation in the acquisition of multispectral data of Earth surface from space with more than 3 million images obtained through the Multispectral Scanner System (MSS) and Thematic Mapper (TM) [Sheffner, 1994]. Today, UAVs with different sensors, including optical, LiDAR, and even SAR, are among the most popular and familiar airborne remote sensing systems.

2.2.1. Photogrammetry

American Society for Photogrammetry and Remote Sensing (ASPRS) has defined the term photogrammetry as the art, technology, and science of acquiring reliable data about the environment and physical reality by steps of recording, measuring, and analyzing photos and patterns of acquired electromagnetic energy and different phenomenon [Wolf et al., 2014]. The word photogrammetry itself consists of three Greek words including photo from photos meaning light, gram from gramma meaning description, and lastly, metry from metron meaning measurement [Valença et al., 2012]. Before the first actual application of photogrammetry, the first photograph was captured by Joseph Niepce, a French inventor who lived in the 18th century, in 1827 through a procedure called heliography [Wolf et al., 2014]. In the late 1840s, the first photogrammetric system was developed by Aimé Laussedat, an officer in the French Army Corps of Engineers, and he is widely recalled as the "father of photogrammetry" [Granshaw, 2019] because of his accomplishments [Jiang et al., 2008]. In other words, the work of Laussedat is the first photogrammetric application for acquiring information about physical reality. In the late 19th century one of the first large-scale topographic mapping initiatives using the photogrammetry technique was carried out in Canada by Eduard Deville, the Surveyor-General of Canada [Collier, 2002]. Albrecht Meydenbauer, a Prussian architect, carried out a pioneering work of photogrammetry by using Laussedat's method to capture photos of various historical landmarks including religious places and other buildings [Jiang et al., 2008]. Thanks to the pioneering accomplishments of Laussedat, Meydenbauer, and other photogrammetry enthusiasts International Society for Photogrammetry (ISP) which is today named International Society for Photogrammetry and Remote Sensing (ISPRS), was established in 1910 and it still exists as a well-known scientific society for photogrammetric research [Fryer, 1996]. After World War II, various aerial photogrammetry campaigns were carried out by countries around the world by photogrammetry specialists and technical staff for mapping wide areas [Polidori, 2021]. This development increased the civilian use of aerial photogrammetry apart from military applications such as reconnaissance. Lately, with advancements in technology and science, utilization of UAVs has increased in various global photogrammetric research and studies.

Compared to satellite remote sensing, photogrammetry offers higher spatial resolution, and lower re-imaging interval, and is especially suitable for small-scale mapping applications. However, satellite remote sensing is generally preferred in large-scale mapping studies because of the large coverage of spaceborne remote sensing systems. Main utilization areas of photogrammetry can be described as cultural heritage documentation [Yastikli, 2007], natural disaster monitoring and management [Chou et al., 2010], forestry research [Aicardi et al., 2016a], precision agriculture studies [Comba et al., 2018], digital twin applications [Mohammadi et al., 2021], VR integration [Sefercik et al., 2021a] and AR integration [Portalés et al., 2010]. Photogrammetry is divided into two main fields terrestrial photogrammetry and aerial photogrammetry. Traditional photogrammetric studies and research are generally within the field of terrestrial photogrammetry. Whether taking photos of objects or extracting building facades. In other words, photogrammetric studies carried out on the ground are entitled terrestrial photogrammetry applications. Also, terrestrial photogrammetry is further identified as close-range photogrammetry if investigated object size and object distance to cameras are both lower than 100 m or 330 ft, and the photographs obtained in such applications are quite convergent and mainly pointed to the center of the objects [Cooper and Robson, 1996]. Aerial photogrammetry is defined as photogrammetric studies carried out by aerial systems, including aircraft, hot air balloons, UAVs, and even live animals including pigeons. However, because UAVs later emerged as an alternative source to aircraft systems which are the conventional platforms for aerial photo acquisition, aerial photogrammetry is further divided into two sections including traditional aerial photogrammetry and optical UAV photogrammetry. While the first demonstration of photogrammetry is carried out using terrestrial systems, later inventions of modern aerial systems increased the interest in aerial photogrammetry. Terrestrial photogrammetry is applied in various applications, including producing 3D object models [Piermattei et al., 2015], measuring building facades [Ordóñez et al., 2010], and monitoring the structural health of buildings [Stayroulaki et al., 2016]. Aerial photogrammetry studies include topographic mapping applications, monitoring of plant growth and health [Sinha et al., 2022], plant disease detection [Neupane and Baysal-Gurel, 2021], forest fire detection [Ollero and Merino, 2006], generating 3D building models [Xie et al., 2012], urban growth monitoring [Kaya and Curran, 2006], building deformation analysis [Varbla et al., 2021], and archeological research [Mozas-Calvache et al., 2012].

In photogrammetry, viewing objects in 3D and thus interpreting the distance between objects or surfaces is based on the principle of stereoscopic viewing which utilizes two or more photos, captured from different view orientations with certain overlap ratios to reconstruct 3D geometry [Linder, 2009]. Because utilizing a single photo, only 2D coordinates of objects can be obtained. Capturing different views of objects is an essential process in extracting the 3D geometry or producing a stereo model. Moreover, objects should be taken with the certain front and side overlap ratios for this procedure to be accomplished. Two photos separated by a base distance are captured for calculating 3D terrain coordinates of object points using 2D image coordinates of the same points which are available at least in two photos. Figure 2.5 shows the geometry for stereo model production with two photos separated by a base distance [Linder, 2009].

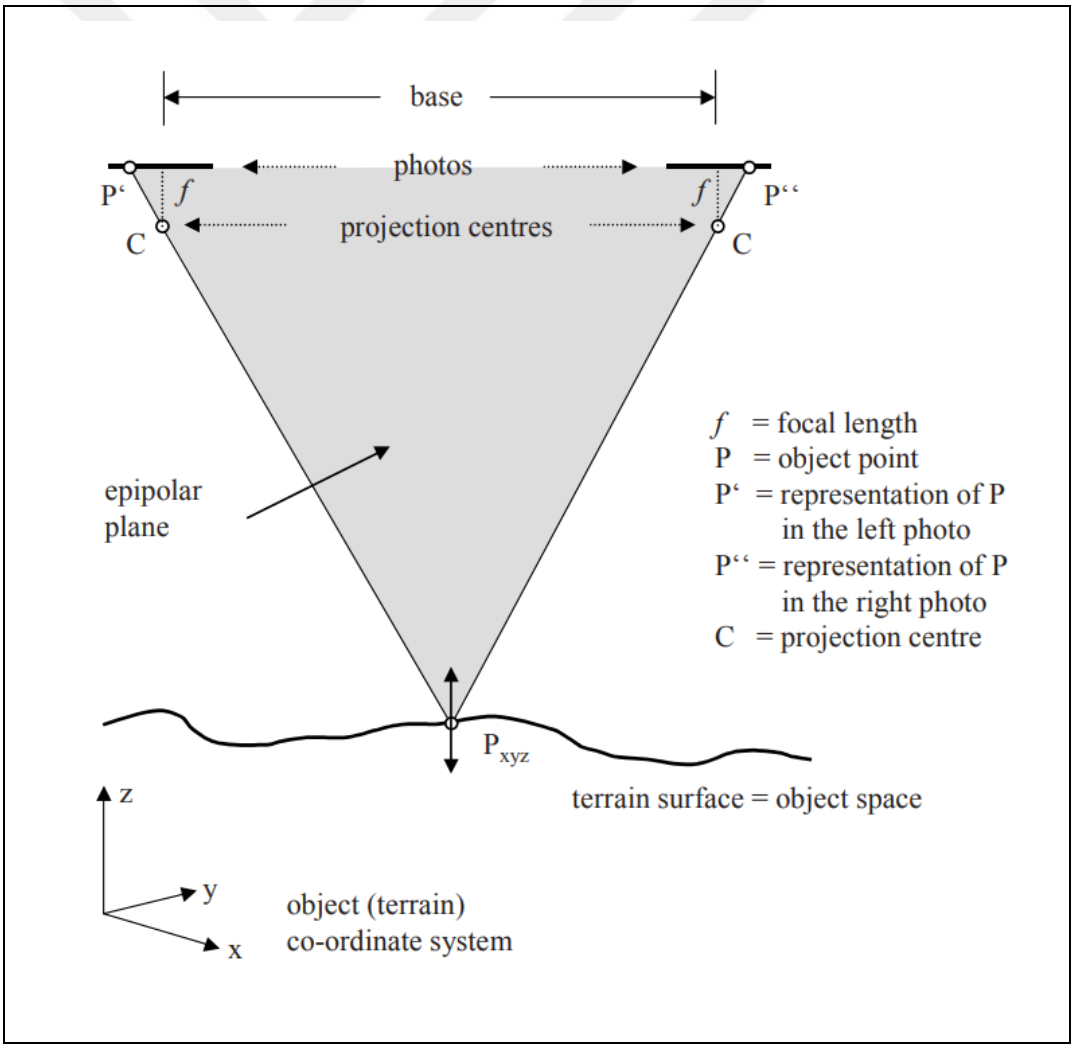

Figure 2.5: The geometry of a stereo model shows the relationship between image coordinates and object coordinates.

In Figure 2.5, C is the projection centre and it is the point where all of the oncoming rays reflected from the ground and objects are intersected in the camera system. On the other hand, *f* is the focal length of the camera system which defines the distance between C and the photo or image coordinate system. P object point is represented in two consecutive photos with a base between them for producing a stereo model of the object. The epipolar plane is the plane that connects object points and lens centers (or Cs) of the two camera systems [Bolles et al., 1987].

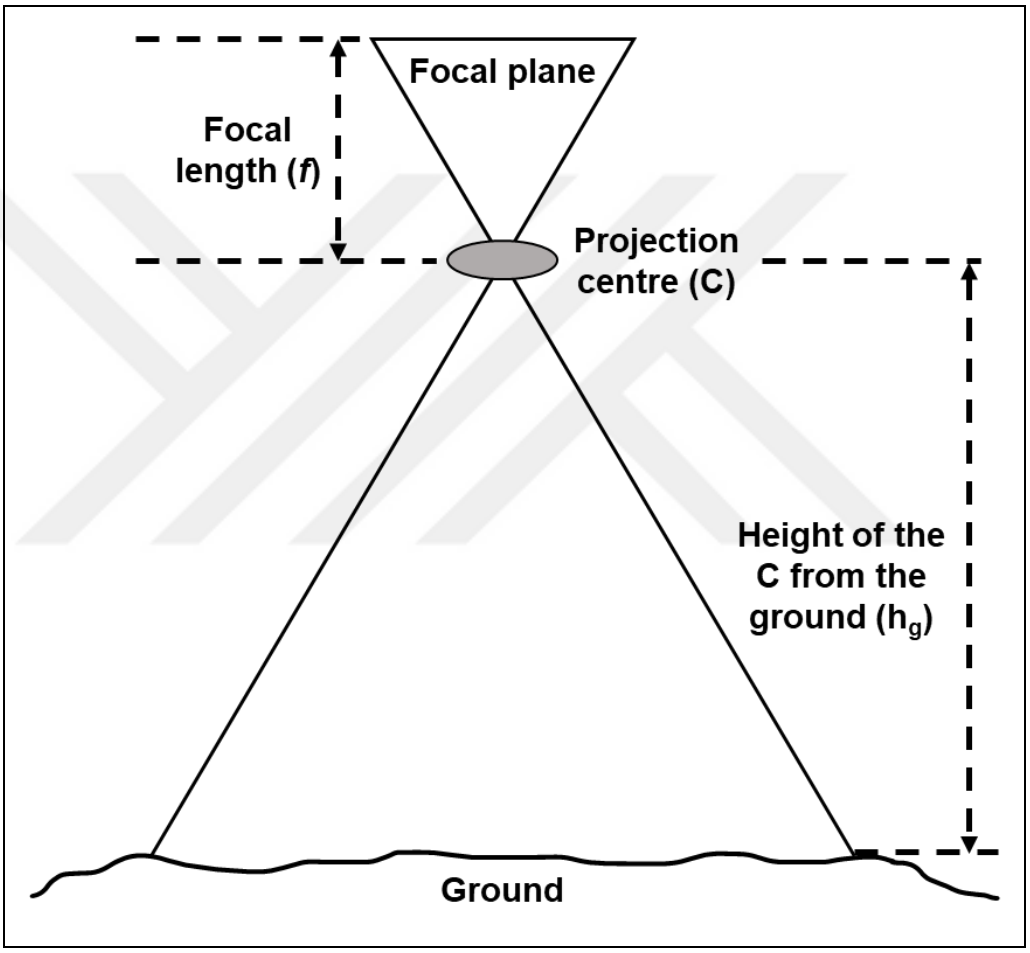

Figure 2.6: Focal length (*f*) and height of the projection centre from the ground (h_c) in a photo capture scenario.

Using the *f* and height of the C from the ground (h_g) the mean photo scale (M_b) and mean photo scale number (m_b) can be calculated as shown in Equation 2.4.

$$M_b = \frac{1}{m_b} = \frac{f}{h_g} \tag{2.4}$$

The collinearity condition describes the relationship between image and object space points. The collinearity condition explains that the vector starting from the C to a particular point on the image is a proportion of the vector from C to the equivalent point on the ground [Habib et al., 2000]. Using the principle of collinearity, the geometry at the time of photo acquisition is realized for reconstructing object position and structure.

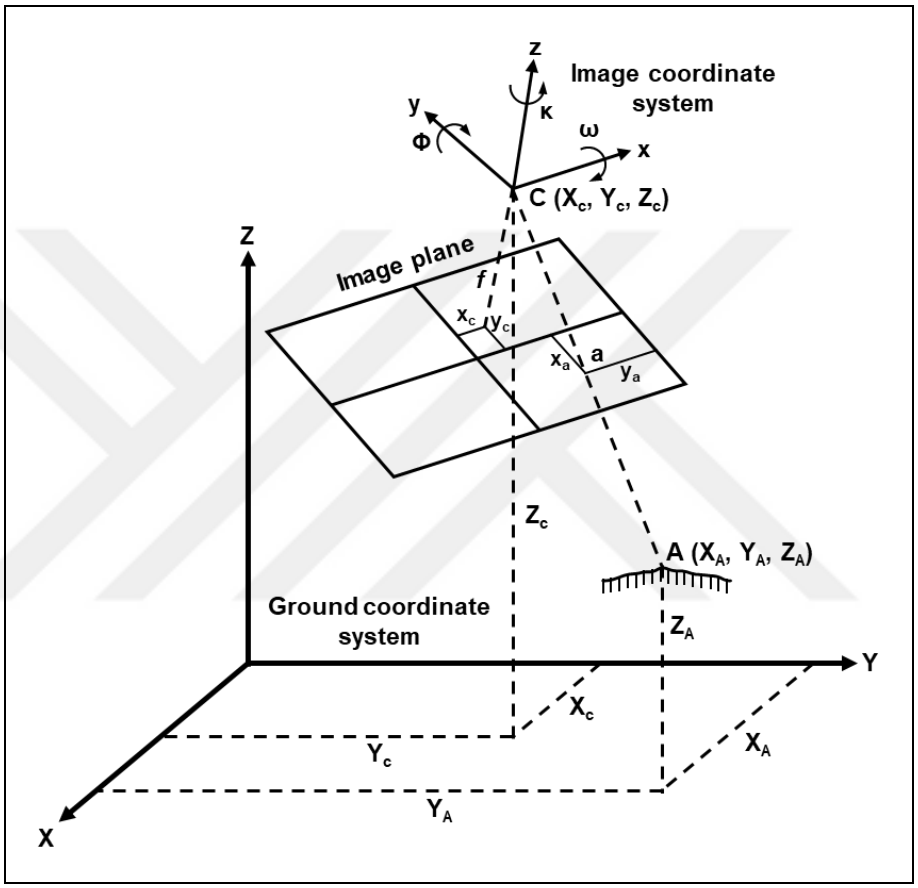

Figure 2.7: The collinearity condition shows the relationship between the image coordinate system and the terrain coordinate system.

The collinearity condition is formulated according to the parameters described by Habib et al. [2000].

$$C = \begin{bmatrix} x_c \\ y_c \\ f \end{bmatrix} \qquad a = \begin{bmatrix} x_a \\ y_a \\ 0 \end{bmatrix} \tag{2.5}$$

In Equation 2.5, the image coordinates of the principal point, the projection of C on the image plane, and image point a, the projection of ground point A on the image

plane, are represented. The vector $\vec{v}$, starting from C to the image point a, and the vector $\vec{V}$, starting from C to the ground point A, can be both expressed using image coordinates as in Equation 2.6.

$$\vec{v} = \begin{bmatrix} x_a - x_c \\ y_a - y_c \\ -f \end{bmatrix} \qquad \vec{V} = \begin{bmatrix} X_A - X_c \\ Y_A - Y_c \\ Z_A - Z_c \end{bmatrix} \tag{2.6}$$

Finally, the relationship between image coordinates and ground coordinates can be explained using Equation 2.7.

$$\vec{v} = \lambda_{scale}\, R^T(\omega\,, \phi\,, \kappa)\, \vec{V} \tag{2.7}$$

In Equation 2.7, λ_{scale} describes the scale factor, R^T identifies the transpose of the 3D matrix for rotation, and ω, ϕ, and κ characterize rotations essential for the alignment of image and ground coordinate systems. Image orientation is an essential step for obtaining 3D coordinates in various applications, including DTM generation, orthophoto computation, and data acquisition for GIS studies [Heipke, 1996]. While establishing a relationship between captured photos through correlation ratio image matching is an important aspect of the image orientation process. An orientation procedure is applied to realize the geometry at the time of photo acquisition, and a 3D model is obtained as a result of this application throughout the photogrammetric evaluation process. The photogrammetric orientation process is divided into two main practices including interior orientation and exterior orientation. Interior orientation is carried out to determine camera geometry and camera parameters such as f and image coordinates of the principal point (x_c, y_c). Also, parameters for lens distortions, including barrel and pincushion distortions are obtained through the interior orientation. General workflow for inner orientation is carried out through the camera calibration task. Camera calibration is done by using a calibration object or through the self-calibration process, which involves using an array of uncalibrated photos to determine the camera parameters and metric specifications of the camera [Remondino and Fraser, 2006]. Nowadays, modern photogrammetric evaluation software realizes the camera parameters automatically by storing the metric properties of the utilized

digital camera in the software database. Still, in some cases where the interior orientation cannot be solved automatically, camera calibration is carried out in a laboratory environment by capturing photos of a calibration object in different viewing geometries and orientations. After the metric properties of the camera system are figured out, interior orientation parameters are identified. Then the exterior orientation is carried out to obtain a scaled 3D model with real-world coordinates by utilizing a set of photos with certain overlapping ratios.

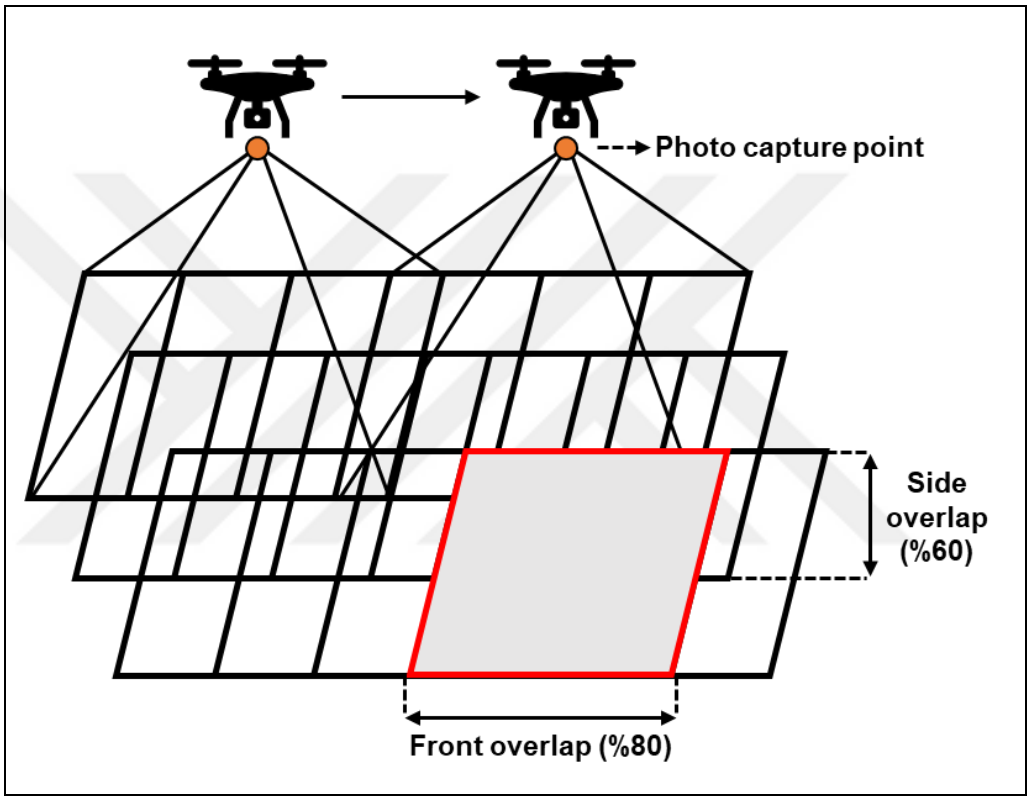

Figure 2.8: Overlap ratios during a photogrammetric flight for an aerial photogrammetry application.

In Figure 2.8 example front and side overlap ratios are shown for a photogrammetric flight plan. The traditional method for exterior orientation is called aerial triangulation, a well-known and conventional method, especially in traditional aircraft photogrammetry. Because the aerial triangulation method requires a human operator and other essential equipment to be carried out, a more autonomous version of this method is developed by Schenk [1997] named automatic aerial triangulation. For exterior orientation at least two photos are required to determine a total of 12 orientation parameters including ground coordinates of C and rotations of photos, ω,

ϕ, and κ. Exterior orientation is done through two consecutive operations including relative orientation and absolute orientation. To obtain positions of points in the ground, coordinates of corresponding points in at least two consecutive images can be utilized. Relative orientation is the process of determining the position and orientation of cameras during the time of photo acquisition [Horn, 1990]. In other words, the geometry of two overlapping images is realized for calculating the distance and orientation between the camera and ground points. The calculation of object points is based on the coplanarity principle which implies that two corresponding image points in two overlapping images and the object point are in the same planar orientation [Grussenmeyer and Khalil, 2002].

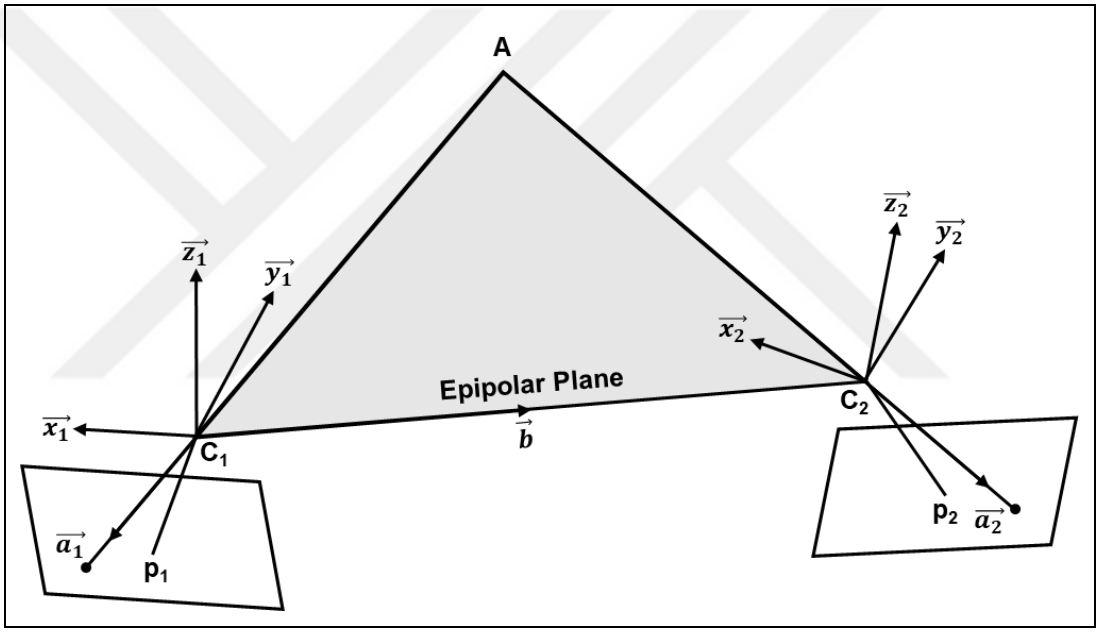

Figure 2.9: Coplanarity principle showing the intersection of rays between two consecutive image points and the object point.

In Figure 2.9, vectors ($\overrightarrow{a_1}, \overrightarrow{a_2}$) between ground point A and corresponding image points and base vector ($\vec{b}$) between two perspective centres (C_1, C_2) are shown in the same epipolar plane as well as principal image points p_1, p_2. A 3D model of the captured environment is obtained as a result of the relative orientation but this model is not scaled and does not have real-world coordinates. Therefore, an additional procedure is carried out for georeferencing the produced 3D model. This procedure is called absolute orientation which is done after the relative operation process. The

absolute orientation process is basically a 3D affine transformation problem utilized for the calculation of ground coordinates.

$$\begin{bmatrix} X_A \\ Y_A \\ Z_A \end{bmatrix} = \lambda_{scale} \begin{bmatrix} A_{11} & A_{12} & A_{13} \\ A_{21} & A_{22} & A_{23} \\ A_{31} & A_{32} & A_{33} \end{bmatrix} + \begin{bmatrix} X_c \\ Y_c \\ Z_c \end{bmatrix} \tag{2.8}$$

Absolute orientation of 3D models is utilized using ground points with known real-world coordinates. These points are generally called ground control points (GCPs), which are homogenously established over the application area and measured using a terrestrial method such as global navigation satellite systems (GNSS). Apart from using GCPs, digital elevation models (DEMs) are utilized for the 3D absolute orientation of stereo models [Rosenholm and Torlegard, 1988]. A scaled version of the study area is obtained through the absolute orientation.

2.2.2. Airborne Laser Scanning

In the scope of airborne remote sensing technologies apart from optical aircraft or UAV systems, airborne laser scanning (ALS) systems are utilized in various research and applications. Laser scanning sensors use optomechanical scanning assemblies, and they utilize laser beams for measuring the distance between the sensor and the illuminated points [Wehr and Lohr, 1999]. In the scientific literature, laser systems are commonly named in two different ways including LiDAR and laser ranging and detection (LADAR). After the invention of the working ruby laser in 1960 by Theodore Harold Maiman, new research and developments in laser technology followed this great accomplishment [Rawicz, 2008]. The emergence of new laser systems followed this development and LiDAR become a commonly utilized alternative to passive sensors including electro-optic (EO) and active sensors such as microwave radio detection and ranging (RADAR) sensors [McManamon, 2012]. Conventional ALS systems are integrated into fixed-wing aircraft or helicopters with flight altitudes of 100-4000 m above ground and they scan objects through the traveling path of the laser footprint [Gallay, 2013]. ALS systems commonly utilize two laser wavelengths for scanning including 1.06 μm and 1.5 μm, and the pulse repetition rate for high-end ALS systems is between 100 kHz (kilohertz) and 200 kHz

[Pfeifer and Briese, 2007]. According to Baltsavias [1999], typical ALS system components without profilers can be listed as:

- a laser range finder (LRF): A system consisting of a laser, optics for transmission and reception, a detector for laser signals, an amplifier, a counter device for time, and other essential electronic parts;
- computer platform, operating system, and essential software for supervision during data retrieval;
- storage system for acquired laser, inertial navigation system (INS), GPS, scanner data, and possibly imagery if there exists an optical camera system for image acquisition;
- a scanner device;
- GPS and a system for attitude measurement or INS in cases where the ALS system does not have different GPS antennas for attitude measurement;
- a platform for positioning and securing system elements;
- GPS stations as the ground reference;
- software for flight mission planning and different postprocessing steps;
- GPS with radio connections or antennas for navigation and receiving corrections in real-time;
- optionally, individual sensors including video and digital CCD-cameras, optical camera systems for photogrammetric application, and other sensors for thermal or multispectral data acquisition;
- optionally, a control mechanism for temperature and humidity.

An ALS system can be seen as a complex platform including various different sensors and electronic components. According to the aim and coverage of the study different configurations exist for the utilized ALS system. While components of ALS systems can be different from each other their prices also vary due to their differentiating complexity. For topographic mapping using the ALS technique, two different calibration processes exist including correcting the determination of laser range and calibration of angular mounting biases by determining the orientation of aircraft relative to the horizon using INS data [Krabill et al., 2000]. Some components and the general operation scheme of an ALS system are shown in Figure 2.10.

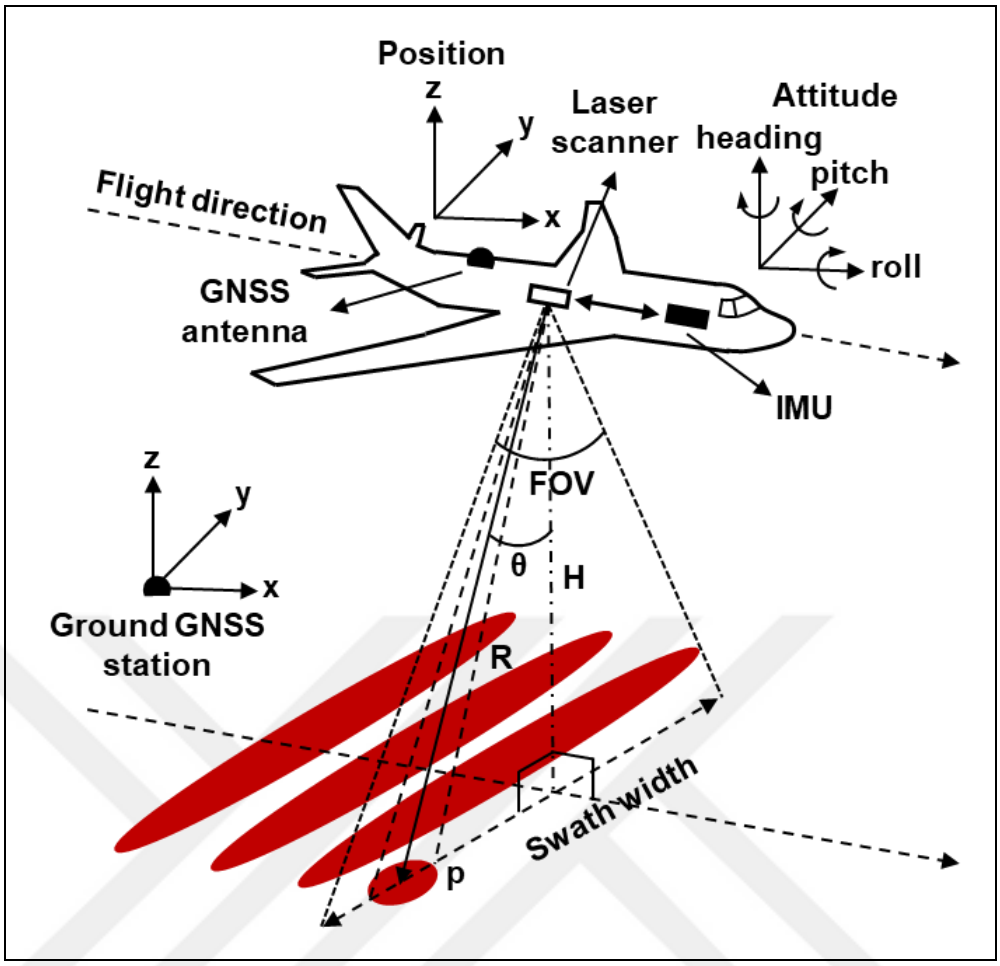

Figure 2.10: The geometry of a typical ALS system with a laser scanner, GNSS antenna, inertial measurement unit (IMU) components, and ground GNSS station.

In Figure 2.10 H is the flying height, θ represents the incidence angle of the laser beam, and field of view (FOV) shows the maximum angular value of θ. Also, R is the slant range of the laser beam during the flight and p is the footprint of the laser beam. An ALS system can be seen as a complex platform including various sensors and electronic components. ALS systems are utilized in a wide range of research and studies including the measurement of individual trees in dense forest areas [Persson et al., 2002], estimating the volume of timber in forest stands [Naesset, 1997], classification of broadleaved and deciduous tree species [Kim et al., 2009], change detection of buildings in urban areas [Murakami et al., 1999], forest growth estimation based on canopy metrics [Næsset and Gobakken, 2005], detection and 3D mapping of vegetation areas [Wagner et al., 2008], estimation of canopy properties such as leaf area index (LAI) and covered ground [Riaño et al., 2004], monitoring of shoreline position change in coastal regions [Robertson et al., 2004], producing flood hazard

maps for disaster management [Costabile et al., 2021], detection of powerlines in forest areas [Zhu and Hyyppä, 2014], monitoring glacier areas and producing glacier inventory [Knoll and Kerschner, 2009]. DSM quality evaluation of satellite data using the ALS data as the reference is another popular topic in remote sensing studies including various research through the years [Ortiz et al., 2012], [Sefercik et al., 2019], [Sefercik et al., 2020]. Generally, ALS DSM is utilized as reference data because 3D topographic point clouds produced using the ALS technique have higher accuracy than traditional remote sensing technologies [Sefercik et al., 2015].

2.3. Optical Unmanned Aerial Vehicle Technology

A UAV or a drone which is the other common acronym for this system is defined as an autonomous aerial system operated by a pilot with a remote controller or a ground control station. UAVs are increasingly utilized in numerous remote sensing applications with each passing day. Also, the complexity and operational capacity of UAV systems are growing with the integration of state-of-the-art equipment including multispectral and hyperspectral digital cameras and real-time kinematic (RTK) GNSS receivers. The term unmanned aerial system (UAS) describes a UAV system with the addition of a ground control station or a remote controller [Nex and Remondino, 2014]. Another international term used by various aviation organizations including International Civil Aviation Organization (ICAO) for UAS is remotely piloted aircraft system (RPAS) [Cary and Coyne, 2011]. UAVs emerged during the period of World War I (1916) however, the idea of a UAV is conceived approximately 2,500 years ago in the ancient era by Archytas of Tarantas who has been credited with the invention of the first autonomous flying machine called the steam-powered pigeon of Archytas in 425 B.C. (before Christ) [Dalamagkidis et al., 2012]. Allegedly, using the energy stored in a mechanism located in its stomach the mechanical pigeon can move its wings to fly roughly 200 m before collapsing to the ground beneath [Valavanis and Kontitsis, 2007]. In 400 B.C., ancient China recorded the concept of a mechanism with vertical flight capability and in 1483 Leonardo Da Vinci, a widely famous renaissance era engineer, architect, and painter, designed a mechanical aircraft that can vertically operate in the air [Prisacariu, 2017]. One of the first use of UAVs was for a military operation when Austrians attacked the city of Venice in 1849, they utilized 200

unmanned balloon platforms with the explosive mechanism to bomb the city [Udeanu et al., 2016]. One of the first demonstrations of unmanned aircraft platforms was the Kettering Bug which was designed in 1917 by Charles Kettering, an American inventor, and engineer, as part of the United States (U.S.) Army project for military operations [Keane and Carr, 2013]. While the World War II era saw the utilization of UAVs for warfare, late 1959 heralded the beginning of the modern UAV era, and during the Vietnam War period (1964-1972) UAVs were substantially used for combat reconnaissance [Cook, 2007]. UAVs were mostly utilized in military operations till the 1990s and after Persian Gulf War in 1991, NASA started to focus on the civil use of UAVs, and a comprehensive research endeavor has begun [Nonami, 2007]. Nowadays, UAVs are utilized for various civilian purposes including scientific and commercial. Also, big manufacturers in the industry such as Da-Jiang Innovations (DJI) are offering professional UAV systems with RGB or multispectral digital cameras and even LiDAR sensors at affordable prices for all consumers.

2.3.1. Classification of Optical UAVs

UAV systems are classified according to their weight, wing type, operational capacity, and purpose of utilization. Different organizations have published their standards regarding this topic. For example, according to UAV Systems Instructions published by the Directorate General of Civil Aviation (DGCA) [2016] which is the regulatory organization for aviation in Turkey, UAV systems are classified into four different groups corresponding to their maximum takeoff weight:

- UAV0: UAVs with maximum takeoff weights between 500 grams (gr) (including) – 4 kilograms (kg),
- UAV1: UAVs with maximum takeoff weights between 4 kg (including) – 25 kg,
- UAV2: UAVs with maximum takeoff weights between 25 kg (including) – 150 kg,
- UAV3: UAVs with a maximum takeoff weight of more than 150 kg (including).

Another classification standard is published by U.S. Army (USA) [2015] in USA Roadmap for UAS 2010-2035. In this classification effort, UAS diversified according

to their maximum takeoff weights, normal operating altitudes, and maximum airspeeds (Table 2.1).

Table 2.1: Classification of UAS according to USA Roadmap for UAS 2010-2035.

UAS Class	Max Takeoff Weight (kg)	Normal Operating Altitude (m)	Airspeed (knots)
Group 1	< approx. 9	< approx. 365 m above ground level (AGL)	< 100
Group 2	approx. 9,5-25	< approx. 1070 m AGL	< 250
Group 3	< approx. 600 kg	< approx. 5490 m mean sea level (MSL)	< 250
Group 4	> approx. 600 kg	< approx. 5490 m MSL	Any Airspeed
Group 5	> approx. 600 kg	> approx. 5490 m MSL	Any Airspeed

Apart from the USA various military organizations publish their own standards about UAS classification. In Minimum Training Requirements for UAS Operators and Pilots which is published by North Atlantic Treaty Organization Standardization Office (NSO) [2019], UAS classified according to their weight class, category, normal operating altitude, and normal mission radius (Table 2.2).

Table 2.2: Classification of UAS according to NSO standards in Minimum Training Requirements for UAS Operators and Pilots.

UAS Class	Category	Normal Operating Altitude (m)	Normal Mission Radius (km)
Class III (> 600 kg)	Strike/Combat	Up to 19812 m MSL	Unlimited/Beyond Line-of-Sight (BLOS)
	High-Altitude, Long Endurance (HALE)	Up to 19812 m MSL	Unlimited/BLOS
	Medium-Altitude, Long Endurance (MALE)	Up to 13716 m MSL	Unlimited/BLOS
Class II (150 – 600 kg)	Tactical	Up to approx. 5486 m AGL	200/Line-of-Sight (LOS)
Class I (< 150 kg)	Small (> 15 kg)	Up to 1524 m AGL	50/LOS
	Mini (< 15 kg)	Up to approx. 914 m AGL	Up to 25 km/LOS
	Micro (< 66 J)	Up to approx. 61 m AGL	Up to 5/LOS

In Table 2.2, micro UAS with a maximum energy state of < 66 J is considered micro UAS and they are not classified or regulated due to their inability to cause any significant harm to human life or property. UAVs are also classified based on their wing types and rotor numbers besides maximum takeoff weight or operational capacity. By their wing types, UAVs are divided into four main classes including:

- Multi-rotor UAVs: These are the most conventional form of UAVs with different rotor designs existing in the industry. In multi-rotor UAVs several rotors are implemented in the UAV platform for vertical lift-off and flight operation,
- Fixed-wing UAVs: In this type of UAV, wings are fixed and motionless, also a landing runway area is generally required in these systems, or they are thrown by hand or a mechanism for lift-off,
- Single-rotor UAVs: These are helicopter-type UAVs that vertically lift off and fly using a single rotor attached to the platform,
- Vertical take-off and landing (VTOL) fixed-wing UAVs: These UAVs are a mixture of multi-rotor UAVs and fixed-wing UAVs while including the advantages and capabilities of both systems.

Based on the number of rotors UAVs are divided into six including monocopter, duocopter, tricopter, quadcopter, hexacopter, and octocopter (Figure 2.11).

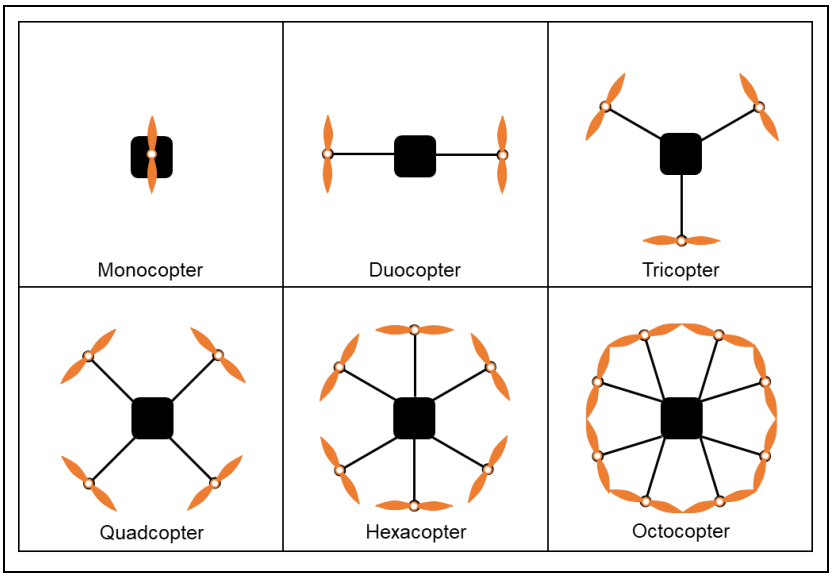

Figure 2.11: UAVs categorized by their rotor numbers.

2.3.2. Legislation

With the growing use of UAVs for various civil purposes in both scientific and commercial areas, several privacy issues, data protection, and ethical problems become imminent [Finn et al., 2014]. Also, due to the increasing complexity and operational capability of UAV systems, these issues become larger affecting a bigger part of society. Because of these concerns, numerous organizations across the globe create regulatory materials and publish their standards about UAVs. However, the present legal framework for UAV regulation raises an obstacle opposing the way of scientific research and technological advancements [Stöcker et al., 2017]. For example, in Turkey UAV laws are regulated by DGCA which published UAV Systems Instructions in 2016. In the first part of UAV Systems Instructions, some clauses regarding the aim and scope are given.

- Purpose – Article 1(1): This Instruction has been prepared to determine the procedures and principles regarding the import, sale, registration, and inscription of civilian UAV systems which will be operated or be utilized in Turkish Airspace, airworthiness maintenance, air traffic services, UAV operations, and qualifications required of people who will use UAV systems.
- Scope – Article 2(1): This Instruction covers the UAVs that will fly in the Turkish Airspace, the relevant systems, real and legal persons who will import, sell, operate or use them, the personnel to be assigned in this context, the UAV team, and the air traffic services to be provided during the use of the airspace.
- Article 2(2): The following UAVs and their systems are out of the scope of this Instruction:

Government unmanned aerial vehicles,

  - UAVs and systems used only in closed areas,
  - Unmanned balloons and systems attached to the ground or any platform,
  - UAVs with a maximum take-off weight of less than 500 gr.

In the second part, principles about classification, imported technical compliance, mandatory equipment, airworthiness, special flight permit, maintenance, and repair are presented.

- Classification – Article 5(1): UAVs are classified according to their maximum take-off weight into four different weight categories including UAV0, UAV1, UAV2 and UAV3.
- Article 5(2): In the test flights to be made within the scope of research and development (R&D) studies, the applicant informs the DGCA about the scope of the test flights, the coordinates of the region to be flown, the altitude, the third-party liability insurance and the pilot information suitable for the relevant category, then guarantees the correctness of given information and obtains permission for the region to be flown.
- Mandatory equipment – Article 7(1): Technical equipment, system elements, and payload components of UAVs classified in the UAV0 class are determined by the preference of the UAV operator/owner/pilot or manufacturer.
- Article 7(2): The UAVs in the UAV1 class must be equipped with at least the following technical features, equipment, and system components:
  - Emergency landing or termination of flight ability in case the command and control data link are interrupted,
  - Continuous monitoring of battery power/fuel level,
  - Strobe lamp,
  - Automatic flight recording system at the UAV or ground control station.
- Article 7(3): For the UAV2 class UAVs, in addition to the equipment essential for the UAV1 class, the following equipment, and the characteristics should be included in the system:
  - Lighting lamps instead of strobe lamps,
  - Redundant navigation system or redundant flight control system or computer,
  - Redundant command and control data link,
  - Suitable communication systems that will enable communication with the air traffic unit if necessary,
- Article 7(4): In addition to the equipment required for the UAV2 class, the following system components must be included in the UAVs classified in the UAV3 class:
  - Mode-S transponder,

  - Detect and avoid systems similar to The Traffic Alert and Collision Avoidance System (TCAS) and Automatic Dependent Surveillance-Broadcast (ADS-B).
- Article 7(5): The UAV, which is classified in the UAV0 class intended to be flown for commercial purposes, must be equipped with at least the technical features, equipment, and system components of the UAV1 class.

In the third part of the Instruction, procedures and principles of the UAV and pilot registration process are explained. Also, requirements for becoming a UAV pilot and mandatory steps to be carried out to register as a pilot are given.

- UAV registration procedures – Article 11(1): The registrations of the UAV0 and UAV1 category systems will be carried out through the "Registration System" created electronically by the DGCA.
- Article 11(2): (Amended: Dated 12/06/2017 and number 52217814-010.07/E.385):
  - Each UAV manufactured in our country is registered in the "Registration System" on the same day by its manufacturer,
  - The information of each UAV sold by the importer company, together with the information of the purchaser, is recorded in the "Registration System" on the same day by the responsible managers of the selling company,
  - The UAV brought from abroad individually or taken over in the country is registered in the "Registration System" within three days at the latest.
- Article 11(3): For UAV0/UAV1 category UAVs, the following information is filled in the Registration System:
  - Manufacturer, brand, model, and serial number of both UAV and its systems,
  - The place and date of manufacture of the UAV and its systems,
  - Maximum take-off weight of the UAV,
  - Name, Turkish Republic (TR) Identity Number/Tax Number, address, and contact information of the owner/operator of the UAV and its systems,
  - Archived criminal record of both owner and pilot of the UAV and its systems,

  - A notarized and certified undertaking by their legal representatives that they accept the legal and criminal responsibilities that may arise in the future for those under the age of 18.
- Article 11(4): The person/enterprise/pilot who owns the commercially utilized UAV0/UAV1 and its systems keeps the following information ready in the file he/she will create, preserves it for a minimum of three years, and submits it during the inspections to be made by public institutions:
  - Registration/ID number obtained from the DGCA,
  - All information about the aircraft,
  - Flight records.
- Article 11(5): The owner/operator/pilot of the UAV0/UAV1 and its systems is responsible for affixing the label to be created by the "Registration System" on the UAV and its systems, or writing the given label code on the UAV system indelibly.
- Pilot license classification and requirements – Article 14(1): Among those who will be issued a UAV pilot license in all classes an archive-registered criminal record is required (even if the periods specified in the 53rd article of the Turkish Penal Code dated 26/9/2004 and numbered 5237 have passed; even if he/she has been imprisoned for one year or more for an intentional crime or he /she has been pardoned), to prove that he/she has not been convicted of crimes against the security of the state, crimes against the constitutional order and the functioning of this order, crimes against sexual immunity, crimes against private life and the confidential sphere of life, manufacture, and trade of drugs or stimulants, theft, fraud, forgery, laundering or smuggling of property values arising from crime, kidnapping or detention of transportation vehicles, or opposition to the Anti-Terror Law numbered 3713 and dated 12/04/1991, Anti-Smuggling Law numbered 5607 and dated 21/03/2007, The Law on Control of Narcotic Substances numbered 2313 and dated 12/06/1933, and the Law on Firearms and Knives and Other Tools numbered 6136 and dated 10/7/1953, or being in action with terrorist organizations, helping these organizations, using public facilities and resources to support these organizations, making propaganda for these organizations.

- Article 14(2): No license is issued by the DGCA for those who will fly UAV0 and UAV1. However, the persons in question have to register in the internet-based Registration System by entering the following information and documents:
  - TR Identity Number,
  - Name-surname and residence information,
  - Phone, e-mail, etc. contact information,
  - A notarized and certified letter of undertaking by their legal representatives that they accept the legal and criminal responsibilities that may arise in the future for those under the age of 18.
- Article 14(3): UAV0 class pilots must be at least 12 years old and UAV1 class pilots must be at least 15 years old.
- Article 14(4): There is no training obligation for those who will fly with UAV0 and UAV1 category aircraft for hobby or sportive purposes. Pilots who will use UAV0 and UAV1 category aircraft for commercial purposes should take the relevant courses in the appendix of this Instruction as 12 hours for UAV0 and 36 hours for UAV1. The authorized training institution gives those who complete this training a UAV Commercial Pilot Certificate. This certificate is sent to the DGCA in the application for UAV pilot registration.
- Article 14(6): Legal and penal liability for damages caused to third parties by UAV pilots under the age of 18 belongs to the legal representative.
- Article 14(7): In addition to the above-mentioned ones, a medical report showing that they can be a class B driver is requested from UAV0 and UAV1 category pilots who will make commercial flights.
- UAV pilot responsibilities – Article 15(1): The UAV pilot is responsible for the safe conduct of the flight and the fulfillment of the administrative, financial and technical rules related to the flight.
- Article 15(2): The UAV pilot is responsible for the use of payloads within the legal framework.
- Article 15(3): The UAV pilot adds the signed commitment that he/she accepts all responsibility for the flight to the flight permit application file.

In the fourth part of the Instruction information about flight permits, no-fly zones, and flight conditions are given and principles about these concepts are explained.

- Flight clearance requirements – Article 17(1): For UAV0 and UAV1 class UAVs:
  - For flights to be performed for sportive and amateur purposes other than commercial activities, the flight permit is automatically issued by the registration system from the DGCA in the free (green) zones, provided that the rules specified in this Instruction are followed. For these classes, it is forbidden to fly in places and times prohibited by the highest local authority,
  - For all kinds of flights to be made in regions subject to special permission (red), an application is made with the UAV Flight Permit Request Form on the official website of the DGCA, together with the justification, ten business days in advance,
  - For all kinds of flights to be made in regions subject to permission, the application is made five working days in advance via the official website created by the DGCA,
  - Applications made via the web-based system created by DGCA for flights below 400 ft (approx. 122 m) in regions subject to permission are reviewed by the relevant civil authorities and, if deemed appropriate, a NOTAM which is a warning broadcast to airmen prepared in a special format to inform flight operations officers in a timely manner about the existence of any aviation service, convenience, management or danger, conditions or any change in them, is published regarding the request. The said permission may be canceled by the relevant civil/military institutions and the DGCA, if necessary,
  - In the case of obtaining a flight permit, it is obligatory for the operator/pilot/individual to comply with the provisions of the Turkish Aeronautical Information Publication (AIP) and other specified rules,
  - Free (green) zones established for the purpose of carrying out flights with UAVs are announced in the en-route (ENR) 5.5 section of the Turkish AIP. The up-to-dateness of the said fields is checked by the DGCA every year,

  - For all kinds of flights to be made above 400 ft in regions subject to permission, an application is made with the UAV Flight Permit Request Form on the official website of the DGCA with its justification, at least ten working days in advance,
- Regions subject to special permission – Article 18(1): It is forbidden to fly in any class of UAV without risk analysis and permission from the DGCA in the areas defined as the special permission (red) zone:
  - Regardless of altitude, at airports, in the field closer than 5 nautical miles (NM) (9 km) from the edge of the nearest runway,
  - Regardless of altitude, in the area with a radius of 5 NM, including navigation aids, heliport, helipad, air park, sea/landing, and take-off areas, etc. published on the official website of the DGCA,
  - For flights over 400 ft,
  - In the "Forbidden, Restricted and Dangerous Areas" in the ENR 5.1 section of the Turkish AIP,
  - Around critical structures, facilities, and assets such as military buildings and facilities, prisons, fuel depots, and stations, weapon/cartridge factories, and warehouses,
  - In the fields declared with NOTAM.
- Article 18(2): In unforeseen emergencies such as search, rescue, and disaster, Flight Permit can be granted exceptionally, provided that the necessary coordination is ensured with the DGCA.
- Flight conditions and space requirements – Article 19(1): In case of flights to be carried out in free (green) zones with UAV0 and UAV1 class UAVs at places and times not prohibited by the highest local authority:
  - Only in cases where visual meteorological conditions are met, flights can be carried out between the hours of sunrise and sunset and in clear weather with a view of at least 2 km,
  - The UAV must be in the pilot's field of view, not exceeding 500 m horizontally,
  - AGL of 400 ft is not exceeded,
  - Flight must be carried out at least 50 m away from people and structures,

In the fifth and final part of the UAV Systems Instructions, legal requirements and sanctions for unauthorized operations are explained.

- Unauthorized operation – Article 26(1): For operations that require permission from the DGCA, in cases where UAV flights are carried out without obtaining permission and operations are carried out outside the airspaces determined by the authorizations, the penalty provisions in the 5th part of the Turkish Civil Aviation Law numbered 2920 are applied to the relevant person and enterprise.

For the aforementioned cases, some legal sanctions and relevant penalty provisions according to the 5th part of the Civil Aviation Law (dated 14/10/1983 and numbered 2920) Article 144 including:

- The responsible operators and managers of companies selling UAVs must duly keep the information of the vehicles sold and the identity information of the purchasers, and record the information about the UAVs with a maximum take-off weight of 500 g (including) in the registration system established by the DGCA on the same day,
- An administrative fine of ten thousand Turkish Liras is imposed on those who make false statements or enter false data during registration,
- Persons flying UAVs in violation of the rules determined by the Ministry of Transport, Maritime Affairs, and Communications or outside the areas determined by the civil authorities are subject to administrative fines from one thousand Turkish Liras to ten thousand Turkish Liras.
- Apart from those listed above, those who do not comply with the rules set by the DGCA regarding UAVs and the measures to be taken to regulate civil aviation within this scope are subject to an administrative fine from one thousand Turkish Liras to ten thousand Turkish Liras.
- Administrative fines to be applied to those flying UAVs outside the designated areas are applied by the local administrative authority, and other administrative fines are applied by the DGCA.

- The procedures and principles regarding the implementation of this article are regulated by the regulation issued jointly by the Ministry of Interior and the Ministry of Transport, Maritime Affairs, and Communications.

2.3.3. Instruments of Optical UAVs

Optical UAV systems are conventionally utilized in both civil and military applications. An optical UAV is a passive remote sensing system generally equipped with a digital camera with RGB, multispectral, or hyperspectral imaging ability. Apart from the optical sensor other electronic components for navigation, communication, and flight operation are integrated into the system. With the technological advancements and maturation of various technological branches, high-tech equipment is added to the components of modern UAV systems. In Figure 2.12 components of DJI Phantom 4 Pro V2.0, a consumer-grade RGB UAV system with an affordable price, are shown as an example [Web 1, 2021].

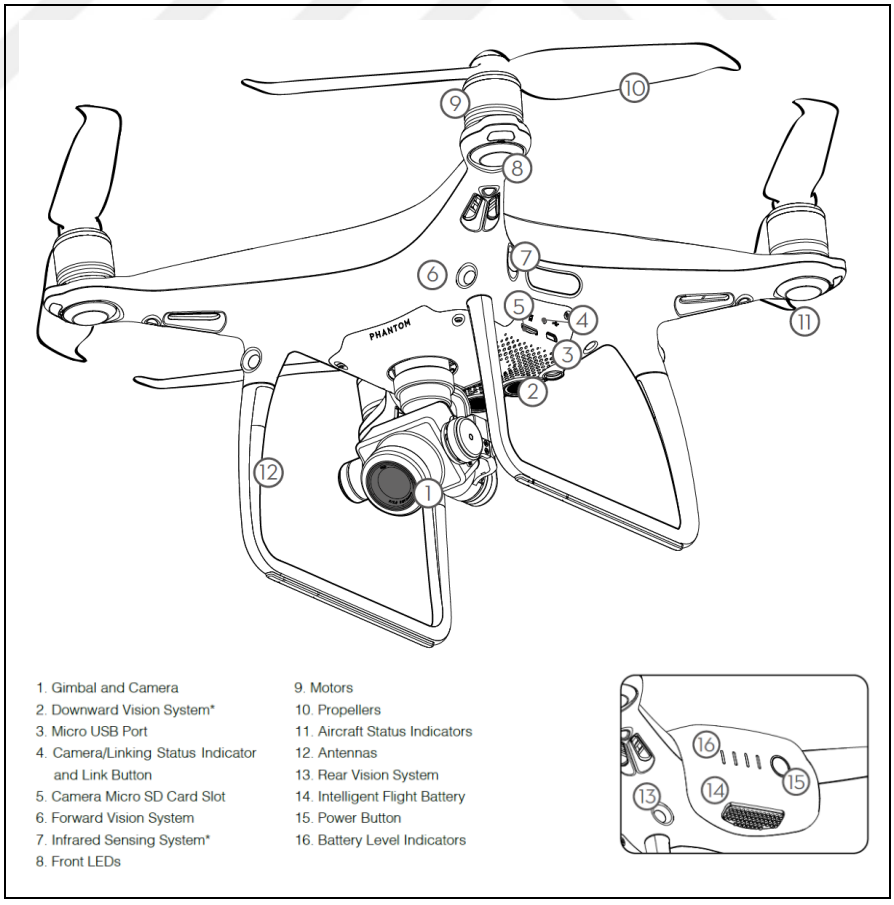

Figure 2.12: Components of DJI Phantom 4 Pro V2.0 UAV.

Apart from the main body of the UAV system a remote controller is utilized for flight operations and communication. Remote controller parts of DJI Phantom 4 Pro V2.0 and some of their functions are shown in Figure 2.13 [Web 1, 2021].

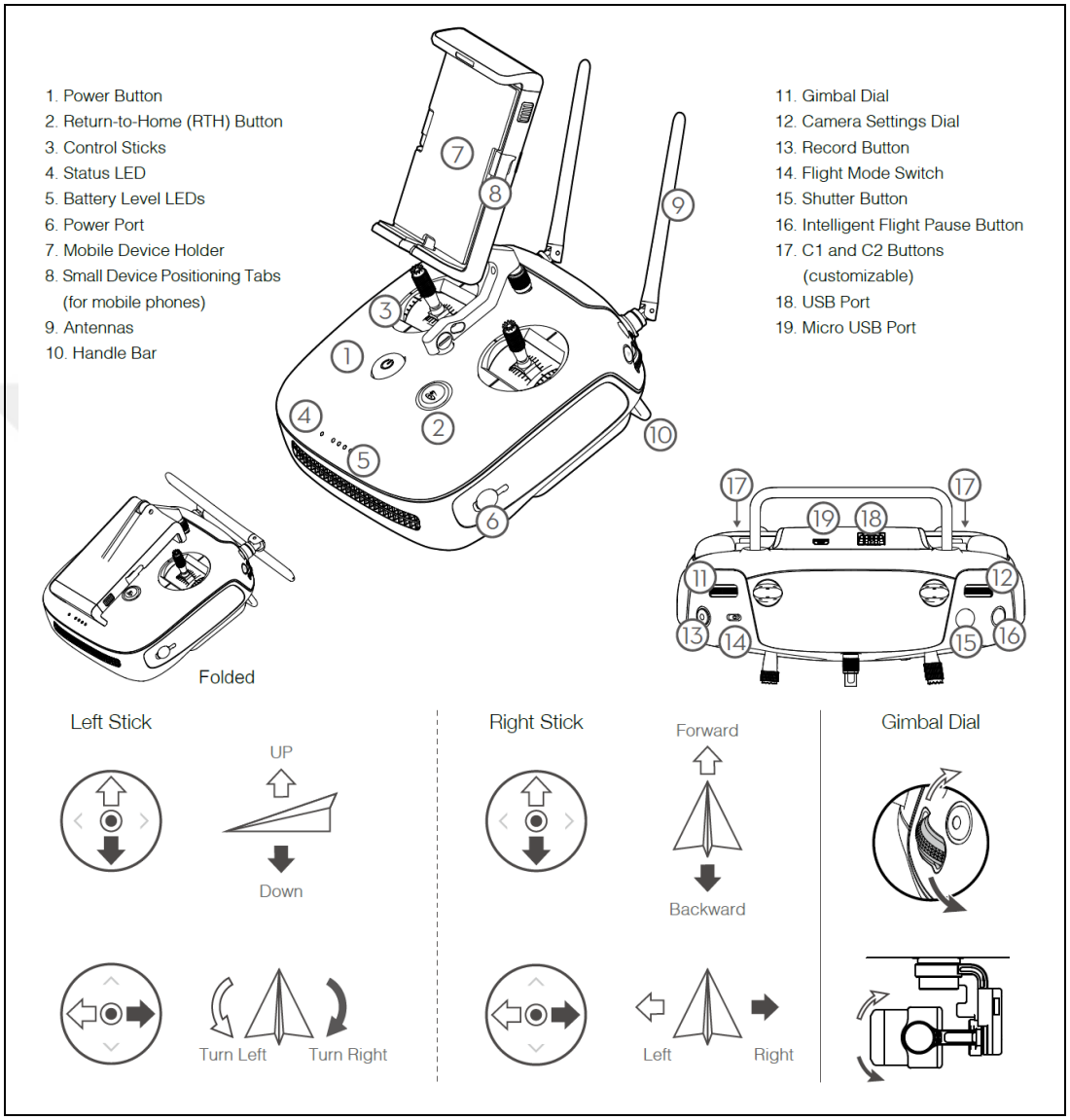

Figure 2.13: Remote controller structure of DJI Phantom 4 Pro V2.0 UAV.

The main components of a UAV system can be listed as a UAV motor, UAV propellers, UAV flight controller, GPS module, electronic speed controller (ESC), power port module, obstacle avoidance sensors, 3-axis gimbal, UAV camera, UAV battery, UAV antennas, downward ultrasonic obstacle avoidance sensor, flight light-emitting diode (LED), joysticks, main remote controller board, and main camera board [Web 2, 2022].

The properties and functions of these components can be described as:

- UAV motor: Quadcopter UAVs have four motors including two clockwise and two counterclockwise turning, for equalizing the force of turning generated by the rotation of propellers. This design is implemented due to Newton's third law of motion, for every action, there is an equal and opposite reaction.
- UAV propellers: For a quadcopter with two pairs of motors rotating in different directions, there are two pairs of propellers for each direction. Propellers generate upwards pushing force for UAVs by producing a pressure difference between the top and bottom of the airfoil surface.
- UAV flight controller: This is the control center of the UAV system which takes input signals from the remote controller, GPS module, obstacle avoidance sensors, and compass and processes these inputs for the ESC to command the motors.
- GPS module: This component operates based on the GNSS method for determining the position of the UAV system on earth. Another function of this element is maintaining stability during flight operations. Also, some advanced UAV systems contain GPS modules with RTK GNSS capability which can determine the precise position of the UAV instantaneously.
- ESC: This component acquires signals processed by the UAV flight controller to supervise the amount of power given to motors during the flight.
- Power port module: Controls the output of batteries and oversees the amount of power transferred to ESC and UAV flight controller.
- Obstacle avoidance sensors: Calculates the distance between the sensor and an obstacle by extracting depth from acquired sensor images, for collision avoidance.
- 3-axis gimbal: For holding the camera steady during the flight, the gimbal system compensates the motion in three different axes for camera stability.
- UAV camera: The imaging sensor utilized for the acquisition of incoming electromagnetic energy and storing the obtained energy as digital photos.
- UAV battery: Generally utilized UAV batteries are lithium polymer batteries with advanced features such as protection for overcharging, temperature data acquisition, and history of the charge cycle.

- UAV antennas: The transmission system is placed in the legs of the UAV for enabling transmission between the UAV and controller. Compass sensors are also placed in the legs for sending the direction of the UAV to the flight controller.
- Downward ultrasonic obstacle avoidance sensor: These sensors utilize sound waves to calculate the altitude of the UAV from the ground.
- Flight LED: These lights flash in different colors for showing the direction the UAV is facing.
- Joysticks: These are used for controlling the movements of the UAV during the flight and each joystick has a differentiating function for moving the UAV in various directions.
- Main remote controller board: This component acquires information about the location, altitude of the UAV, and view of the camera, and transfer received information to the flight controller.
- Main camera board: Receives and processes the information gathered from the digital camera and gimbal system to provide solid camera footage while also controlling the writing of acquired photos to a storage unit.

2.3.4. Optical UAV Utilization Areas

With their high-resolution data acquisition and ability to capture areas within short time intervals repeatedly UAV systems are increasingly used in numerous scientific research and commercial applications. The ability to integrate different sensors into the platform and changeable flight altitude are important factors in the high preferability of UAVs in the scientific community. Some of the utilization areas of optical UAVs can be listed as:

- Smart agriculture or farming applications: Classification of crops [Kwak and Park, 2019], estimation of crop growth parameters based on UAV data [Tao et al., 2020], biomass estimation of croplands [Bending et al., 2014], estimation of crop water stress [Park et al., 2017], disease detection in croplands [Kerkech et al., 2020], crop pest monitoring [Yue et al., 2012], detection of leaf nitrogen concentration and prediction of plant height [Osco et al., 2020], determination

of nitrogen application and yield prediction of crops [Maresma et al., 2016], calculation of leaf area index (LAI) for crops [Comba et al., 2020], chlorophyll content estimation for different crop coverages [Qiao et al., 2022], evapotranspiration estimation in croplands [Niu et al., 2020], vegetation index estimation for high-throughput phenotyping of crops [Khan et al., 2018], evaluating the influence of soil heterogeneity on crop development and crop yield estimation [Falco et al., 2021].

- Forestry applications: Producing forest inventories [Wallace et al., 2012], growth estimation for individual trees [Guerra-Hernández et al., 2017], estimation of forest LAI [Zhang et al., 2019], individual tree detection and classification [Nevalainen et al., 2017], disease detection in forests [Qin et al., 2021], quantification of forest gaps [Getzin et al., 2014], monitoring of post-fire recovery process in forest areas [Aicardi et al., 2016b], monitoring of forest degradation [Ghulam, 2014], measurement of leaf angle distribution in forest canopies [McNeil et al., 2016].
- Disaster management: Forest fire monitoring [Casbeer et al., 2005], monitoring and documentation of landslides [Lindner et al., 2016], damage degree evaluation of areas affected by earthquakes [Chen et al., 2016], flood hazard mapping [Annis et al., 2020], hurricane-induced damage assessment [Greenwood et al., 2020], land subsidence monitoring in mining areas [Ignjatović Stupar et al., 2020], volcanic plume measurements [Mori et al., 2016], oil spill detection on the sea surface [Jiao et al., 2019].
- Apart from these applications UAVs are utilized in cultural heritage documentation [Jo and Hong, 2019], structural health monitoring [Kang and Cha, 2018], 3D modeling of buildings and other structures [Skondras et al., 2022], BIM studies [Barrile et al., 2019], monitoring of glacier dynamics [Immerzeel et al., 2014], monitoring of coastal dune changes [Laporte-Fauret et al., 2019], monitoring of gas pipelines [Hausamann et al., 2005], crack detection for bridge inspection applications [Lei et al., 2018], AR applications [Zhang et al., 2019], VR integration studies [Sefercik et al., 2021a], LULC studies [Sefercik et al., 2021b], archeological research [Lin et al., 2011], distress detection in road structure [Tan and Li, 2019], methane emission monitoring in landfill areas [Fjelsted et al., 2019], air pollution measurement [Villa et al.,

2016], water pollution monitoring [Zang et al., 2012], quantitative soil salinity estimation in areas with different vegetation density [Hu et al., 2019].

2.3.5. Fundamentals of Optical UAVs

Optical UAVs with the ability to capture high-resolution aerial photos periodically between specific time intervals are utilized in numerous applications and studies including smart agriculture applications, forestry applications, disaster detection, and monitoring, cultural heritage documentation, structural health monitoring, 3D modeling of buildings and objects, BIM studies, monitoring of glacier dynamics and coastal dune changes, inspection of engineering structures, AR and VR integration studies, LULC studies, archeological research, methane emission monitoring in landfill areas, air and water pollution monitoring, soil salinity estimation.

The smart agriculture or farming concept involves the utilization of technologies and systems such as the Internet of Things (IoT), AI, and remote sensing including satellite systems and UAVs to modernize conventional agricultural techniques for increasing crop yield in a sustainable and clean environment [Gondchawar and Kawitkar, 2016], [Bu and Wang, 2019]. Smart agriculture not only provides aid in compensating food requirements of the increasing population but also stands as a promising concept for situations like food shortages and establishing self-sufficient farms during the COVID-19 pandemic [Chamola et al., 2020], [Maddikunta et al., 2021].

In the scope of the smart agriculture concept UAVs are used in various applications. For classifying crops in a cabbage cultivation area Kwak and Park [2019] utilized a UAV with a multispectral camera that has green, red, and NIR bands. Acquiring multi-temporal UAV images over the area they investigated the effect of texture features extracted from gray-level co-occurrence matrix (GLCM) on the classification of UAV data using machine learning classification methods random forest and support vector machines (SVMs). When results are examined, classification accuracy was significantly improved when texture features were employed especially using only one UAV orthomosaic where time-series UAV data is not available or difficult to obtain.

Assessment of crop growth is another important application in smart agriculture where various growth indicators are calculated and analyzed. Tao et al. [2020] employed hyperspectral UAV data for estimating AGB and LAI indicators over a winter wheat cropland for assessment of crop growth. When results are examined, the estimation of AGB and LAI is boosted while combining vegetation indices and red-edge parameters obtained using hyperspectral UAV data.

The efficiency of water use and crop productivity can be improved by monitoring the water status of crops, therefore, Park et al. [2017] utilized a UAV with a high-resolution thermal camera for mapping plant water stress over orchards of nectarine and peach. By interpreting the thermal UAV data, a water stress index is calculated for detecting crop water stress, especially at the early stages.

Disease detection in croplands can improve the efficiency and mobility of crop management, especially in pesticide application so Kerkech et al. [2020] applied the deep learning segmentation method on thermal and RGB UAV imagery for detecting Mildew disease in a vineyard. Using a fully convolutional neural network approach for the classification of infected crops accuracy of more than %92 at the grape-vine level and %87 at the leaf level was achieved.

Due to the effect of leaf nitrogen concentration on plant height growth, Osco et al. [2020] utilized multispectral UAV imagery for estimating the nitrogen condition and height of maize plants. Utilizing the vegetation indices such as NDVI, normalized difference red-edge index (NDRE), soil adjusted vegetation index (SAVI), and green normalized difference vegetation index (GNDVI) with supervised machine learning approaches including random forest leaf nitrogen concentration and plant height were predicted for maize cropland.

Maresma et al. [2016] utilized multispectral UAV data, several vegetation indices, the Soil Plant Analysis Development (SPAD) chlorophyll meter, a tool for measuring chlorophyll concentrations, and crop height for estimating crop yield for maize plants. When results are investigated it has been found that for predicting final grain yield during nitrogen treatment, the wide dynamic range vegetation index (WDRVI) demonstrated better results than other used vegetation indices.

Estimation of evapotranspiration is a crucial task for water management in agricultural applications thus Hoffmann et al. [2016] used thermal UAV images to estimate evapotranspiration over a barley field. Utilizing thermal UAV data land surface temperature was calculated and used for evapotranspiration estimation.

Forestry is defined as the science, art, and practice dealing with the creation, conservation, and management of forests and resources associated with forests for human welfare and in a sustainable approach to meet wanted objectives, requirements, and values [Web 8, 2013]. UAV systems emerged as an alternative to conventional aerial photography and satellite imagery for forestry applications with their advantages including low operational cost, flexibility in spatial and temporal resolution control, and data acquisition in high intensity [Tang and Shao, 2015].

UAV systems are used in different forestry applications and studies. For producing forest inventories Wallace et al. [2012] utilized a UAV with a LiDAR sensor and a video camera. Combining LiDAR data with obtained video data 3D point clouds were generated showing the location of trees, tree heights, and crown width for producing the forest inventory of the investigated area.

Guerra-Hernández et al. [2017] utilized UAV data obtained between different periods to individually estimate trees' growth in an area. Using the acquired multi-temporal UAV aerial photos positions of trees were determined and parameters including individual tree height, diameter, biomass, as well as changes in these parameters are estimated for the entire study.

Zhang et al. [2019] utilized UAV aerial photos to estimate forest LAI, a crucial forest structural parameter in the photosynthesis process. Using the canopy cover and forest height information obtained from UAV data forest LAI was estimated and results indicated that in the LAI estimation process canopy cover and forest height were complementary.

To investigate the performance of hyperspectral UAV data in the detection of individual trees and classification of tree species Nevalainen et al. [2017] utilized RGB and hyperspectral UAV aerial photos captured over boreal forest areas. Using the 3D point clouds generated utilizing high resolution RGB aerial photos, and spectral features obtained from hyperspectral UAV data individual trees were identified and various tree species were classified.

Identification of pine wood nematode disease is vital for prevention and control so Qin et al. [2021] utilized multispectral UAV data for identifying pine nematode. Using a deep learning approach for the detection of pine nematode mean overall accuracy of 79% was achieved and as a result, it is indicated that multispectral UAV data has great potential for finding previously undiscovered pine nematode disease areas.

Forest gaps that can be formed by human interference or natural phenomenon can be of different sizes including large (>100 m2) to small (<10 m2) and detection of very small gaps is difficult utilizing conventional aerial or satellite data, therefore, Getzin et al. [2014] utilized UAV data for detecting small gaps which generally have an area of <5 m2 in both managed and unmanaged forest areas.

One of the primary natural phenomena influencing forest ecosystems is wildfires so it is crucial to examine possible effects on post-fire regeneration dynamics and to take preventive measures. For this purpose, Aicardi et al. [2016b] conducted a change detection analysis using DSMs obtained from ALS and UAV data acquired in different periods.

Natural disasters pose a great threat to humanity and they often push human survival instinct to its limits by causing heavy, and regularly unpredictable loss of human life, and inflicting extensive property and infrastructure damage [Erdelj and Natalizio, 2016]. UAVs equipped with various instruments present many opportunities in disaster management and high-resolution UAV data can be utilized in producing hazard maps, generating comprehensive surface models, detailed building renderings, extensive elevation models, and other features of disaster regions [Adams and Friedland, 2011].

Forest fires inflict heavy damage to properties and the environment every year and access to the disaster region is not possible in a typical forest fire scenario due to impassable terrain features so Casbeer et al. [2005] proposed a system consisting of small UAVs for monitoring the situation. A UAV path planning algorithm is developed for the utilization of infrared data collected in real-time by UAVs to monitor forest fire in an area.

Landslides, caused primarily after an extensive rainfall or after snow melting in spring, can cause extreme damage to properties and infrastructure, thus monitoring landslide events is of utmost importance for taking preventive steps and mitigating harmful effects. Therefore, Lindner et al. [2016] utilized a UAV for inspecting the landslide event periodically, and using the UAV data a DSM was generated for tracking fissures, obtaining velocity, flow direction, and mass balances.

Earthquakes, which are one of the most catastrophic natural disasters occurring in millions worldwide every year, cause extreme damage to buildings, infrastructure, loss of life, and injury [Dong and Shan, 2013]. For earthquake-induced damage degree evaluation, Chen et al. [2016] inspected five targets including the building, the road,

the vegetation, the riverway, the mountain, and the vegetation by applying the SVM classification algorithm to UAV data and a damage degree evaluation index was obtained for assessing damage intensity.

Remote sensing is an efficient tool for flood hazard simulations and it also enables forecasting and mitigating inundations in primary rivers around the globe. For testing the performance of high-resolution UAV data in flood hazard mapping, Annis et al. [2020] compared the DEM produced using UAV aerial photos with a benchmark LiDAR DEM, and the results show that UAV-derived DEM could be a suitable alternative to LiDAR DEMs for flood hazard mapping in small basins.

Apart from fields of smart agriculture or farming, forestry, and disaster management UAVs are utilized in various applications. Cultural heritage documentation for systematic management against deformation in cultural heritage sites is an example application where UAVs are utilized. For producing the 3D model of a cultural heritage site Jo and Hong [2019] applied terrestrial laser scanning and UAV photogrammetry techniques.

Due to the high cost of installing and maintaining sensors in conventional structural health monitoring deep learning-based crack detection applications are used with UAV data. For conducting a structural health monitoring study Kang and Cha [2018] applied a deep learning approach to UAV data for detecting cracks in concrete surfaces.

The inspection and detection of the potential source areas for rockfall on rock cliffs by conducting susceptibility analysis based on remote sensing are of utmost importance in rockfall hazard management. Therefore, for rock mass recognition and superimposing related rock discontinuities and susceptibility of rockfall onto the actual slopes Zhang et al. [2019] applied the AR mapping approach to UAV data.

VR technology is a powerful tool for visualizing geospatial data and the generation of 3D real-like mesh models from images. For creating a 3D VR tour application for a university campus area Sefercik et al. [2021a] integrated high-quality 3D textured mesh models, generated utilizing high-resolution UAV aerial photos, into the Unity game engine.

2.4. Virtual and Augmented Reality

VR and AR concepts are becoming more familiar in the scientific community and also the industry. With the developments in computer and electronics technology, these concepts are increasingly applied in many areas including both commercial and scientific. The idea of realizing the physical reality inside another environment including a virtual domain, or combining the concept of virtuality with reality fascinated humanity since the early stages of computer graphics development. Computer graphics can be defined as the science and art of visual communication through a display component of a computer and its devices for interaction, and generally, the visual part of this communication is carried out in the direction of computer-to-human, with the human-to-computer direction is guided via instruments such as a mouse, keyboard, game controller device, joystick, or an overlay with touch-sensitive feature [Hughes et al., 2013]. Some utilization areas and purposes of the computer graphics are user interface visualization, interactive plotting and production of graph materials in fields of business, science, and technology, representation of geographical elements in cartography, diagnostic and surgical planning in medicine area, and computer-aided design (CAD), multimedia systems, producing simulations and animations for entertainment and visualization in the field of science [Foley et al., 1993]. In addition, advancements in game engine technology further expand the potential and applicability of both VR and AR in various fields. A game engine can be defined as the framework which conceals the low-level details of different functions or processes including graphics, physics, input detection, audio playback and control, scripting, AI, networking, and core utilities that lays the foundations of the video game, by utilizing consisting of a group of various utilities and interfaces [Sherrod, 2007]. As the number of free 3D graphics-based game engines such as Unity, Unreal Engine, CryEngine, Godot, Armory, Source Engine, and Amazon Lumberyard grow, greater opportunities appear for AR and VR applications. Apart from the game engine component, 3D models are another important factor in AR and VR application development. The quality and complexity of the 3D model affect the visual capability, immersive ability, and operating performance of the applications. While the higher quality 3D models are better for visualization, the increased size of polygon and vertex data can also mean an increased workload for the application. The optical UAV

technique is an efficient tool for producing realistic and high-quality 3D mesh models. Different objects including buildings, roads, trees, vegetation, etc., can be captured and modeled utilizing aerial UAV photos.

2.4.1. Virtual Reality Concept

As presented by Sutherland [1965], the ultimate computer display, would be a room or a controlled environment within which the computer system can supervise and manipulate the existence of matter to a limit that even a chair visualized in this room would be realistic enough to sit in as if there is a real chair in front of the user. Today, computer systems have not reached that point but a remarkable development has been made in computer graphics including 3D realistic applications which provide users the opportunity to look into a virtual copy of the physical reality. VR can be defined as an advanced human-computer interface that offers participants to interact with the simulation of a realistic environment [Latta and Oberg, 1994]. A VR computer hardware consists minimally of a head-mounted display that has sensors to monitor the change of position between head movements in a 3D coordinate system, a data glove for tracking the hand and finger movement to locate the position of the glove in space, and finally a tracking device [Helsel, 1992]. The foundation of VR technology can be traced back to the late 1960s, with the development of the first head-mounted display by Sutherland [1968] and his team called the Sword of Damocles which can measure the position of the head via a sensor (Figure 2.14).

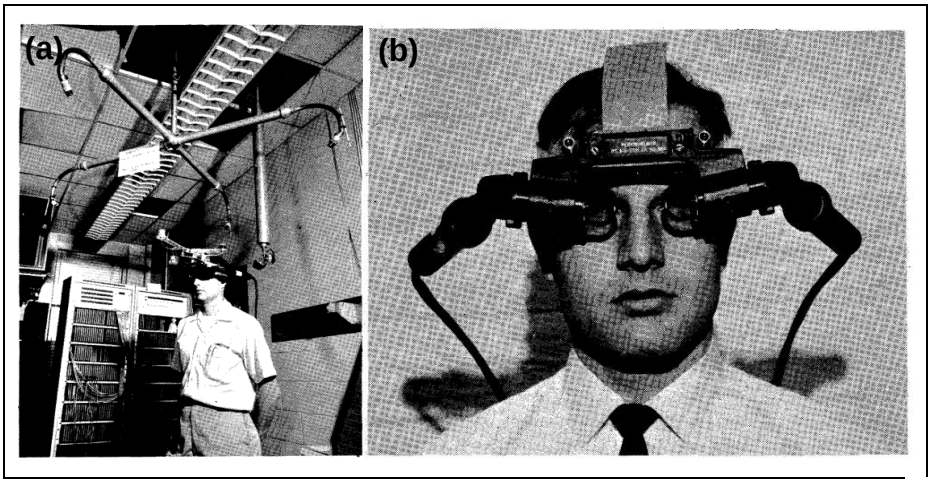

Figure 2.14: a) General view and b) close-up view of the Sword of Damocles the first head-mounted display.

Today, with advanced computer systems, modern head-mounted displays, and other movement tracking sensors VR has evolved much more advanced than when it first appeared. As suggested by the Cipresso et al. [2018] according to the level of immersion provided to the users, VR systems are classified into three categories:

- Non-immersive VR systems which utilized computer systems to realize the physical reality in a virtual domain, are the most basic form of this technology.
- Immersive VR systems offer users a whole simulated experience with the inclusion of different devices including a head-mounted display for providing a better view of the environment via positional changes of the head, alongside the audio and haptic sensory output hardware.
- Semi-immersive VR systems including Fish Tank VR are classified between non-immersive and immersive systems. Fish Tank VR system operates based on 3D viewing of a stereo image scene on a computer display utilizing a perspective projection linked to track the head movement of the user [Ware et al., 1993].

Visualization of an environment and rendering of 3D objects in a VR system is carried out based on two main techniques including the geometry-based method where the virtual environment is generated by producing 3D models of objects in an area of interest, and the image-based method, where the artificial domain is realized by generating panoramas for each set of photos captured within a specific viewpoint [Huang et al., 1998]. Both techniques have advantages and disadvantages according to their features [Ong and Nee, 2004]. The advantages of the image-based rendering method are:

- Offering an easy way for constructing a high-quality virtual environment with realistic and immersive effects,
- Regardless of the modeled real-world area the complexity of the produced virtual environment is consistent,
- Because of the relatively low size of the data demanded in this method, real-time interactivity is efficient.

However, as Ong and Nee [2004] pointed out, due to a lack of interactivity in the image-based rendering method, an immersive environment cannot be provided although the quality of the generated virtual environment can be very high. Compared to the image-based approach geometry-based one offers an immersive experience by providing the ability for users to interact with the virtual environment but the relatively large size of the data can constrain the performance of the VR application. VR technology is utilized in various applications including producing 3D virtual tours for various attraction sites [Zhu and Fan, 2016], visualization of cultural heritage in the virtual environment [Gaitatzes et al., 2001], archeological exhibition research [Bruno et al., 2010], creation of a virtual classroom for the educational purpose [Liou and Chang, 2018], producing an educational and training tool for medicinal procedures [Izard et al., 2018], forensic examination of injuries [Koller et al., 2019], adjunctive treatment of burn pain in adults during physical therapy [Hoffman et al., 2000], exposure therapy for anxiety disorders [Powers and Emmelkamp, 2008], producing an immersive greenhouse for precision agriculture training [Carruth et al., 2020], and producing a 3D VR tour application for a university campus [Sefercik et al., 2021a].

2.4.2. Augmented Reality Concept

AR is a variation of VR that enables users to view the real world with virtual objects superimposed upon or fused with the physical reality rather than completely immersing the user inside a virtual atmosphere [Azuma, 1997]. While VR technology simulates a virtual environment resembling the real world, AR systems add virtual elements into the real world by augmenting physical reality with computer graphics. The emergence of the AR term has been attributed to Tom Caudell who coined the term in 1990 to characterize a display device that combined virtual elements with reality [Green et al., 2017]. The combination of computer graphics and the real world can be multisensory and might contain the augmentation of an image with virtual graphics, the audio detection, and amplification, or the utilization of haptic feedback to elevate the sense of touch [Reinhart and Patron, 2003]. An AR application can be in two different forms the marker-based AR application where the digital camera must perceive a distinct visual cue to display the corresponding information or markerless AR application which utilizes the spatial data including mobile phone GPS and

compass, or image recognition technique, where the camera input data is compared against a bundle of imagery for detecting the matching one [Johnson et al., 2010]. AR systems should have properties such as the combination of real and virtual elements in a realistic environment, interactive and real-time operation, and alignment of real and virtual components with each other [Azuma et al., 2001]. As described by Milgram and Kishino [1994] mixed reality (MR) is a branch of VR-related technology that involves the combination of real and virtual environments as represented in the idea of the virtuality continuum which establishes a link between AR and augmented virtuality (AV) (Figure 2.15).

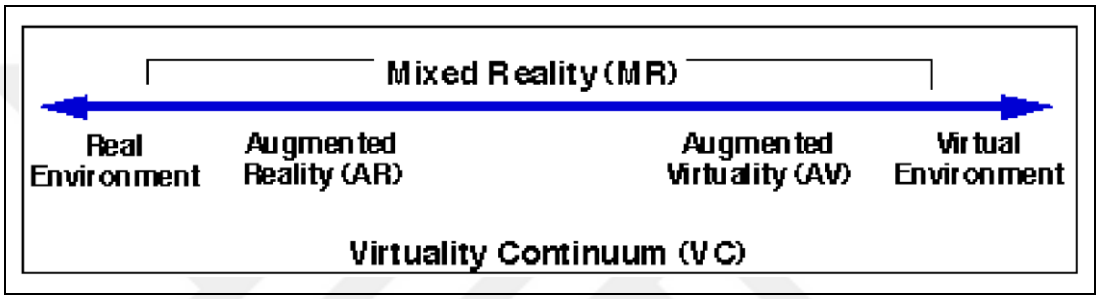

Figure 2.15: The virtuality continuum.

Utilization fields of AR technology can be described as architecture and urban planning [Cirulis and Brigmanis, 2013], cultural heritage visualization [Vlahakis et al., 2001], development of an AR-based teaching system [Freitas and Campos, 2008], assisting and improving manufacturing processes [Ong et al., 2008], designing a computer-aided surgery system [Birkfellner et al., 2002], assisting patients in rehabilitation exercises for physical therapy [Sousa et al., 2016], precision agriculture applications [Huuskonen and Oksanen, 2018], assisting forensic investigation [Streefkerk et al., 2013].

2.4.3. Integration of UAV Data and Virtual Reality

VR technology is increasingly utilized in the integration of 3D mesh models for the visualization of geospatial data in an artificial environment. Moreover, for producing immersive VR applications to offer users a more realistic experience it is essential to produce high-quality real-like 3D mesh models with texture. High-resolution UAV data is a prominent source for producing high-quality 3D textured

mesh models. Integration of produced 3D mesh models into a game engine for creating a VR application is a familiar concept in the scientific literature. Different tools and methods are utilized in the integration of UAV-derived 3D meshes into the virtual environment.

For creating a VR application to remotely monitor the structural health of historical buildings Bacco et al. [2020] utilized UAV data for producing realistic 3D textured mesh models and a wireless sensor network for detecting structural damages. Produced 3D meshes were integrated into the Unity game engine with corresponding wireless sensor data for offering users an interactive interface for monitoring the actual status of the historical site.

To produce a photorealistic 3D textured mesh model of a cultural heritage site Püschel et al. [2008] utilized terrestrial photos and UAV aerial photos for covering building facades in high detail. After texture mapping of generated 3D mesh was carried out in Blender, open-source cross-platform software for modeling, animation, and rendering [Web 9, 2022], the 3D textured mesh model was exported in VR Modeling Language (VRML), a format for displaying 3D objects in a network-based artificial environment [Taubin et al., 1998], for providing users to view the 3D mesh in a virtual environment.

For generating a hyper-realistic 3D model of a university campus area which includes various structures Berrett et al. [2021] utilized UAV aerial photos and terrestrial photos. After 3D textured mesh models were generated they were integrated into Unreal Engine 4, a multi-platform game development software [Web 10, 2022], for creating an immersive 3D VR tour application.

3. STUDY AREA AND UTILIZED MATERIALS

In this part, the study area and utilized materials as both hardware such as UAV, GNSS receiver, polycarbonate GCPs, and software such as the photogrammetric evaluation software and game engine development platform are presented. Also, information about used materials and their specifications are given in this section for further information.

3.1. Study Area

The study area is the GTU Campus which is positioned on the western side of the Gebze district of Kocaeli, Turkey. The Campus is located between 40°48′08″-40°49′12″N and 29°20′42″-29°21′59″E and the total area is approx. 2.5 km^2. The topography in the area is relatively flat with the orthometric height in the area variating between 1-50 m. There are also different land cover classes in the area including forest, agricultural, built-up area, road and water bodies. Inside the Campus area, there are densely forested regions and dense vegetation, especially on the northern side which can issue a challenge for the optical UAV techniques due to the heavily covered forest understory. In addition, the location contains buildings and trees with differentiating heights and orientations resulting in a complex atmosphere that demands conducting flight operations at different heights for obtaining aerial photos. Also, the complexity of areas in the GTU Campus is differentiating so a proper UAV flight planning procedure is essential to be carried to determine the required level of detail while capturing each area. For example, when comparing the northern side with the southern side the vegetation cover is larger in the north while the southern part has a lower density of vegetation. When the distribution of buildings on the Campus is examined, it is seen that there are more administrative buildings in the northern part, while there are more faculty buildings in the southern part. In Figure 3.1 the UAV orhomosaic of the GTU Campus in the World Geodetic System 1984 (WGS84) datum and the geographic coordinate system is shown.

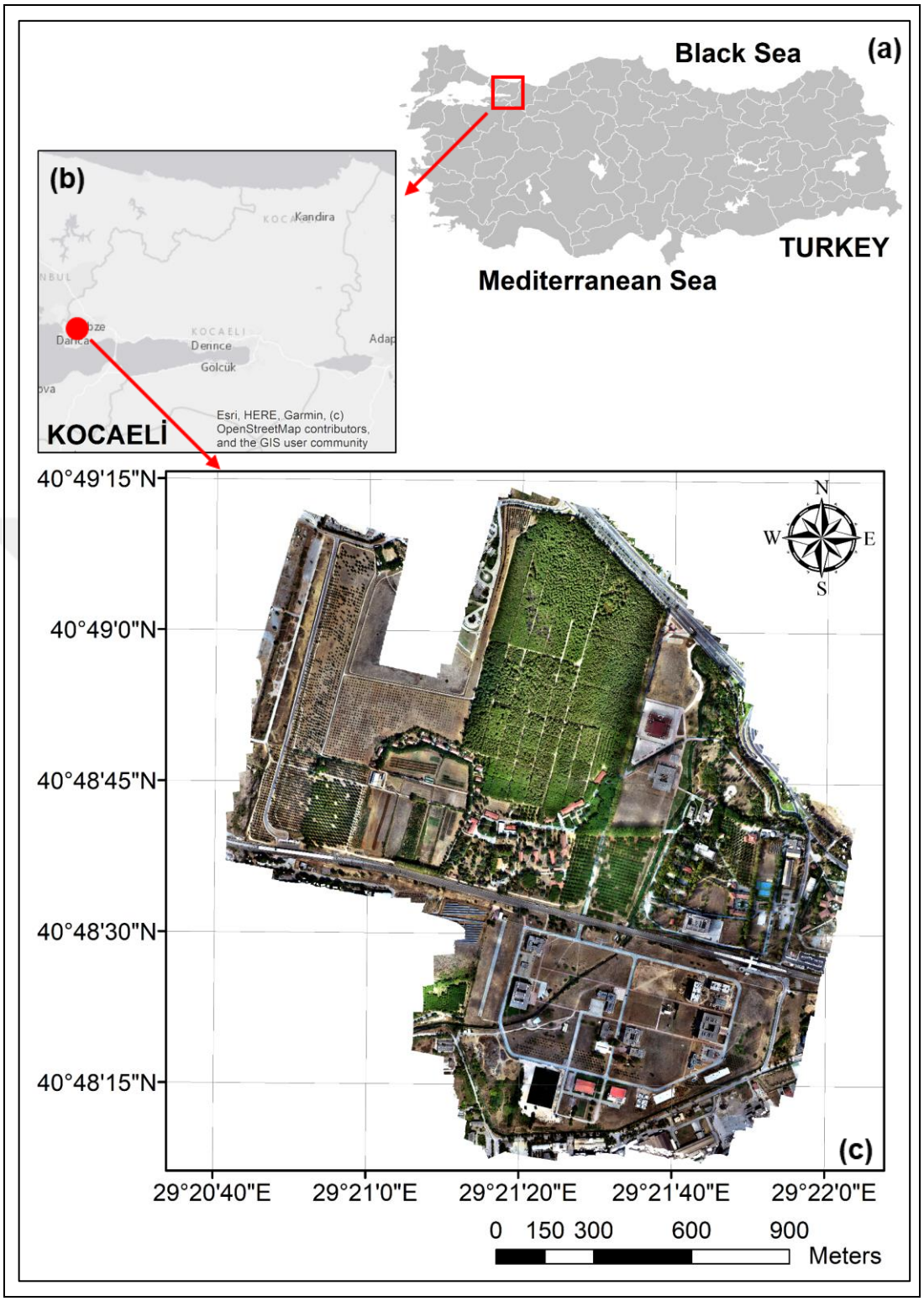

Figure 3.1: a) Location of Kocaeli province in Turkey. b) Position of GTU Campus in Kocaeli. c) The UAV orthomosaic of the study area in the WGS84 datum and geographic coordinate system.

3.2. Utilized Materials

Information about utilized DJI Phantom 4 Pro V2.0 UAV, CHC i80 GNSS receiver, and polycarbonate GCPs and their properties are given in this section. Moreover, specifications of utilized materials are also presented. All of the utilized equipment is available at GTU Geomatics Engineering Department's Advanced Remote Sensing Technology Laboratory (ARTLAB).

3.2.1. DJI Phantom 4 Pro V2.0 UAV

In UAV flights DJI Phantom 4 Pro V2.0 UAV with 20 megapixel Sony Exmor RGB digital camera was utilized. This utilized UAV is widely used in the industry for both scientific and commercial purposes due to its affordable price and performance. Also, the high effective pixel resolution of this UAV can be utilized for capturing high-resolution aerial photos of the building and other objects for generating high-quality 3D models. Specifications about the DJI Phantom 4 Pro V2.0 UAV is given in Table 3.1. In Figure 3.2 the utilized UAV is displayed with the remote controller which is used in flight operations.

Table 3.1: Specifications of DJI Phantom 4 Pro V2.0 UAV.

DJI Phantom 4 Pro V2.0 UAV	
Specification	**Value**
Camera	4K, HD, 1080p, 1”, effective pixel resolution 20 MP
Gimbal	3-axis (pitch, roll, yaw)
Image Size	3:2 Aspect Ratio: 5472×3648 4:3 Aspect Ratio: 4864×3648 16:9 Aspect Ratio: 5472×3078
Flight duration	Max. 30 minutes
Weight	1375 g
Speed	Max 20 m/s in S-mode
Wind speed resistance	Max. 10 m/s
Outdoor positioning module	GPS/GLONASS dual
Hover Accuracy Range	± 0.1 m V, ± 0.5 m H (Vision)

Figure 3.2: DJI Phantom 4 UAV and its remote controller.

3.2.2. CHC i80 GNSS Receiver

In terrestrial GNSS measurements to obtain 3D coordinates of established GCPs CHC i80 GNSS receiver with RTK GNSS ability is utilized. This GNSS receiver has the ability to operate as a rover while applying the network RTK GNSS technique to measure points. Due to this ability of the CHC i80 GNSS receiver without the requirement of a base GNSS station placed in the survey area point coordinates can be instantaneously measured with less labor and lower cost. In Figure 3.3 CHC i80 GNSS receiver is shown and its specifications are given in Table 3.2.

Figure 3.3: CHC i80 GNSS Receiver.

Table 3.2: Specifications of CHC i80 GNSS Receiver.

CHC i80 GNSS Receiver	
Specification	**Value**
GNSS technology	GPS, GLONASS, GALILEO, BeiDou, SBAS, NavIC
Operating system	Linux
Working modes	Static, VRS RTK, UHF RTK, all surveying modes
Internal Memory	32 GB
Positioning accuracy RTK	± 0.8 cm H, ± 1.5 cm V with initialization reliability >99.9%
Battery	Dual; Static up to 10 h, Cellular receive only up to 9h, UHF receive/transmit up to 6h
Network-RTK	Available

3.2.3. Polycarbonate Ground Control Point

For absolute orientation of acquired UAV aerial photos, polycarbonate GCPs were established and measured over the study area. These GCPs consist of two rectangle-shaped polycarbonate sheets combined to form a cross shape and each sheet has a length and width size of 100 x 25 cm. Also, the center of part of these sheets was painted black for increasing the contrast and thus making the center point of the GCP more visible.

Figure 3.4: A polycarbonate GCP consisting of two combined sheets.

3.3. Utilized Software

Information about used software for 3D textured meh model and orthomosaic generation, Agisoft Metashape Professional, and the software utilized in the creation of the 3D VR tour application, Unity game engine is presented in this part.

3.3.1. Agisoft Metashape Professional

For the generation of high-resolution 3D textured mesh models and UAV orthomosaic, Agisoft Metashape Professional version 1.7.0 which is a photogrammetric evaluation software was utilized. Agisoft Metashape aligns aerial photos or another form of imagery based on the SfM technique which offers the ability to reconstruct high-resolution 3D geometry by utilizing an array of overlapping photos acquired with a specific offset [Westoby et al., 2012]. The general workflow of the SfM method starts with the correspondence search stage which consists of feature extraction, matching, and geometric verification, and the later stage is the reconstruction which consists of initializing the model with two-view reconstruction, registration of new images, triangulation of scene points, outlier filtering, and utilizing bundle adjustment to refine the construction [Schonberger and Frahm, 2016]. The operating principle of the SfM technique is shown in Figure 3.5 [Web 3, 2022].

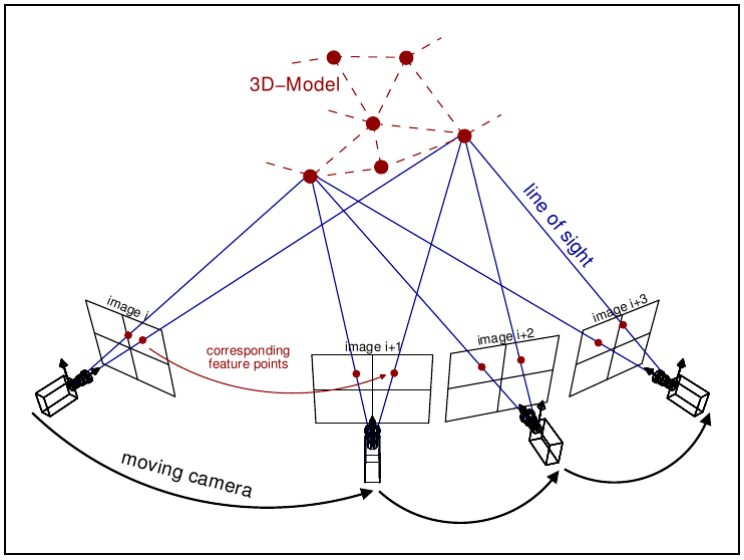

Figure 3.5: The SfM technique utilizes 2D overlapping images with offset to reconstruct 3D geometry.

In Figure 3.6 general workflow SfM technique with input images and output point cloud data is displayed [Schonberger and Frahm, 2016].

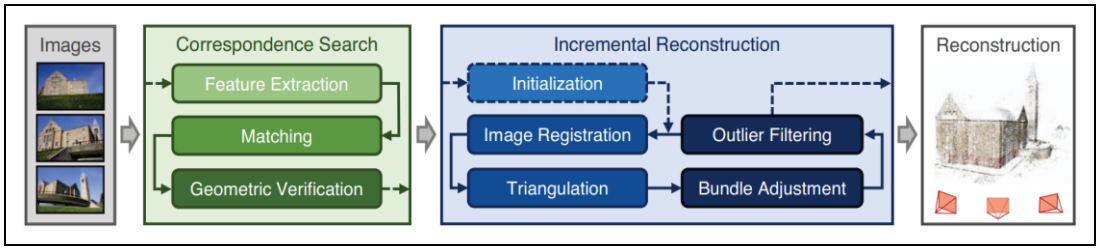

Figure 3.6: Workflow of the SfM technique with input as the image data and the output as the point cloud data.

SfM method uses 2D image data to produce 3D data in the form of the point cloud data which is a vector data type consisting of points with 3D coordinates and usually a color value. Produced point cloud data can then be used to generate 3D textured mesh models, DSMs, or orthomosaics.

3.3.2. Unity3D

Integration of produced 3D textured mesh models and creation of 3D VR tour application was carried out in Unity, otherwise known as Unity3D, which is a cross-platform game development platform utilized by a wide community due to free to use software and convenient user interface. The first version of Unity (1.0.0) which is described as a toolset utilized to build games and has the technological capability for executing the interactions, the audio, the physics, the graphics, and lastly the networking, was developed in June 2005 by David Helgason, Joachim Ante, and Nicholas Francis, and by 2008, the platform had become more prominent and sophisticated and utilized by a wider community [Web 4, 2013]. Unity supports mobile platforms including iOS, Android, desktop platforms including Windows, Mac, Linux, web platforms such as WebGL, console platforms such as PlayStation, Xbox, Nintendo Switch, Stadia, and VR platforms. The programming language Unity is based on C#, also called C-sharp, and all other languages that can be used in Unity are object-oriented [Web 5, 2022]. In Unity, 2D and 3D applications can be developed and with the help of the built-in physics engine, object-oriented projects can be carried out [Web 6, 2022]. The creation of a 3D VR tour creation for the GTU Campus was done

using the Unity game engine version 2021.2.7f1. In Figure 3.7 the user interface screen of the Unity game engine is displayed.

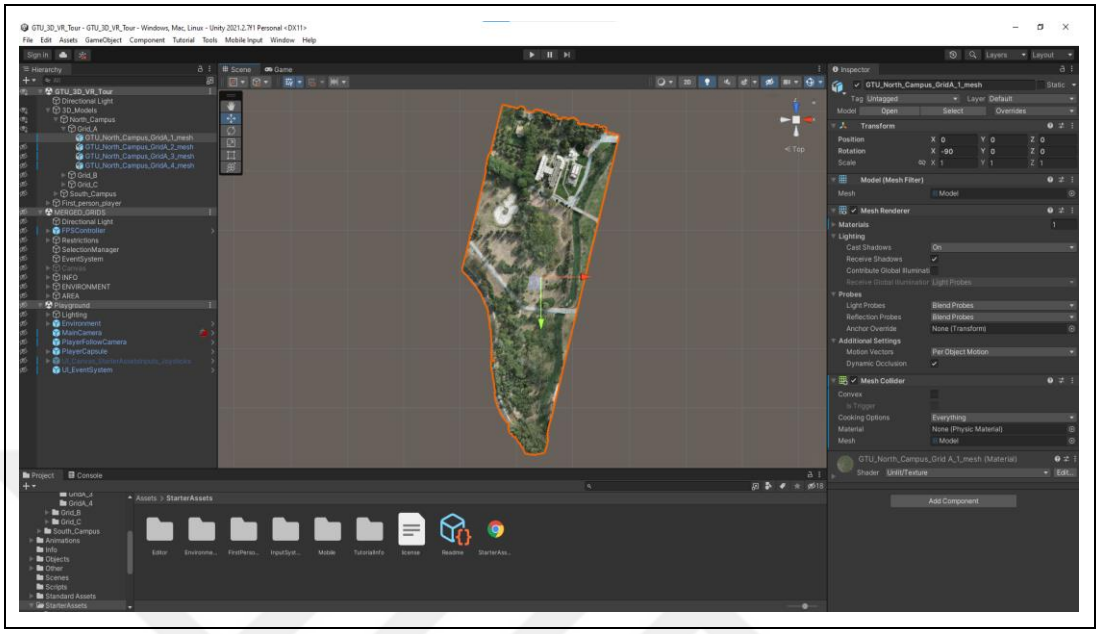

Figure 3.7: The user interface of the Unity game engine.

4. METHODOLOGY

The methodology of the thesis study consists of three main parts including optical UAV data acquisition, orthomosaic generation using optical UAV data in Agisoft Metashape Professional, and creation of 3D VR tour application in Unity game engine. The utilized methodology and corresponding software used in processes are shown in Figure 4.1.

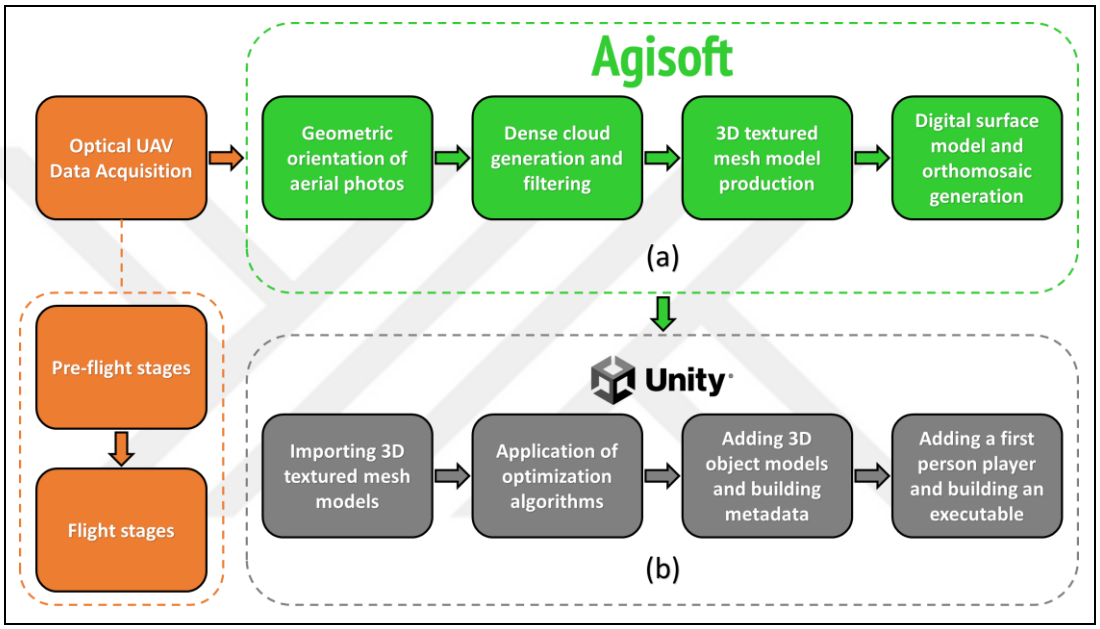

Figure 4.1: The methodology followed in this thesis study. a) Optical UAV data acquisition steps including pre-flight and flight stages. b) Orthomosaic generation steps using optical UAV in Agisoft Metashape Professional. c) 3D VR Tour Creation steps in Unity game engine.

4.1. Optical UAV Data Acquisition

The first part of the methodology is the optical UAV data acquisition which consists of pre-flight stages which cover UAV flight planning and terrestrial GNSS measurements both carried out before the UAV flights, and the later part flight stages consist of the preparation of UAV for flight operations and transfer of the captured aerial photos to the computer.

4.1.1. Pre-Flight Stages

Pre-flight stages or operations carried out before UAV flights are the determination of the study, preparation of UAV flight plans for covering the area with aerial photos, and establishment of GCPs according to prepared flight plans and terrestrial GNSS measurements. In Figure 4.2 the workflow applied in the pre-flight stages is represented.

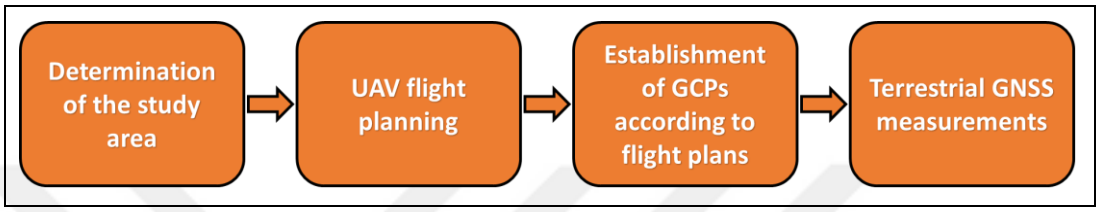

Figure 4.2: The methodology applied in the pre-flight stages.

After the study area was determined as the GTU Campus, for covering the whole area with the minimum number of aerial photos flight plans were prepared using Pix4Dcapture UAV flight planning software. The entire study area was covered with polygonal, bundle grid, and circular flights in both nadir and oblique camera orientation for acquiring buildings facades in detail and also capturing different views of objects which are not visible in nadir looking. Some of the prepared flight plans are displayed in Figure 4.3.

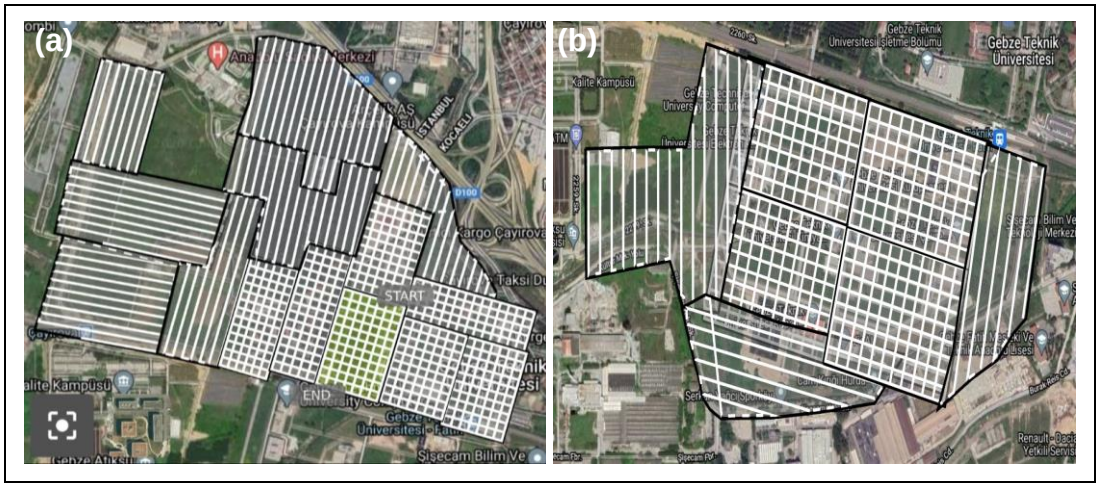

Figure 4.3: UAV flight plans with different flight modes prepared using the Pix4DCapture software for a) North Campus and b) South Campus.

Polygonal flights were generally preferred in forest and agricultural areas, while bundle-grid and circular flights were applied to capture built-up regions. For bundle-grid and circular flights, the camera view angle was selected as 70° (off-nadir 20°) while in polygonal flights nadir view was chosen. After, preparing the UAV flight plans 86 mobile GCPs were established over the study area and their coordinates are acquired by using the continuously operating reference stations (CORS) RTK GNSS technique. Minimum front and side overlap ratios were chosen as 80% and 60%, respectively. Moreover, the flight altitude was selected as 80 m for both polygonal and bundle grid flights and 30 m for circular flight orientation. The establishment of a GCP is shown in Figure 4.4.

Figure 4.4: The establishment of a GCP.

4.1.2. Flight Stages

After the pre-flight stages were accomplished the UAV batteries were prepared and a suitable Secure Digital (SD) card with a 32 gigabyte (GB) memory was selected as a storage unit for aerial photos. In addition, IMU and compass calibration processes were carried out using the DJI Ground Station (GS) Pro software before the flight for a proper flight operation. IMU and compass components of the UAV are affected by various parameters including electromagnetic areas in the environment so after conducting some flight operations a calibration process is essential to be carried out.

After the calibration process was done, according to prepared flight plans a total of 32 UAV flights were carried out, and 8333 aerial photos were captured with a ground sampling distance (GSD) of ≤2.2 cm. Finally, acquired aerial photos were transferred to a computer using the SD card. In Figure 4.5 workflow followed in the flight stages is given.

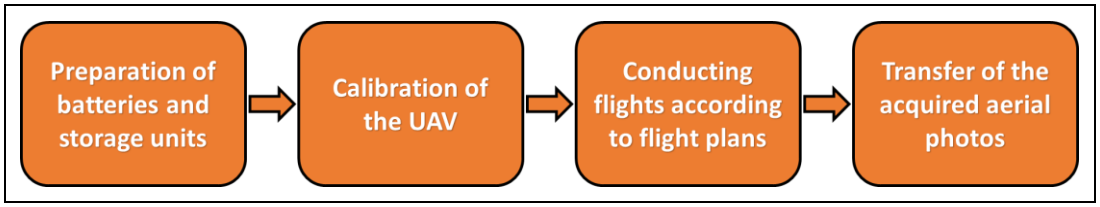

Figure 4.5: Workflow followed in the flight stages.

4.2. Orthomosaic Generation Using Optical UAV Data

3D textured mesh model and orthomosaic generation processes were carried out in Agisoft Metashape Professional software. The subsections of this process are the geometric orientation of aerial photos, dense cloud generation and filtering, 3D textured mesh model production, and generation of both DSM and orthomosaic.

4.2.1. Geometric Orientation Steps

Before the aerial photo orientation, the inner orientation of the utilized UAV camera was carried out automatically in Agisoft Metashape and the required parameters are obtained. Geometric orientation of aerial photos was conducted in two main parts the relative alignment of the aerial photos and absolute orientation using GCPs. Because the number of acquired aerial photos was higher than 2000, the chunk-based work necessity has arisen and a high-end HP Z4 G4 model workstation with Intel® Xeon® W-2133 CPU @ 3.60 GHz, NVIDIA Quadro P2000 GPU, and 64 GBs of RAM was utilized for processing the huge number of aerial photos. As mentioned before Agisoft Metashape operates based on the SfM method for orientation of aerial photos. So, captured aerial photos as shown in Figure 4.6 are matched and oriented according to their correlations using the SfM technique.

Figure 4.6: A set of aerial photos captured in circular flight mode for aerial photo orientation using the SfM method.

However, before the geometric orientation process was carried out a masking operation was applied to photos for eliminating the effect of noise in the orientation process which can be caused by background pixels especially apparent in photos captured in oblique viewing geometry during bundle-grid and circular flights. Moreover, by filtering the points with low correlation values the accuracy of orientation was increased. The masking process was carried out by selecting and then filtering the background pixels in the aerial photos (Figure 4.7).

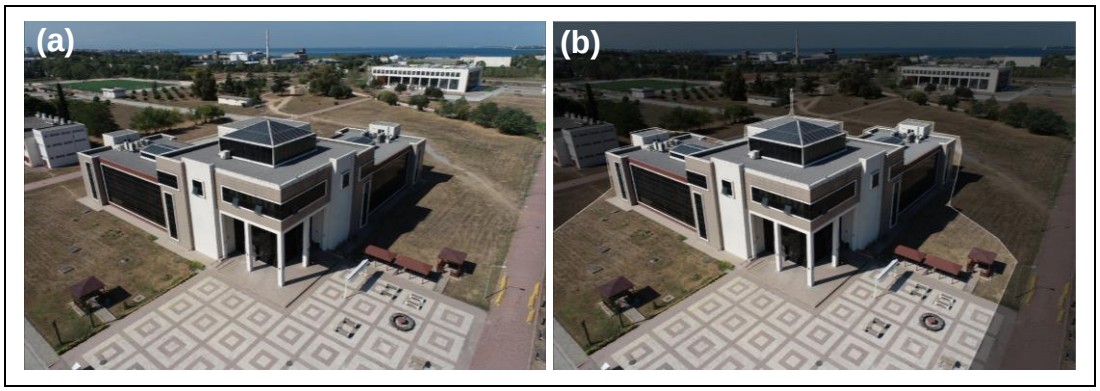

Figure 4.7: An aerial photo a) before and b) after the masking process.

After the masking process is completed, the relative alignment of aerial photos was carried out for each created chunk in Agisoft Metashape using the settings shown

in Figure 4.8, and sparsely point clouds with a total size of >73 million points were acquired.

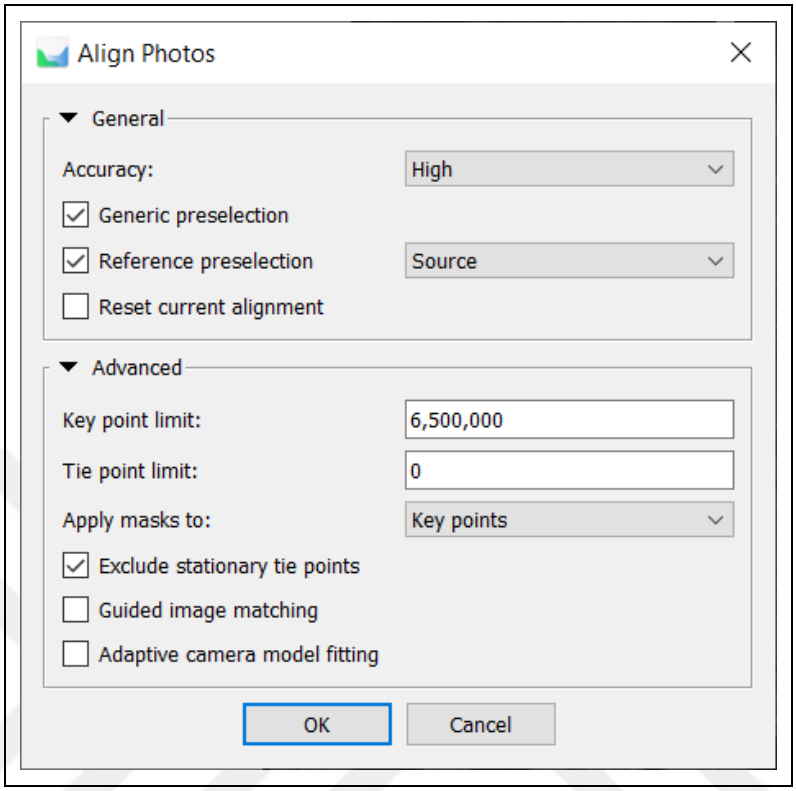

Figure 4.8: The settings utilized for relative orientation of aerial photos.

In Figure 4.8 utilized parameters in relative orientation are described as [Web 7, 2021]:

- Accuracy: Higher the accuracy setting more accurate estimations of camera positions can be obtained. Lower accuracy can be utilized to get rough estimates of camera positions but in a shorter period of time compared to higher accuracy settings. At the high accuracy, the software uses the original photo size, but at the medium and low accuracy settings, photo sizes are downscaled by a factor of 4 and 16, respectively.
- Generic preselection: Due to the large size of photos in some projects, the alignment process can take excessive time. So, the image pair preselection setting may quicken this process due to the selection of some image pairs for the matching process. By using a generic preselection option overlapping photo pairs are chosen by matching them utilizing a lower accuracy option.

- Reference preselection: Reference preselection setting can be carried out using three different options including source preselection which finds overlapping photo pairs based on the measured camera locations, estimated preselection which uses exterior orientation parameters calculated during the photo-alignment process, and sequential preselection which utilizes the sequence of aerial photos for determining correspondence between aerial photos.
- Reset current alignment: This option resets the geometry produced by the relative orientation process and deletes the produced sparse point cloud.
- Key point limit: This number indicates the number of maximum feature points on aerial photos to be utilized during relative orientation of aerial photos. Setting the value as zero provides Agisoft Metashape the ability to find the maximum number of key points possible.
- Tie point limit: This number shows the maximum number of matching points for every photo and selecting the value as zero removes the upper limit of matching points.
- Apply mask to: If the masking process was carried out before the relative orientation of aerial photos, this setting can be used to apply masks to key points or tie points for eliminating the filtered pixels from the process.
- Exclude stationary tie points: This setting enables excluding tie points that remain stationary on multiple photos and also helps in the elimination of false tie points.
- Guided image matching: This setting increases the key point number for every photo without a significant increase in processing time as if the value of the key point limit was increased manually before the process.
- Adaptive camera model fitting: Camera parameters are automatically selected to be utilized in adjustment based on their estimations of reliability.

Because the high accuracy settings were sufficient in producing a high-resolution 3D textured mesh model and orthomosaic generation, this option was selected as high. Other options apart from key point and tie point limits were selected as default. The key point limit was selected as 6,500,000 for using a large number of feature points and the tie point limit is determined as zero for allowing the software to use the maximum number of possible tie points in relative orientation. Also, masks

were applied to key points for eliminating the influence of background pixels. Absolute orientation was carried out by importing GCP coordinates and then selecting GCPs in corresponding aerial photos (Figure 4.9).

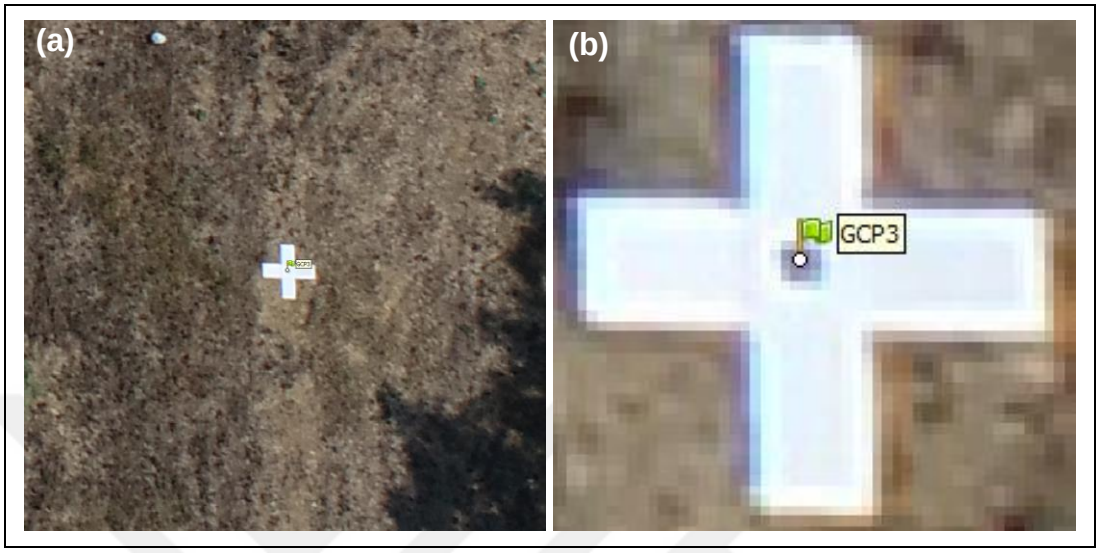

Figure 4.9: a) Zoomed-out and b) zoomed-in views of a GCP, utilized in the absolute orientation process.

The geometric accuracy of this process was calculated according to GCP selection as root mean square error (RMSE) in both cm and pixels as shown in Equation 4.1 [Web 7, 2021].

$$RMSE = \sqrt{\frac{\sum_{i=1}^{n}\left(\hat{X}_i - X_i\right)^2 + \left(\hat{Y}_i - Y_i\right)^2 + \left(\hat{Z}_i - Z_i\right)^2}{n}} \tag{4.1}$$

Finally, the geometric accuracy was obtained as ± 2 cm (~0.9 pixels) according to RMSE calculated in Equation 4.1 where for each camera position of i, $\hat{X}i$, $\hat{Y}i$, $\hat{Z}i$ display estimated values and Xi, Yi, Zi represent actual input values.

4.2.2. Dense Point Cloud Generation

After the geometric orientation and acquirement of sparse point clouds, the dense point cloud generation process was carried out. The sparse point cloud displays the topography and objects in the form of 3D vector data but in low resolution. A more

real-like and prominent characterization is essential for producing high-quality 3D mesh models. So, by using depth map data, constructed by extracting depth information from overlapping aerial photos, dense point clouds with a total size of approx. 1,5 billion points were generated. The settings utilized in dense point cloud generation are shown in Figure 4.10.

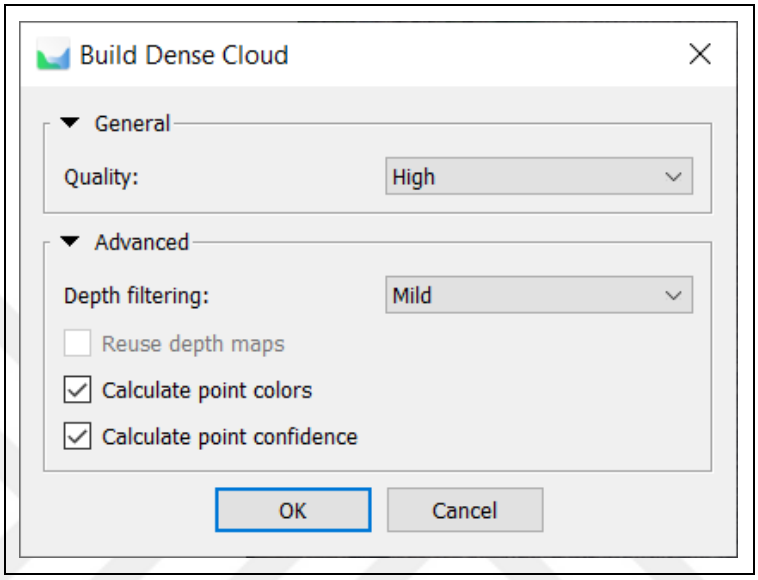

Figure 4.10: The settings utilized in the dense point cloud generation.

In Figure 4.10 utilized parameters in dense point cloud generation are explained as [Web 7, 2021]:

- Quality: Determines the preferred quality of the generated depth maps and a higher quality setting can be utilized to acquire a more detailed geometry with higher accuracy but in increased processing time.
- Depth filtering: Due to some elements including noisy and roughly focused photos, there can be some outliers among generated points. The depth filtering setting offers four modes including mild, aggressive, moderate, and disabled which differentiate from each other according to the aggressiveness of the filtering algorithm.
- Calculate point colors and point confidence: These settings can be used to calculate the color values of points and the number of depth maps used to generate each point in a dense cloud, respectively.

In this process, quality was chosen as high for acquiring a better 3D geometry and depth filtering mode was chosen mild as default. Even utilizing a workstation with a relatively high RAM capacity of 64 GB, generation of dense point clouds took 5-12 hours per chunk. Also, because of distortions in viewing geometry and the influence of forest, vegetation, and water body land cover classes, some noisy parts emerged in dense point clouds. The noise data in dense point clouds were filtered by selecting and classifying noisy points. In Figure 4.11 general views of generated dense point cloud before and after the filtering process are displayed.

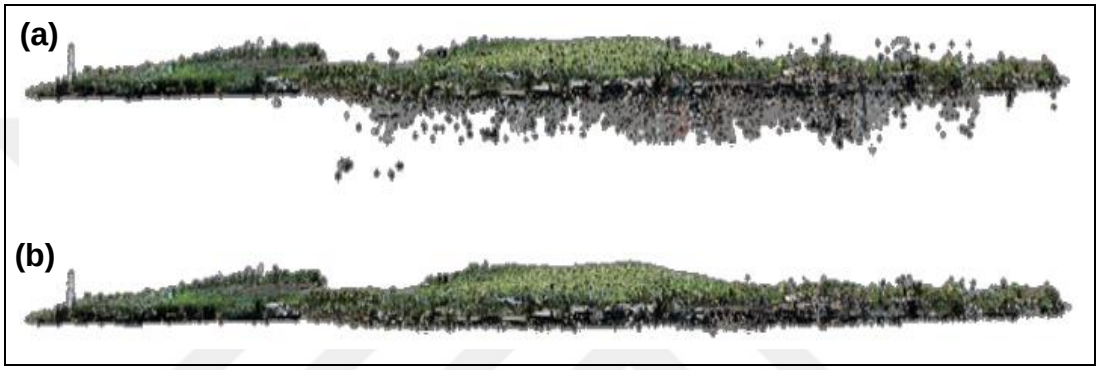

Figure 4.11: a) Unfiltered dense point cloud data. b) Filtered dense point cloud data.

4.2.3. 3D Mesh Model Generation

Point cloud data display topography and objects above it in non-continuous point-based vector format, for models to be more real-like and detailed, it is crucial to generate 3D meshes using the dense cloud data. Moreover, by visualizing objects in continuous data format without any gaps a more immersive 3D VR tour experience can be provided. Therefore, utilizing filtered dense point cloud 3D mesh models of the GTU Campus were generated and interpolation was applied to fill holes that may emerge due to the low number of points in certain parts. In addition, because of the number of predicted faces or triangles and thus excessive size of the polygonal data, a mesh decimation operation was carried out and the total number of faces in generated 3D mesh models was reduced to approx. 430 million. However, there were faces with rough geometry and isolated polygons in generated 3D mesh models so a manual mesh filtering process was carried out. In Figure 4.12 the utilized settings in the mesh model generation are displayed.

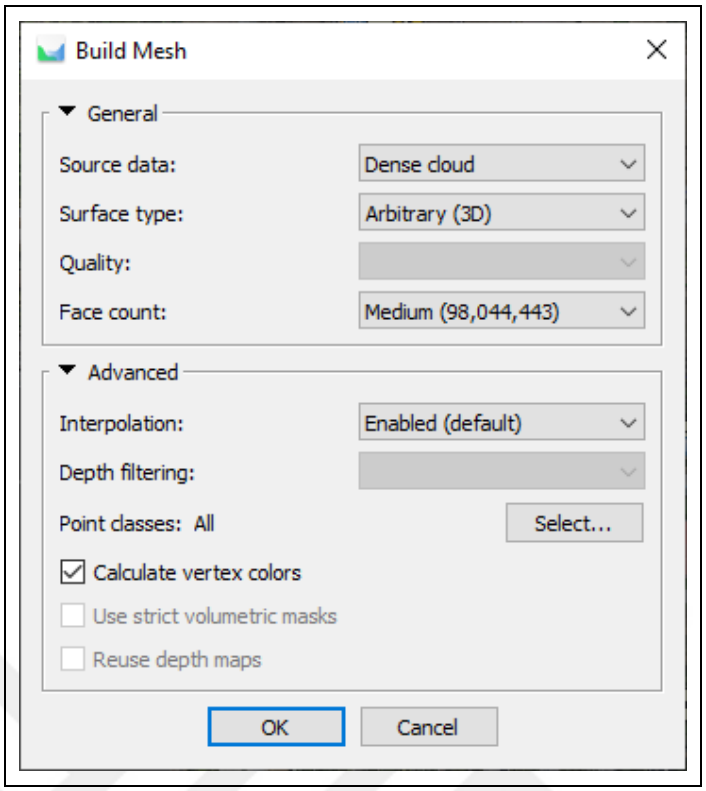

Figure 4.12: The settings utilized in the mesh model generation process.

In Figure 4.12 utilized parameters in mesh model generation are explained as [Web 7, 2021]:

- Source data: This setting selects the source data such as sparse cloud, dense cloud, and depth maps utilized for the mesh generation process.
- Surface type: Surface type can be selected as arbitrary (3D) which can be used for modeling different kinds of objects, especially the closed ones such as statues and buildings, and height field (2.5D) which is optimized for modeling surfaces with a planar orientation such as terrains or base reliefs.
- Quality: Designates the desired reconstruction quality of the depth maps if they are chosen as the source type.
- Face count: Determines the upper limit for the number of polygons in the generated 3D mesh model by applying mesh decimation. According to the level of detail preferred in the final mesh three options high, medium, and low can be selected.
- Interpolation: Specifies if an interpolation process will be carried out during 3D mesh generation. If the disabled option is selected only areas that appear in the

dense point cloud are reconstructed, while the enabled (default) option is used to apply interpolation for covering holes and gaps. Also, the extrapolated option can be utilized to generate a holeless mesh with extrapolated geometry.

During the 3D mesh generation process source type was selected as the dense point cloud for generating models with complex and detailed geometry. Also, face count was selected as the medium for reducing the number of faces in mesh models and interpolation was enabled for covering holes and gaps that may appear in the meshes.

4.2.4. 3D Textured Mesh Model Generation

For acquiring 3D mesh models much like their physical counterparts, it is necessary to apply texture graphics with high resolution to them. In Agisoft Metashape, 3D mesh models are displayed in the shaded mode which visualizes objects with colors however in lower resolution compared to a texture graphic. In Figure 4.13 the used settings for 3D textured mesh model generation are shown.

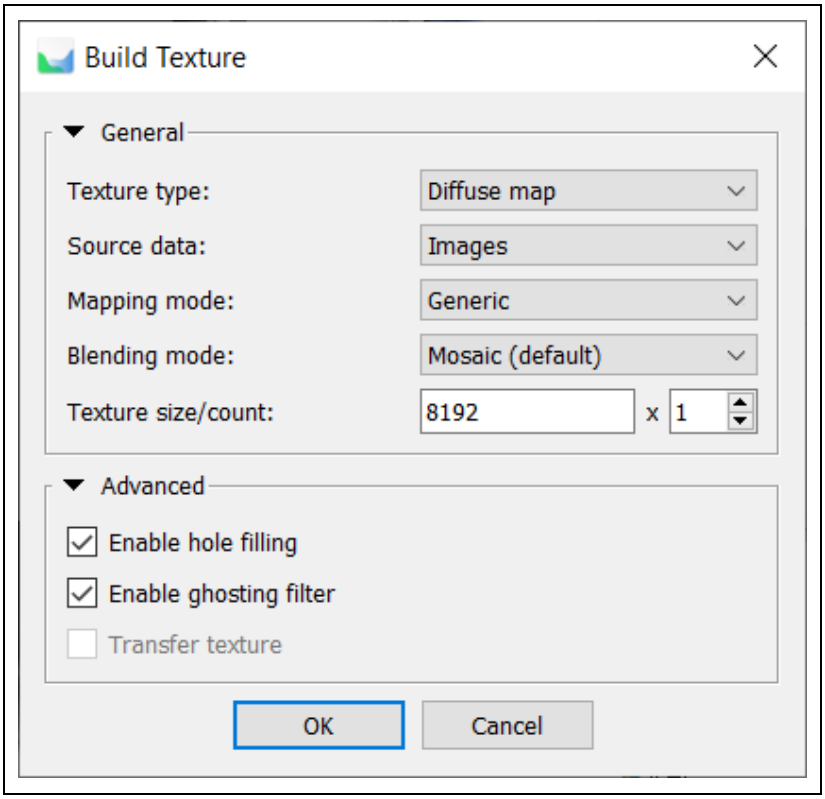

Figure 4.13: The settings utilized in 3D textured mesh model generation.

In Figure 4.13 utilized parameters in 3D textured mesh model generation are identified as [Web 7, 2021]:

- Texture type: This setting indicates the generated texture map type including the diffuse map which is the basic texture with color values, the normal map which allows calculating illumination of model sections, and the occlusion map which is a texture containing pre-calculated information about shading.
- Source data: Selects the source data type such as aligned images and 3D model for building the color texture map.
- Mapping mode: This setting determines the way object texture will be packed in the generated texture atlas. The default mode is generic mapping mode which allows texture atlas parameterization for arbitrary geometry, and other options for mapping mode are listed as orthophoto, adaptive orthophoto, spherical, single camera, and keep uv.
- Blending mode: This chooses the way pixel color values obtained from various aerial photos will be combined in the generated texture graphic. Selectable options for available blending modes are mosaic, average, max intensity, min intensity, and disabled.
- Texture size/count: Indicates the width and height of the texture atlas in total pixels and chooses the number of files for exporting the texture data.
- Enable hole filling: This is a default setting that helps to eliminate the salt-and-pepper effect due to the complex surface with several tiny parts shading other sections of the model.
- Enable ghosting filter: If there are some structures with thin bodies or objects in motion which are not reconstructed as a section of the polygonal model, this option can be enabled for avoiding the ghosting effect on the generated texture.

Using high-resolution aerial photos, a texture was produced and applied to 3D mesh models for generating 3D textured mesh models (Figure 4.14). In 3D texture mesh model generation all options except texture size which was selected as 8192 x 8129 pixels for generating high-resolution texture graphics, were determined as default preselected values.

Figure 4.14: a) A 3D mesh model without texture. b) A 3D mesh model with texture.

4.2.5. Digital Surface Model Generation

For generating the orthomosaic of the GTU Campus a DSM is required to be produced by utilizing a filtered dense point cloud. Settings utilized in this DSM generation are displayed in Figure 4.15. In this step, the projection setting was chosen as geographic which allows displaying DSM in the geographic coordinate system. Also, the coordinate system was selected as the Turkish National Reference Frame (TUREF) Transverse Mercator (TM) zone 30. Finally using the settings shown in Figure 4.15 a DSM with a pixel resolution of 5,89 cm was obtained.

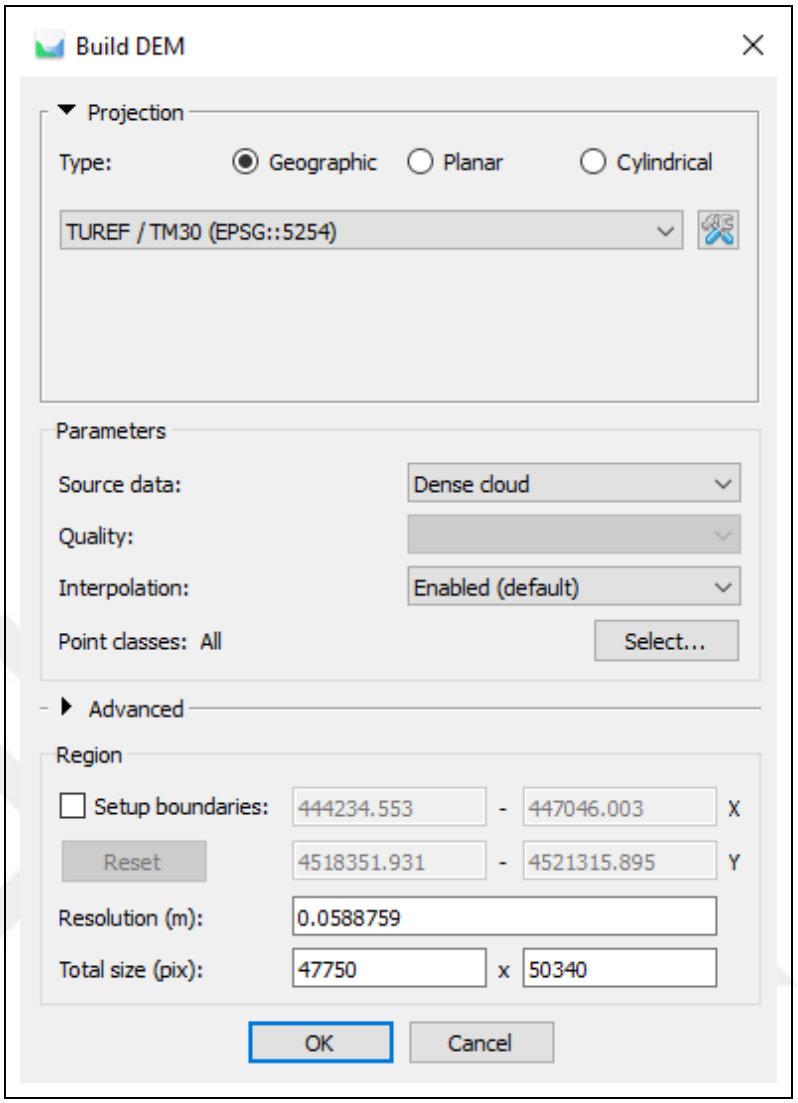

Figure 4.15: The utilized settings for DSM generation.

4.2.6. Orthomosaic Generation

After a DSM was generated high-resolution UAV orthomosaic of the GTU Campus was obtained using the settings displayed in Figure 4.16. The pixel resolution of the UAV orthomosaic was obtained as 2.39 cm. The UAV orthomosaic was generated for providing a general view of the Campus for the created 3D VR tour application.

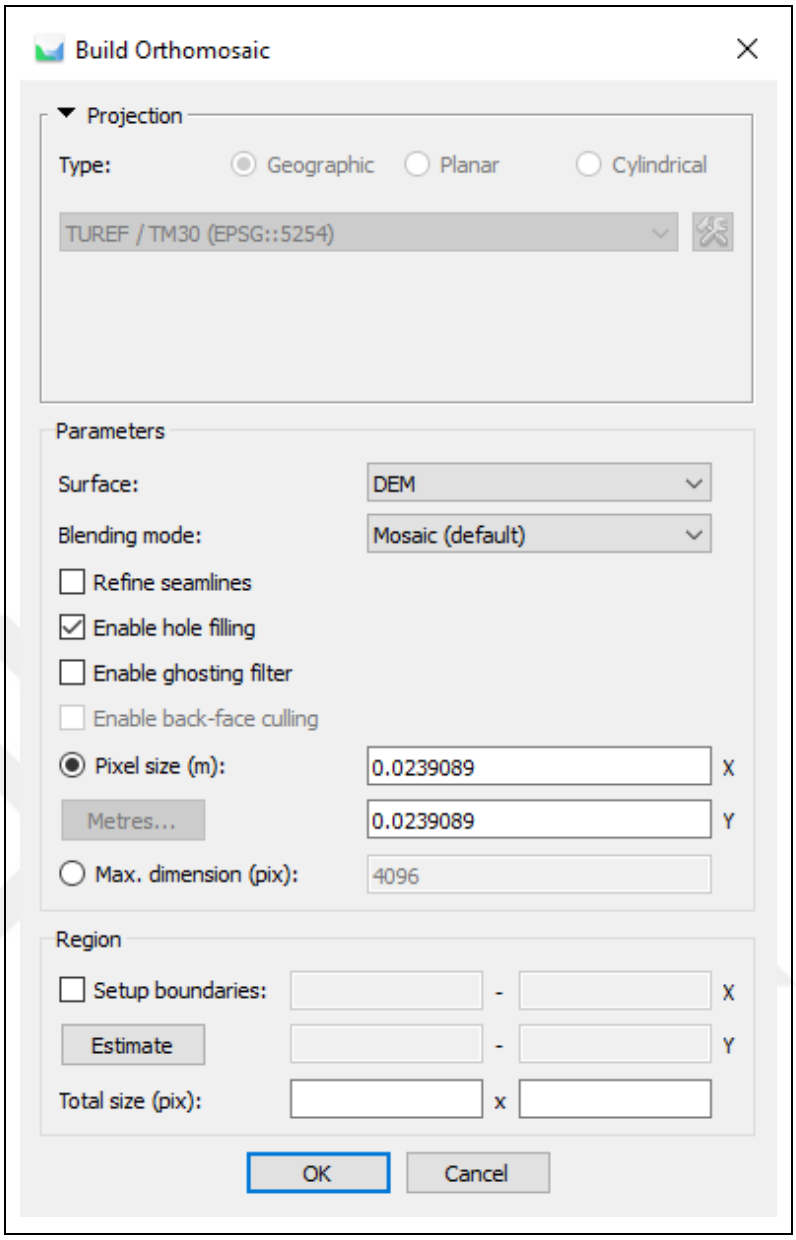

Figure 4.16: The utilized settings for orthomosaic generation.

4.3. 3D Virtual Reality Tour Creation

After generating high-resolution 3D textured mesh models and UAV orthomosaic of the GTU Campus, the Unity game engine was utilized for VR integration of the generated data and the creation of the 3D VR tour application. Steps of 3D VR tour creation include 3D textured mesh model importation, setting up the environment, application of rendering optimization algorithms, first-person player implementation, and building and executable.

4.3.1. 3D Textured Mesh Model Importation

Importing of generated 3D textured mesh models to Unity was carried out by exporting these meshes from the Agisoft Metashape in a suitable data format for efficiency and performance. Wavefront OBJ data format which was supported by Unity was selected in the export process. Wavefront OBJ format is conventionally used in exporting 3D meshes and it keeps both 3D coordinates of points and polygonal data and is supported by various 3D CAD software [Kato and Ohno, 2009]. In addition, a material that has texture and properties of shader object's lighting is essential to be created in Unity for displaying imported textures along with the 3D mesh models. Also, utilizing the inspector window properties of created materials were edited via selecting shader type as unlit/texture for providing smoother views of 3D textured meshes. Finally, the max size of the high-resolution textures was selected as 16384 x 16384 pixels for a better presentation of 3D meshes.

4.3.2. Setting Up the Environment

For offering users a more immersive and realistic experience a directional light object was implemented into the application and also 3D premade object models and interactive information panels were added. Also, by adding the additional objects into the 3D VR tour application a more detailed and complex environment will be provided to users while utilizing the application.

4.3.2.1. 3D Premade Object Addition

For better visualization of the objects such as trees, benches, arbors, lighting poles, and tables across the GTU Campus 3D premade models these objects were added. Due to limitations of the optical UAV technique in capturing detailed views of objects smaller compared to buildings, 3D textured mesh models of some objects were not acquired in high detail even using the high-resolution aerial photos for 3D texture mesh model generation. In Figure 4.17 an example of 3D premade object model addition to the 3D VR tour application is displayed.

Figure 4.17: Addition of a 3D premade object model into the application.

4.3.2.2. Interactive Information Panel Production

Providing an informative experience to users during the 3D VR tour, interactive information panels with textual metadata about buildings including building name, block number, total floor area, and total usage area, were added to the application. In Figure 4.18 an example of interactive information panel addition is displayed.

Figure 4.18: Addition of an interactive information panel to the application.

4.3.3. Rendering Optimization Algorithm Application

Due to the excessive number of faces in imported 3D mesh models and thus large polygonal data size, rendering optimization algorithms including occlusion culling and space subdivision were applied by utilizing tools in the Unity game engine. Occlusion culling algorithms are used for recognizing and rendering visible areas of 3D models so that objects positioned on the back of a distinct viewpoint are not rendered for increasing the performance of the applications and overcoming bottlenecks in hardware [Coorg and Teller, 1997]. Optimization algorithms applied in this process have a small impact on processing time, making the operation much more efficient.

4.3.4. First Person Player Implementation

By providing users the ability to walk around buildings and objects as if they doing it in physical reality, a more immersive VR tour experience can be realized. So, a player component with a first-person camera was implemented to the 3D VR tour application for a real-like virtual experience. The first-person player has components including a character controller, a capsule mesh object, scripts for enabling the movement of the player, and a camera programmed to follow the motion of the player. Also, a collider component was added to the first-person player for giving the player the ability to detect and contact the faces of 3D meshes in the application [Jafri et al., 2017]. The implementation of the first-person player is shown in Figure 4.19.

Figure 4.19: Implementation of the first-person player.

4.3.5. Building an Executable

Finally, an executable file compatible with Windows was built for the created 3D VR tour application in Unity. While building the executable graphic options were selected as the highest possible quality for improving the visualization of the created application.

5. RESULTS

Results including acquired point clouds, generated 3D textured mesh models, UAV orthomosaic, and scenes from the created 3D VR tour application are presented in this section.

5.1. Orthomosaic Generation Using Optical UAV Data

Process results of ortomosaic generation using optical UAV data such as generated sparse point clouds, dense point clouds, 3D textured mesh models, DSM, and orthomosaic of the GTU Campus are displayed in this part.

5.1.1. Geometric Orientation Results

The merged version of generated sparse point clouds is given in Figure 5.1. A total of 86 mobile GCPs were established and utilized for the geometric orientation process which was carried out with a RMSE of ± 2 cm (~0.9 pixels).

Figure 5.1: Sparse point cloud of the GTU Campus.

5.1.2. Dense Point Cloud

Dense point clouds of the GTU Campus are displayed in a merged form in Figure 5.2. When the dense point cloud of the GTU Campus is examined, it is observed that the dense cloud visualizes the topography and objects above it in more detail and complexity compared to the sparse point cloud which can be deemed as the rough visualization of the area.

Figure 5.2: Dense point cloud of the GTU Campus.

5.1.3. 3D Textured Mesh Model

The merged 3D textured mesh model of the GTU Campus is shown in Figure 5.3. Because each of the generated 3D textured mesh models have real world coordinates they became a merged, single model when combined together. When the 3D textured mesh model is examined, it is seen that the displaying capability of the 3D textured mesh is much higher than the dense point cloud due to gapless geometry and continuous data format. The topography and objects are displayed in more detail and complexity.

Figure 5.3: 3D textured mesh model of the GTU Campus.

5.1.4. Digital Surface Model

Generated DSM of the Campus Area was presented in Figure 5.4.

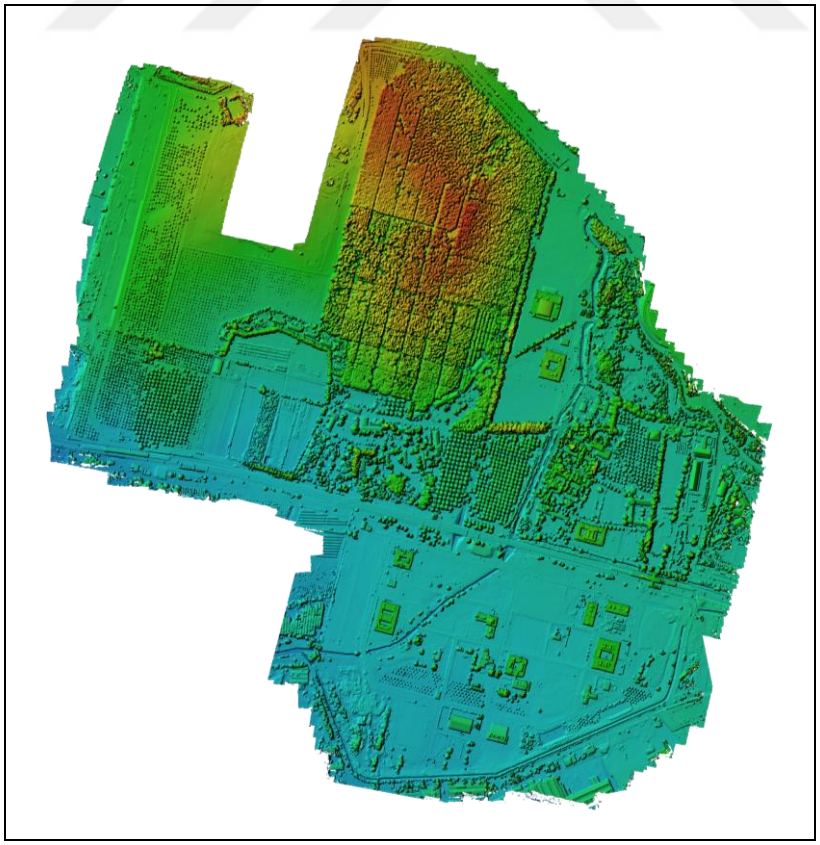

Figure 5.4: Generated DSM of the GTU Campus.

5.1.5. Orthomosaic

The generated UAV orthomosaic of the GTU Campus is displayed in Figure 5.5.

Figure 5.5: Generated UAV orthomosaic of the GTU Campus.

5.2. 3D Virtual Reality Tour Creation

Sample scenes from the created 3D VR tour application of the GTU Campus are shown in Figure 5.6 with 3D textured mesh models of buildings and 3D pre-made object models displayed in scenes. Also, interactive information panel with pop-up window ability can be seen in Figure 5.7.

Figure 5.6: Sample scenes from the created 3D VR tour application.

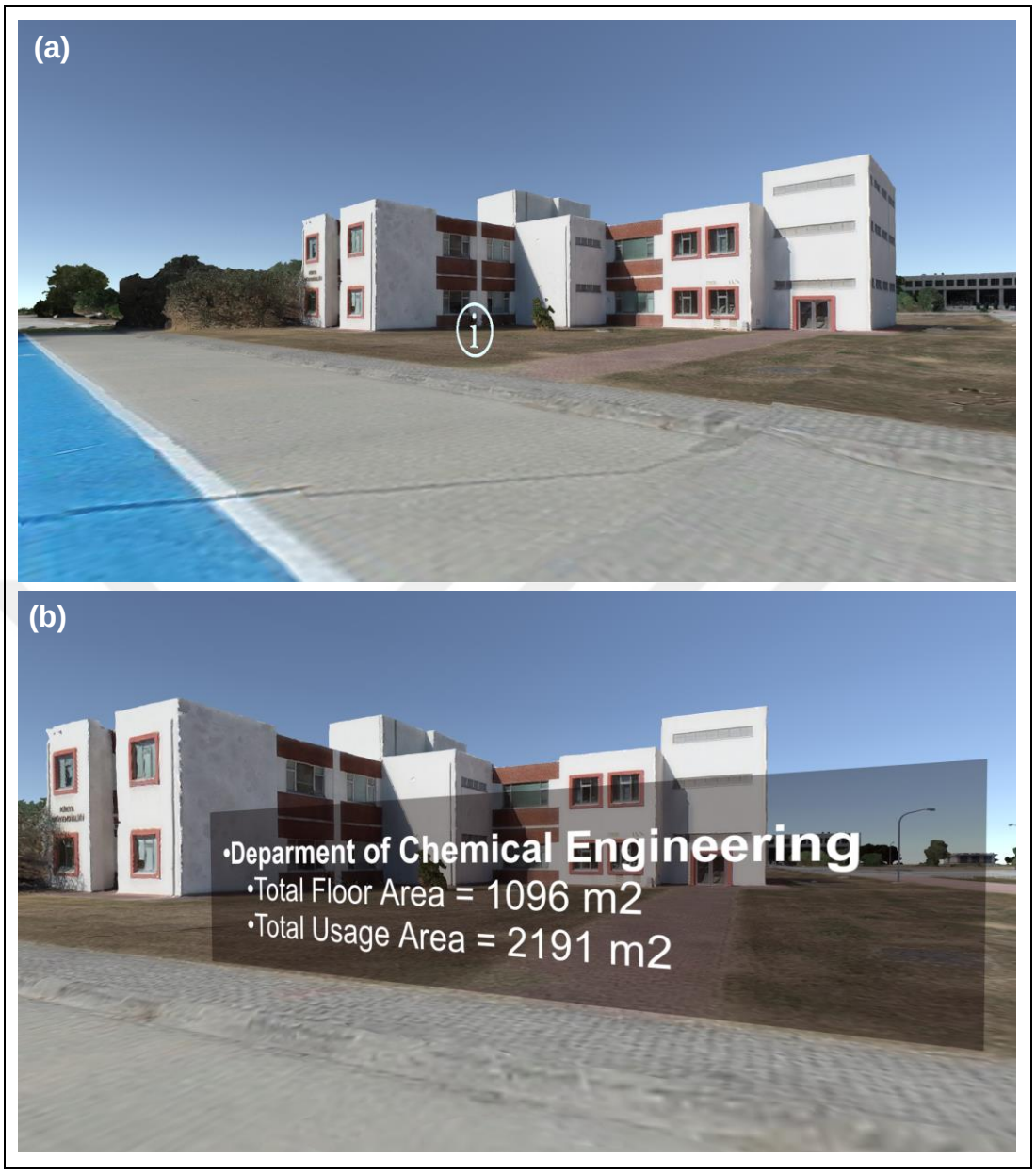

Figure 5.7: An interactive information panel a) inactive and b) activated.

6. CONCLUSION and DISCUSSION

In the produced 3D textured mesh models some gaps and holes are visible, especially on the thin walls covering the building roofs (Figure 6.1). The primary cause of this problem is the non-continuous vertical geometry of some objects in which the aerial photo orientation process results have a small number of points because of low correlation. Therefore, an inadequate number of points are utilized in the interpolation process which causes gaps and holes. These holes were filled via executing the hole filling tool in Agisoft Metashape software.

Figure 6.1: Interpolation effect on a rooftop wall due to points with low correlation.

These holes were filled via executing the hole filling tool in Agisoft Metashape software. Optical remote sensing systems do not have the ability to penetrate densely forested or vegetated areas compared to LiDAR or large wavelength SAR systems because of using the passive remote sensing principle for viewing. Therefore, capturing forest and vegetation understory is impossible using an optical system with nadir viewing. Because of this issue, it is of utmost importance to conduct flight operations in different viewing modes or geometries and oblique camera orientations. Apart from the generally preferred polygonal flights with nadir-view, it is crucial to carry out UAV flights in different flight modes including bundle-grid and circular modes. In Figure 6.2 an example of the aforementioned problem is displayed.

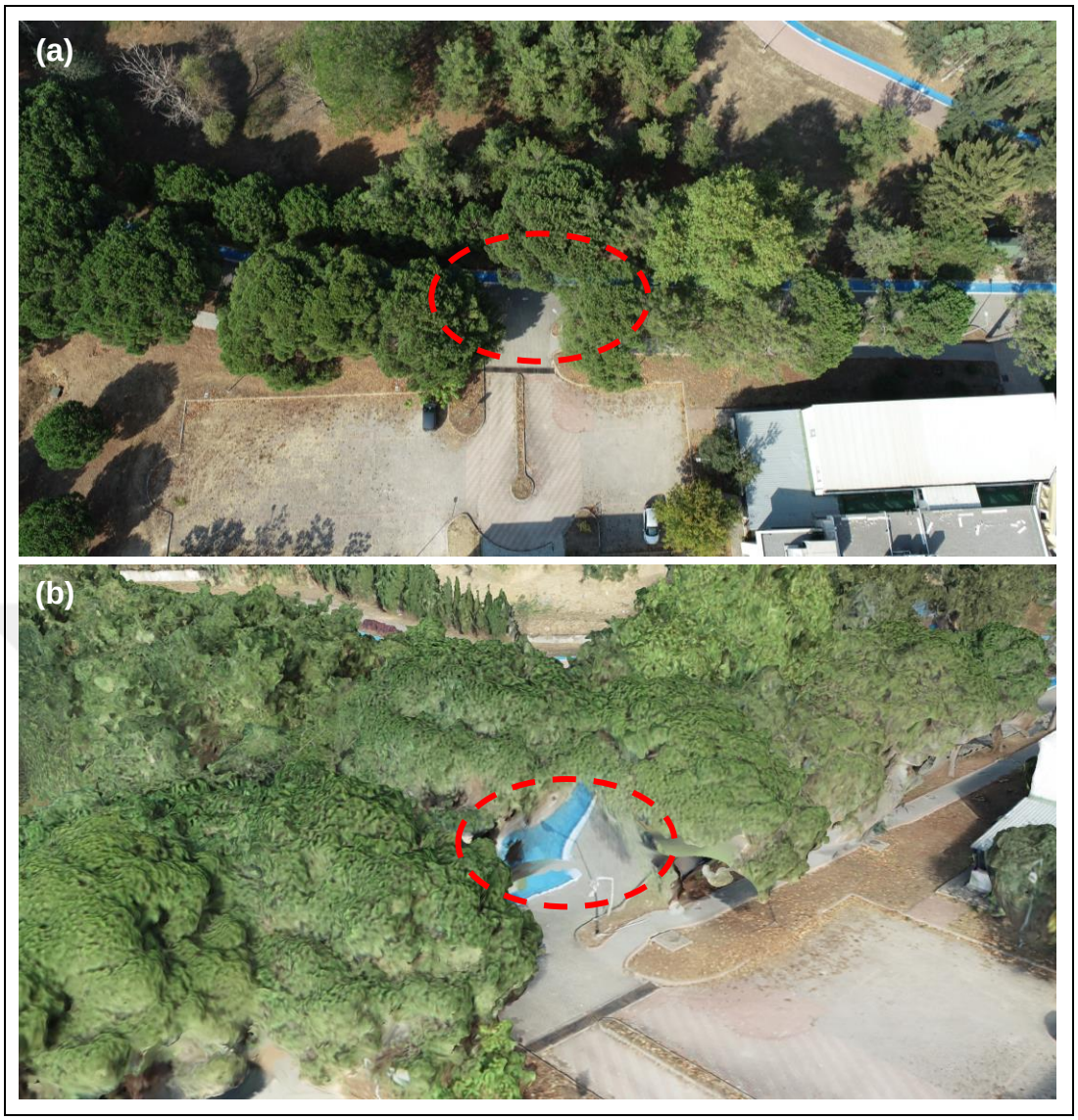

Figure 6.2: a) An aerial photo of the GTU Campus. b) The 3D textured mesh model of the region covered by dense trees.

As Figure 6.2 is examined, due to the low number of points under dense trees, a bicycle road was displayed in incorrect geometry in the generated 3D textured mesh model. In cases like this, two solutions can be recommended if the problem cannot be solved by using the optical UAV technique. The first one is carrying out a LiDAR UAV flight in the area where the issue persists. However, it is important that the utilized LiDAR sensor operates based on multiple signal returns (more than two) for penetrating dense vegetation. The second one is to conduct TLS surveys with an integrated camera to obtain point cloud data with color and then merge the obtained colorful point cloud data with UAV dense point cloud data for reconstruction of the 3D textured mesh model.

In this thesis study, the GTU Campus area was captured by using a UAV platform with a high-resolution RGB camera for the purpose of generating high-quality 3D textured mesh models which were integrated into a synthetic environment for creating a 3D VR tour application. Acquired aerial photos were oriented using Agisoft Metashape Professional software using 86 GCPs and the geometric accuracy was calculated as the RMSE of ±2 cm (~0.9 pixels). Then, sparse and dense point clouds were generated. However, due to the influence of some land cover classes including forests, a filtering process was carried out for removing the noisy parts of dense clouds. Utilizing the filtered dense point clouds, solid 3D mesh models were generated, and using the obtained aerial photos high-resolution texture graphics were constructed and then applied to 3D meshes for the production of 3D textured mesh models. VR integration process was realized using the Unity game for 3D mesh model importation and rendering optimization algorithms were applied for better performance. In addition, premade 3D object models of arbors, benches, lighting poles, trees, and tables were placed in the application for creating a more genuine VR tour application. Also, interactive information panels with textual building metadata including building name, block number, total floor, and usage area, were placed in the virtual environment for informing visitors about the Campus buildings. Finally, a first-person player was implemented for users to freely move inside the Campus and interact with objects. Overall, a qualified 3D VR tour application was developed by integrating 3D textured mesh models, generated using high-resolution UAV aerial photos, into the virtual environment through using the Unity game engine. The created application will be available through the official GTU website for visitors to reach. Moreover, the generated 3D textured mesh model of the Campus can be utilized for purposes of planning, management, and construction. Also, because of having real-world coordinates, the 3D mesh can be integrated into a bigger dataset for BIM studies or the creation of a 3D smart city model.

REFERENCES

Adams S. M., Friedland C. J., (2011), "A survey of unmanned aerial vehicle (UAV) usage for imagery collection in disaster research and management", 9th International Workshop on Remote Sensing for Disaster Response, 8, 1-8, California, USA, 15-16 September.

Aggarwal S., (2004), "Principles of remote sensing", Satellite Remote Sensing and GIS Applications in Agricultural Meteorology, 23 (2), 23-28.

Aicardi I., Dabove P., Lingua A. M., Piras M., (2016a), "Integration between TLS and UAV photogrammetry techniques for forestry applications", Iforest-Biogeosciences and Forestry, 10 (1), 41.

Aicardi I., Garbarino M., Lingua A., Lingua E., Marzano R., Piras M., (2016b), "Monitoring post-fire forest recovery using multitemporal digital surface models generated from different platforms", EARSeL eProceedings, 15 (1), 1-8.

Annis A., Nardi F., Petroselli A., Apollonio C., Arcangeletti E., Tauro F., Grimaldi S., (2020), "UAV-DEMs for small-scale flood hazard mapping", Water, 12 (6), 1717.

Azuma R. T., (1997), "A survey of augmented reality", Presence: Teleoperators & Virtual Environments, 6 (4), 355-385.

Azuma R., Baillot Y., Behringer R., Feiner S., Julier S., MacIntyre B., (2001), "Recent advances in augmented reality", IEEE Computer Graphics and Applications, 21 (6), 34-47.

Bacco M., Barsocchi P., Cassará P., Germanese D., Gotta A., Leone G. R., Moroni D., Pascali M. A., Tampucci M., (2020), "Monitoring ancient buildings: Real deployment of an IoT system enhanced by UAVs and virtual reality", IEEE Access, 8, 50131-50148.

Baltsavias E. P., (1999), "Airborne laser scanning: existing systems and firms and other resources", ISPRS Journal of Photogrammetry and Remote sensing, 54 (2-3), 164-198.

Barrile V., Fotia A., Candela G., Bernardo E., (2019), "Integration of 3D model from UAV survey in BIM environment", The International Archives of Photogrammetry, Remote Sensing and Spatial Information Sciences, 42, 195-199.

Bendig J., Bolten A., Bennertz S., Broscheit J., Eichfuss S., Bareth G., (2014), "Estimating biomass of barley using crop surface models (CSMs) derived from UAV-based RGB imaging", Remote sensing, 6 (11), 10395-10412.

Berrett B. E., Vernon C. A., Beckstrand H., Pollei M., Markert K., Franke K. W., Hedengren J. D., (2021), "Large-scale reality modeling of a university campus using

combined UAV and terrestrial photogrammetry for historical preservation and practical use", Drones, 5 (4), 136.

Birkfellner W., Figl M., Huber K., Watzinger F., Wanschitz F., Hummel J., Hanel R., Greimel W., Homolka P., Ewers R., Bergmann H., (2002), "A head-mounted operating binocular for augmented reality visualization in medicine-design and initial evaluation", IEEE Transactions on Medical Imaging, 21 (8), 991-997.

Bolles R. C., Baker H. H., Marimont D. H., (1987), "Epipolar-plane image analysis: An approach to determining structure from motion", International Journal of Computer Vision, 1 (1), 7-55.

Brooks F. P., (1999), "What's real about virtual reality?", IEEE Computer Graphics and Applications, 19 (6), 16-27.

Bruno F., Bruno S., De Sensi G., Luchi M. L., Mancuso S., Muzzupappa M., (2010), "From 3D reconstruction to virtual reality: A complete methodology for digital archaeological exhibition", Journal of Cultural Heritage, 11 (1), 42-49.

Bu F., Wang X., (2019), "A smart agriculture IoT system based on deep reinforcement learning", Future Generation Computer Systems, 99, 500-507.

Campbell J. B., Wynne R. H., (2011), "Introduction to remote sensing", 5th Edition, Guilford Press.

Carruth D. W., Hudson C., Fox A. A., Deb S., (2020), "User interface for an immersive virtual reality greenhouse for training precision agriculture", International Conference on Human-Computer Interaction, 35-46, Springer, Cham.

Cary L., Coyne J., (2011), "ICAO unmanned aircraft systems (UAS)", Circular 328, In 2011–2012 UAS Yearbook – UAS: The Global Perspective, 112-115, Blyenburgh & Co., Paris, France.

Casbeer D. W., Beard R. W., McLain T. W., Li S. M., Mehra R. K., (2005), "Forest fire monitoring with multiple small UAVs", American Control Conference, 3530-3535, Oregon, USA, 8-10 June.

Castleman K. R., (1996), "Digital image processing", Prentice Hall Press.

Chamola V., Hassija V., Gupta V., Guizani M., (2020), "A comprehensive review of the COVID-19 pandemic and the role of IoT, drones, AI, blockchain, and 5G in managing its impact", IEEE Access, 8, 90225-90265.

Chen J., Liu H., Zheng J., Lv M., Yan B., Hu X., Gao Y., (2016), "Damage degree evaluation of earthquake area using UAV aerial image", International Journal of Aerospace Engineering, 2052603.

Chou T. Y., Yeh M. L., Chen Y. C., Chen Y. H., (2010), "Disaster monitoring and management by the unmanned aerial vehicle technology", Proceedings of the ISPRS TC VII Symposium, 38 (7B), 137-142, Vienna, Austria, 5-7 July.

Cipresso P., Giglioli I. A. C., Raya M. A., Riva G., (2018), “The past, present, and future of virtual and augmented reality research: a network and cluster analysis of the literature”, Frontiers in Psychology, 9, 2086.

Cirulis A., Brigmanis K. B., (2013), “3D outdoor augmented reality for architecture and urban planning”, Procedia Computer Science, 25, 71-79.

Collier P., (2002), “The impact on topographic mapping of developments in land and air survey: 1900-1939”, Cartography and Geographic Information Science, 29 (3), 155-174.

Comba L., Biglia A., Aimonino D. R., Gay P., (2018), “Unsupervised detection of vineyards by 3D point-cloud UAV photogrammetry for precision agriculture”, Computers and Electronics in Agriculture, 155, 84-95.

Cook K. L., (2007), “The silent force multiplier: The history and role of UAVs in warfare”, IEEE Aerospace Conference, 1-7, Montana, USA, 3-10 March.

Cooper M. A. R., Robson S., (1996), “Close range photogrammetry and machine vision”, Whittles Publishing.

Coorg S., Teller S., 1997, “Real-time occlusion culling for models with large occluders”, In Proceedings of the Symposium on Interactive 3D Graphics, 83-90, Providence RI, USA, 27-30 April.

Costabile P., Costanzo C., De Lorenzo G., De Santis R., Penna N., Macchione F., (2021), “Terrestrial and airborne laser scanning and 2-D modelling for 3-D flood hazard maps in urban areas: New opportunities and perspectives”, Environmental Modelling & Software, 135, 104889.

Dalamagkidis K., Valavanis K. P., Piegl L. A., (2012), “Aviation history and unmanned flight”, On Integrating Unmanned Aircraft Systems into the National Airspace System, 11-42, Springer, Dordrecht.

Dalponte M., Bruzzone L., Vescovo L., Gianelle D., (2009), “The role of spectral resolution and classifier complexity in the analysis of hyperspectral images of forest areas”, Remote Sensing of Environment, 113 (11), 2345-2355.

DGCA, (2016), “Unmanned aerial vehicle systems instructions”.

Dong L., Shan J., (2013), “A comprehensive review of earthquake-induced building damage detection with remote sensing techniques”, ISPRS Journal of Photogrammetry and Remote Sensing, 84, 85-99.

Erdelj M., Natalizio E., (2016), “UAV-assisted disaster management: Applications and open issues”, International Conference on Computing, Networking and Communications, 1-5, Hawaii, USA, 15-18 February.

Falco N., Wainwright H. M., Dafflon B., Ulrich C., Soom F., Peterson J. E., Brown B. J., Schaettle K. B., Williamson M., Cothren J. D., Ham R. G., McEntire J. A., Hubbard

S. S., (2021), “Influence of soil heterogeneity on soybean plant development and crop yield evaluated using time-series of UAV and ground-based geophysical imagery”, Scientific Reports, 11 (1), 1-17.

Fauvel M., Tarabalka Y., Benediktsson J. A., Chanussot J., Tilton J. C., (2012), “Advances in spectral-spatial classification of hyperspectral images”, Proceedings of the IEEE, 101 (3), 652-675.

Finn R. L., Wright D., Jacques L., De Hert P., (2014), “Study on privacy, data protection and ethical risks in civil remotely piloted aircraft systems operations: Final report,” European Commission, Brussels, Belgium.

Fjelsted L., Christensen A. G., Larsen J. E., Kjeldsen P., Scheutz C., (2019), “Assessment of a landfill methane emission screening method using an unmanned aerial vehicle mounted thermal infrared camera–A field study”, Waste Management, 87, 893-904.

Foley J. D., Van Dam A., Feiner S. K., Hughes J. F., Phillips R. L., (1993), “Introduction to Computer Graphics”, Addison-Wesley Professional.

Freitas R., Campos P., (2008), “SMART: a System of augmented reality for teaching 2nd grade students”, Proceedings of the 22nd British Computer Society Conference on Human-Computer Interaction, 27-30, Liverpool, United Kingdom, 1-5 September.

Fryer J. G., (1996), “Close range photogrammetry and machine vision”, Whittles Publishing.

Gaitatzes A., Christopoulos D., Roussou M., (2001), “Reviving the past: cultural heritage meets virtual reality”, Conference on Virtual Reality, Archeology, and Cultural Heritage, 103-110, Glyfada, Greece, 28-30 November.

Gallay M., (2013), “Direct acquisition of data: airborne laser scanning”, Geomorphological Techniques, 2 (1.4), 1-17.

Gerhards M., Schlerf M., Mallick K., Udelhoven T., (2019), “Challenges and future perspectives of multi-/Hyperspectral thermal infrared remote sensing for crop water-stress detection: A review”, Remote Sensing, 11 (10), 1240.

Getzin S., Nuske R. S., Wiegand K., (2014), “Using unmanned aerial vehicles (UAV) to quantify spatial gap patterns in forests”, Remote Sensing, 6 (8), 6988-7004.

Ghulam A., (2014), “Monitoring tropical forest degradation in Betampona Nature Reserve, Madagascar using multisource remote sensing data fusion”, IEEE Journal of Selected Topics in Applied Earth Observations and Remote Sensing, 7 (12), 4960-4971.

Gondchawar N., Kawitkar R. S., (2016), “IoT based smart agriculture”, International Journal of Advanced Research in Computer and Communication Engineering, 5 (6), 838-842.

Granshaw S. I., (2019), “Laussedat bicentenary: origins of photogrammetry”, The Photogrammetric Record, 34 (166), 128-147.

Green J., Green T., Brown A., (2017), “Augmented reality in the K-12 classroom”, TechTrends, 61 (6), 603-605.

Greenwood F., Nelson E. L., Greenough P. G., (2020), “Flying into the hurricane: A case study of UAV use in damage assessment during the 2017 hurricanes in Texas and Florida”, PLoS one, 15 (2), e0227808.

Gregory J., (2018), “Game engine architecture”, 3rd Edition, AK Peters/CRC Press.

Grussenmeyer P., Khalil O. A., (2002), “Solutions for exterior orientation in photogrammetry: a review”, The Photogrammetric Record, 17 (100), 615-634.

Guerra-Hernández J., González-Ferreiro E., Monleón V. J., Faias S. P., Tomé M., Díaz-Varela R. A., (2017), “Use of multi-temporal UAV-derived imagery for estimating individual tree growth in Pinus pinea stands”, Forests, 8 (8), 300.

Gupta R. P., (2006), “Remote sensing geology”, 3rd Edition, Springer.

Habib A., Asmamaw A., Kelley D., May M., (2000), “Linear features in photogrammetry”, Report No. 450, Department of Civil and Environmental Engineering and Geodetic Science, The Ohio State University.

Hausamann D., Zirnig W., Schreier G., Strobl P., (2005), “Monitoring of gas pipelines – a civil UAV application”, Aircraft Engineering and Aerospace Technology, 77 (5), 352-360.

Heipke C., (1997), “Automation of interior, relative, and absolute orientation”, ISPRS Journal of Photogrammetry and Remote Sensing, 52 (1), 1-19.

Helsel S., (1992), “Virtual reality and education”, Educational Technology, 32 (5), 38-42.

Hoffman H. G., Patterson D. R., Carrougher G. J., (2000), “Use of virtual reality for adjunctive treatment of adult burn pain during physical therapy: a controlled study”, The Clinical Journal of Pain, 16 (3), 244-250.

Hoffmann H., Nieto H., Jensen R., Guzinski R., Zarco-Tejada P., Friborg T., (2016), “Estimating evaporation with thermal UAV data and two-source energy balance models”, Hydrology and Earth System Sciences, 20 (2), 697-713.

Horler D. N. H., Dockray M., Barber J., (1983), “The red edge of plant leaf reflectance”, International Journal of Remote Sensing, 4 (2), 273-288.

Horn B. K., (1990), “Relative orientation”, International Journal of Computer Vision, 4 (1), 59-78.

Hu J., Peng J., Zhou Y., Xu D., Zhao R., Jiang Q., Fu T., Wang F., Shi Z., (2019), "Quantitative estimation of soil salinity using UAV-borne hyperspectral and satellite multispectral images", Remote Sensing, 11, 736.

Huang H. C., Nain S. H., Hung Y. P., Cheng T., (1998), "Disparity-based view morphing – a new technique for image-based rendering", In Proceedings of the ACM Symposium on Virtual Reality Software and Technology, 9-16, Taipei, Taiwan, 2-5 November.

Hughes J. F., Van Dam A., McGuire M., Sklar D. F., Foley J. D., Feiner S. K., Akeley K., (2013), "Computer graphics: Principles and practice", 3rd Edition, Addison-Wesley Professional.

Huuskonen J., Oksanen T., (2018), "Soil sampling with drones and augmented reality in precision agriculture", Computers and Electronics in agriculture, 154, 25-35.

Ignjatović Stupar D., Rošer J., Vulić M., (2020), "Investigation of unmanned aerial vehicles-based photogrammetry for large mine subsidence monitoring", Minerals, 10 (2), 196.

Immerzeel W. W., Kraaijenbrink P. D., Shea J. M., Shrestha A. B., Pellicciotti F., Bierkens M. F., de Jong S. M., (2014), "High-resolution monitoring of Himalayan glacier dynamics using unmanned aerial vehicles", Remote Sensing of Environment, 150, 93-103.

Izard S. G., Juanes J. A., García Peñalvo F. J., Estella J. M., Ledesma M., Ruisoto P., (2018), "Virtual reality as an educational and training tool for medicine", Journal of Medical Systems, 42 (3), 1-5.

Jafri R., Campos R. L., Ali S. A., Arabnia H. R., 2017, "Visual and infrared sensor data-based obstacle detection for the visually impaired using the Google project tango tablet development kit and the unity engine", IEEE Access, 6, 443-454.

Jiang R., Jáuregui D. V., White K. R., (2008), "Close-range photogrammetry applications in bridge measurement: Literature review", Measurement, 41 (8), 823-834.

Jiao Z., Jia G., Cai Y., (2019), "A new approach to oil spill detection that combines deep learning with unmanned aerial vehicles", Computers & Industrial Engineering, 135, 1300-1311.

Jo Y. H., Hong S., (2019), "Three-dimensional digital documentation of cultural heritage site based on the convergence of terrestrial laser scanning and unmanned aerial vehicle photogrammetry", ISPRS International Journal of Geo-Information, 8 (2), 53.

Johnson L., Levine A., Smith R., Stone S., (2010), "Simple augmented reality", The 2010 Horizon Report, 21-24.

Kang D., Cha Y. J., (2018), "Autonomous UAVs for structural health monitoring using deep learning and an ultrasonic beacon system with geo-tagging", Computer-Aided Civil and Infrastructure Engineering, 33 (10), 885-902.

Kato A., Ohno N., (2009), "Construction of three-dimensional tooth model by micro-computed tomography and application for data sharing", Clinical Oral Investigations, 13 (1), 43-46.

Kaufman Y. J., Gao B. C., (1992), "Remote sensing of water vapor in the near IR from EOS/MODIS", IEEE Transactions on Geoscience and Remote Sensing, 30 (5), 871-884.

Kaya S., Curran P. J., (2006), "Monitoring urban growth on the European side of the Istanbul metropolitan area: A case study", International Journal of Applied Earth Observation and Geoinformation, 8 (1), 18-25.

Keane J. F., Carr S. S., (2013), "A brief history of early unmanned aircraft", Johns Hopkins APL Technical Digest, 32 (3), 558-571.

Kerkech M., Hafiane A., Canals R., (2020), "Vine disease detection in UAV multispectral images using optimized image registration and deep learning segmentation approach", Computers and Electronics in Agriculture, 174, 105446.

Khan Z., Rahimi-Eichi V., Haefele S., Garnett T., Miklavcic S. J., (2018), "Estimation of vegetation indices for high-throughput phenotyping of wheat using aerial imaging", Plant Methods, 14 (1), 1-11.

Kim S., McGaughey R. J., Andersen H. E., Schreuder G., (2009), "Tree species differentiation using intensity data derived from leaf-on and leaf-off airborne laser scanner data", Remote Sensing of Environment, 113 (8), 1575-1586.

Klemas V., (2013), "Airborne remote sensing of coastal features and processes: An overview", Journal of Coastal Research, 29 (2), 239-255.

Knoll C., Kerschner H., (2009), "A glacier inventory for South Tyrol, Italy, based on airborne laser-scanner data", Annals of Glaciology, 50 (53), 46-52.

Koller S., Ebert L. C., Martinez R. M., Sieberth T., (2019), "Using virtual reality for forensic examinations of injuries", Forensic Science International, 295, 30-35.

Krabill W. B., Wright C. W., Swift R. N., Frederick E. B., Manizade S. S., Yungel J. K., Martin C. F., Sonntag J. G., Duffy M., Hulslander W., Brock J. C., (2000), "Airborne laser mapping of Assateague National Seashore Beach", Photogrammetric Engineering & Remote Sensing, 66 (1), 65-71.

Kwak G. H., Park N. W., (2019), "Impact of texture information on crop classification with machine learning and UAV images" Applied Sciences, 9 (4), 643.

Laporte-Fauret Q., Marieu V., Castelle B., Michalet R., Bujan S., Rosebery D., (2019), "Low-cost UAV for high-resolution and large-scale coastal dune change monitoring using photogrammetry", Journal of Marine Science and Engineering, 7 (3), 63.

Latta J. N., Oberg D. J., (1994), "A conceptual virtual reality model", IEEE Computer Graphics and Applications, 14 (1), 23-29.

Le Maire G., Marsden C., Nouvellon Y., Grinand C., Hakamada R., Stape J. L., Laclau J. P., (2011), "MODIS NDVI time-series allow the monitoring of Eucalyptus plantation biomass", Remote Sensing of Environment, 115 (10), 2613-2625.

Lei B., Wang N., Xu P., Song G., (2018), "New crack detection method for bridge inspection using UAV incorporating image processing", Journal of Aerospace Engineering, 31 (5), 04018058.

Li Q., Zhong R., Huang J., Gong H., (2011), "Comparison of two retrieval methods with combined passive and active microwave remote sensing observations for soil moisture. Mathematical and computer modelling", 54 (3-4), 1181-1193.

Liang S., Li X., Wang J., (2012), "Advanced remote sensing: terrestrial information extraction and applications", Academic Press.

Lillesand T., Kiefer R. W., Chipman J., (2015), "Remote sensing and image interpretation", 7nd Edition, John Wiley & Sons.

Lin A. Y. M., Novo A., Har-Noy S., Ricklin N. D., Stamatiou K., (2011), "Combining GeoEye-1 satellite remote sensing, UAV aerial imaging, and geophysical surveys in anomaly detection applied to archaeology", IEEE Journal of Selected Topics in Applied Earth Observations and Remote Sensing, 4 (4), 870-876.

Linder W., (2009), "Digital photogrammetry: A practical course", Springer.

Lindner G., Schraml K., Mansberger R., Hübl J., (2016), "UAV monitoring and documentation of a large landslide", Applied Geomatics, 8 (1), 1-11.

Liou W. K., Chang C. Y., (2018), "Virtual reality classroom applied to science education", 23rd International Scientific-Professional Conference on Information Technology, 1-4, Žabljak, Montenegro, 19-24 February.

Maddikunta P. K. R., Hakak S., Alazab M., Bhattacharya S., Gadekallu T. R., Khan W. Z., Pham Q. V., (2021), "Unmanned aerial vehicles in smart agriculture: Applications, requirements, and challenges", IEEE Sensors Journal, 21 (16), 17608-17619.

Maresma Á., Ariza M., Martínez E., Lloveras J., Martínez-Casasnovas J. A., (2016), "Analysis of vegetation indices to determine nitrogen application and yield prediction in maize (Zea mays L.) from a standard UAV service", Remote Sensing, 8 (12), 973.

Mather P. M., Koch M., (2011), "Computer processing of remotely-sensed images: an introduction", 4th Edition, John Wiley & Sons.

McManamon P., (2012), “Review of ladar: a historic, yet emerging, sensor technology with rich phenomenology”, Optical Engineering, 51 (6), 060901.

McNeil B. E., Pisek J., Lepisk H., Flamenco E. A., (2016), “Measuring leaf angle distribution in broadleaf canopies using UAVs”, Agricultural and Forest Meteorology, 218, 204-208.

Milgram P., Kishino F., (1994), “A taxonomy of mixed reality visual displays”, IEICE Transactions on Information and Systems, 77 (12), 1321-1329.

Mohammadi M., Rashidi M., Mousavi V., Karami A., Yu Y., Samali B., (2021), “Quality evaluation of digital twins generated based on UAV photogrammetry and TLS: Bridge case study”, Remote Sensing, 13 (17), 3499.

Mori T., Hashimoto T., Terada A., Yoshimoto M., Kazahaya R., Shinohara H., Tanaka, R., (2016), “Volcanic plume measurements using a UAV for the 2014 Mt. Ontake eruption”, Earth, Planets and Space, 68 (1), 1-18.

Mozas-Calvache A. T., Pérez-García J. L., Cardenal-Escarcena F. J., Mata-Castro E., Delgado-García J., (2012), “Method for photogrammetric surveying of archaeological sites with light aerial platforms”, Journal of Archaeological Science, 39 (2), 521-530.

Murakami H., Nakagawa K., Hasegawa H., Shibata T., Iwanami E., (1999), “Change detection of buildings using an airborne laser scanner”, ISPRS Journal of Photogrammetry and Remote Sensing, 54 (2-3), 148-152.

Naesset E., (1997), “Estimating timber volume of forest stands using airborne laser scanner data”, Remote Sensing of Environment, 61 (2), 246-253.

Næsset, E., Gobakken, T., (2005), “Estimating forest growth using canopy metrics derived from airborne laser scanner data”, Remote Sensing of Environment, 96 (3-4), 453-465.

Neupane K., Baysal-Gurel F., (2021), “Automatic identification and monitoring of plant diseases using unmanned aerial vehicles: A review”, Remote Sensing, 13 (19), 3841.

Nevalainen O., Honkavaara E., Tuominen S., Viljanen N., Hakala T., Yu X., Hyyppä J., Saari H., Pölönen I., Imai N.N., Tommaselli A. M. G., (2017), “Individual tree detection and classification with UAV-based photogrammetric point clouds and hyperspectral imaging”, Remote Sensing, 9 (3), 185.

Nex F., Remondino F. (2014), “UAV for 3D mapping applications: a review”, Applied Geomatics, 6 (1), 1-15.

Niu H., Hollenbeck D., Zhao T., Wang D., Chen Y., (2020), “Evapotranspiration estimation with small UAVs in precision agriculture”, Sensors, 20 (22), 6427.

Nonami K., (2007), “Prospect and recent research & development for civil use autonomous unmanned aircraft as UAV and MAV”, Journal of System Design and Dynamics, 1 (2), 120-128.

NSO, (2019), “Minimum training requirements for unmanned aircraft systems (UAS) operators and pilots”, STANAG 4670 – ATP – 3.3.8.1, Ed. B, Ver. 1.

Ollero A., Merino L., (2006), “Unmanned aerial vehicles as tools for forest-fire fighting”, Forest Ecology and Management, 234 (1), S263.

Ong S. K., Nee A. Y. C., (2004), “A brief introduction of VR and AR applications in manufacturing”, In: Ong S. K., Nee A. Y. C. (Eds.) Virtual and Augmented Reality Applications in Manufacturing, 1-11, Springer.

Ong S. K., Yuan M. L., Nee A. Y., (2008), “Augmented reality applications in manufacturing: a survey”, International Journal of Production Research, 46 (10), 2707-2742.

Ordóñez C., Martínez J., Arias P., Armesto, J., (2010), “Measuring building façades with a low-cost close-range photogrammetry system”, Automation in Construction, 19 (6), 742-749.

Ortiz S. M., Breidenbach J., Knuth R., Kändler G., (2012), “The influence of DEM quality on mapping accuracy of coniferous-and deciduous-dominated forest using TerraSAR-X images”, Remote Sensing, 4 (3), 661-681.

Osco L. P., Junior J. M., Ramos A. P. M., Furuya D. E. G., Santana D. C., Teodoro L. P. R., Gonçalves W. N., Baio F. H. R., Pistori, H., Junior C. A. d. S., Teodoro, P. E., (2020), “Leaf nitrogen concentration and plant height prediction for maize using UAV-based multispectral imagery and machine learning techniques”, Remote Sensing, 12 (19), 3237.

Pantelidis V. S., (1993), “Virtual reality in the classroom”, Educational Technology, 33(4), 23-27.

Park S., Ryu D., Fuentes S., Chung H., Hernández-Montes E., O’Connell M., (2017), “Adaptive estimation of crop water stress in nectarine and peach orchards using high-resolution imagery from an unmanned aerial vehicle (UAV)”, Remote Sensing, 9 (8), 828.

Persson, A., Holmgren, J., Soderman, U., (2002), “Detecting and measuring individual trees using an airborne laser scanner”, Photogrammetric Engineering and Remote Sensing, 68 (9), 925-932.

Pfeifer N., Briese C., (2007), “Geometrical aspects of airborne laser scanning and terrestrial laser scanning”, International Archives of Photogrammetry, Remote Sensing and Spatial Information Sciences, 36 (3/W52), 311-319.

Piermattei L., Carturan L., Guarnieri A., (2015), “Use of terrestrial photogrammetry based on structure-from-motion for mass balance estimation of a small glacier in the Italian alps”, Earth Surface Processes and Landforms, 40 (13), 1791-1802.

Polidori L., (2021), “Words as tracers in the history of science and technology: the case of photogrammetry and remote sensing”, Geo-spatial Information Science, 24 (1), 167-177.

Portalés C., Lerma J. L., Navarro S. (2010), “Augmented reality and photogrammetry: A synergy to visualize physical and virtual city environments”, ISPRS Journal of Photogrammetry and Remote Sensing, 65 (1), 134-142.

Powers M. B., Emmelkamp P. M., (2008), “Virtual reality exposure therapy for anxiety disorders: A meta-analysis”, Journal of Anxiety Disorders, 22 (3), 561-569.

Prisacariu V., (2017), “The history and the evolution of UAVs from the beginning till the 70s”, Journal of Defense Resources Management, 8 (1), 181-189.

Püschel H., Sauerbier M., Eisenbeiss H., (2008), “A 3D model of Castle Landenberg (CH) from combined photogrammetric processing of terrestrial and UAV based images”, International Archives of the Photogrammetry, Remote Sensing and Spatial Information Sciences, 37 (B6b), 93-98.

Qiao L., Tang W., Gao D., Zhao R., An L., Li M., Sun H., Song D., (2022), “UAV-based chlorophyll content estimation by evaluating vegetation index responses under different crop coverages”, Computers and Electronics in Agriculture, 196, 106775.

Qin J., Wang B., Wu Y., Lu Q., Zhu H., (2021), “Identifying pine wood nematode disease using UAV images and deep learning algorithms”, Remote Sensing, 13 (2), 162.

Rawicz A. H., (2008), “Theodore Harold Maiman and the invention of laser”, in Photonics, Devices, and Systems IV, 7138, 1-7, Prague, Czech Republic, 27-29 August.

Reinhart G., Patron C., (2003), “Integrating augmented reality in the assembly domain-fundamentals, benefits and applications”, CIRP Annals, 52 (1), 5-8.

Remondino F., Fraser C., (2006), “Digital camera calibration methods: considerations and comparisons”, International Archives of the Photogrammetry, Remote Sensing and Spatial Information Sciences, 36 (5), 266-272.

Riaño D., Valladares F., Condés S., Chuvieco E., (2004), “Estimation of leaf area index and covered ground from airborne laser scanner (Lidar) in two contrasting forests”, Agricultural and Forest Meteorology, 124 (3-4), 269-275.

Robertson W., Whitman D., Zhang K., Leatherman S. P., (2004), “Mapping shoreline position using airborne laser altimetry”, Journal of Coastal Research, 20 (3), 884-892.

Rosenholm D. A. N., Torlegard K., (1988), “Three-dimensional absolute orientation of stereo models using digital elevation models”, Photogrammetric Engineering and Remote Sensing, 54 (10), 1385-1389.

Schenk T., (1997), “Towards automatic aerial triangulation”, ISPRS Journal of Photogrammetry and Remote Sensing, 52 (3), 110-121.

Schonberger J. L., Frahm J. M., (2016), “Structure-from-motion revisited”, In Proceedings of the IEEE Conference on Computer Vision and Pattern Recognition, 4104-4113, Nevada, USA, 27-30 June.

Sefercik U. G., Buyuksalih G., Atalay C., (2020), “DSM generation with bistatic TanDEM-X InSAR pairs and quality validation in inclined topographies and various land cover classes”, Arabian Journal of Geosciences, 13 (13), 1-15.

Sefercik U. G., Buyuksalih G., Jacobsen K., Bayburt S., (2019), “DSM quality of Korean satellite KOMPSAT-3 in comparison to AW3D30 and Sentinel-1A in respect of airborne laser scanning”, KSCE Journal of Civil Engineering, 23 (7), 3162-3173.

Sefercik U. G., Glennie C., Singhania A., Hauser D., (2015), “Area-based quality control of airborne laser scanning 3D models for different land classes using terrestrial laser scanning: sample survey in Houston, USA”, International Journal of Remote Sensing, 36 (23), 5916-5934.

Sefercik U. G., Kavzoglu T., Colkesen I., Adali S., Dinc S., Nazar M., Ozturk M. Y., (2021b), “Land cover classification performance of multispectral RTK UAVs”, Int. Arch. Photogramm. Remote Sens. Spatial Inf. Sci., XLVI-4/W5-2021, 489–492.

Sefercik U. G., Kavzoglu T., Nazar M., Atalay C., Madak M., (2021a), “UAV-based 3D virtual tour creation”, Int. Arch. Photogramm. Remote Sens. Spatial Inf. Sci., XLVI-4/W5-2021, 493-499.

Seward A., Ashraf S., Reeves R., Bromley C., (2018), “Improved environmental monitoring of surface geothermal features through comparisons of thermal infrared, satellite remote sensing and terrestrial calorimetry”, Geothermics, 73, 60-73.

Sheffner E. J., (1994), “The Landsat program: recent history and prospects”, Photogrammetric Engineering and Remote Sensing, 60 (6), 735-744.

Sherrod A., (2007), “Ultimate 3D game engine design & architecture”. Charles River Media.

Sinha R., Quirós J. J., Sankaran S., Khot L. R., (2022), “High resolution aerial photogrammetry based 3D mapping of fruit crop canopies for precision inputs management”, Information Processing in Agriculture, 9 (1), 11-23.

Sinha S., Jeganathan C., Sharma L. K., Nathawat M. S., (2015), “A review of radar remote sensing for biomass estimation”, International Journal of Environmental Science and Technology, 12 (5), 1779-1792.

Skondras A., Karachaliou E., Tavantzis I., Tokas N., Valari E., Skalidi I., Bouvet G. A., Stylianidis E., (2022), "UAV mapping and 3D modeling as a tool for promotion and management of the urban space", Drones, 6 (5), 115.

Sousa M., Vieira J., Medeiros D., Arsenio A., Jorge J., (2016), "SleeveAR: Augmented reality for rehabilitation using realtime feedback", In Proceedings of the 21st International Conference on Intelligent User Interfaces, 175-185, California, USA, 7-10 March.

Stavroulaki M. E., Riveiro B., Drosopoulos G. A., Solla M., Koutsianitis P., Stavroulakis G. E., (2016), "Modelling and strength evaluation of masonry bridges using terrestrial photogrammetry and finite elements", Advances in Engineering Software, 101, 136-148.

Stöcker C., Bennett R., Nex F., Gerke M., Zevenbergen J., (2017), "Review of the current state of UAV regulations", Remote Sensing, 9 (5), 459.

Streefkerk J. W., Houben M., Amerongen P. V., Haar F. T., Dijk J., (2013), "The art of csi: An augmented reality tool (art) to annotate crime scenes in forensic investigation", In International Conference on Virtual, Augmented and Mixed Reality, 330-339.

Sublime J., (2021), "The 2011 Tohoku tsunami from the sky: A review on the evolution of artificial intelligence methods for damage assessment", Geosciences, 11 (3), 133.

Sutherland I. E., (1965), "The ultimate display", Proceedings of the International Federation of Information Processing Congress, 506-508, New York, USA, 24-29 May.

Sutherland I. E., (1968), "A head-mounted three dimensional display", In Proceedings of Fall Joint Computer Conference, 757-764, Washington, D.C., USA, 9-11 December.

Tan Y., Li Y., (2019), "UAV photogrammetry-based 3D road distress detection", ISPRS International Journal of Geo-Information, 8 (9), 409.

Tao H., Feng H., Xu L., Miao M., Long H., Yue J., Li Z., Yang G., Yang X., Fan, L, (2020), "Estimation of crop growth parameters using UAV-based hyperspectral remote sensing data", Sensors, 20 (5), 1296.

Tatem A. J., Goetz S. J., Hay S. I., (2008), "Fifty years of earth observation satellites: Views from above have lead to countless advances on the ground in both scientific knowledge and daily life", American Scientist, 96 (5), 390.

Taubin G., Horn W. P., Lazarus F., Rossignac J., (1998), "Geometry coding and VRML", Proceedings of the IEEE, 86(6), 1228-1243.

Thenkabail P. S., (2015), "Remotely sensed data characterization, classification, and accuracies", CRC Press.

Townshend J. R., (1981), “The spatial resolving power of earth resources satellites”, Progress in Physical Geography, 5 (1), 32-55.

Tucker C. J., (1980), “Remote sensing of leaf water content in the near infrared”, Remote Sensing of Environment, 10 (1), 23-32.

Udeanu G., Dobrescu A., Oltean M., 2016, “Unmanned aerial vehicle in military operations”, Sci. Res. Educ. Air Force, 1, 199–205.

USA, (2015), “Eyes of the army: U.S. Army roadmap for unmanned aircraft systems 2010-2035”.

Valavanis K. P., Kontitsis M., (2007), “A historical perspective on unmanned aerial vehicles”, Advances in Unmanned Aerial Vehicles, 15-46, Springer, Dordrecht.

Valença J., Júlio E. N. B. S., Araújo H. J., (2012), “Applications of photogrammetry to structural assessment”, Experimental Techniques, 36 (5), 71-81.

Varbla S., Ellmann A., Puust R., (2021), “Centimetre-range deformations of built environment revealed by drone-based photogrammetry”, Automation in Construction, 128, 103787.

Verde N., Mallinis G., Tsakiri-Strati M., Georgiadis C., Patias P., (2018), “Assessment of radiometric resolution impact on remote sensing data classification accuracy”, Remote Sensing, 10 (8), 1267.

Villa T. F., Salimi F., Morton K., Morawska L., Gonzalez F., (2016), “Development and validation of a UAV based system for air pollution measurements”, Sensors, 16 (12), 2202.

Vlahakis V., Ioannidis N., Karigiannis J., Tsotros M., Gounaris M., Almeida L., Stricker D., Gleu T., Christou I. T., Carlucci R., (2001), “ARCHEOGUIDE: First results of an augmented reality, mobile computing system in cultural heritage sites”, Proceedings of the Conference on Virtual Reality, Archeology and Cultural Heritage, 131-139, Glyfada, Greece, 28-30 November.

Wagner W., Hollaus M., Briese C., Ducic V., (2008), “3D vegetation mapping using small-footprint full-waveform airborne laser scanners”, International Journal of Remote Sensing, 29 (5), 1433-1452.

Wallace L., Lucieer A., Watson C., Turner D., (2012), “Development of a UAV-LiDAR system with application to forest inventory”, Remote Sensing, 4 (6), 1519-1543.

Ware C., Arthur K., Booth K. S., (1993), “Fish tank virtual reality”, Proc. of the INTERACT '93 and CHI '93 Conf. on Human Factors in Computing Systems, 37-42, Amsterdam, Netherlands, 24-29 April.

Web 1, (2021), https://dl.djicdn.com/downloads/phantom_4_pro/20211129/QSG/pro_v2.0/Phantom_4_Pro_v2.0_Quick_Start_Guide_EN.pdf, (Accessed: 16/06/2022).

Web 2, (2022), https://www.dronefly.com/the-anatomy-of-a-drone, (Accessed: 16/06/2022).

Web 3, (2022), http://theia-sfm.org/sfm.html, (Accessed: 20/06/2022).
Web 4, (2013), https://insights.dice.com/2013/06/03/how-unity3d-become-a-game-development-beast/, (Accessed: 20/06/2022).

Web 5, (2022), https://unity.com/how-to/learning-c-sharp-unity-beginners#:~:text=The%20language%20that's%20used%20in,variables%2C%20functions%2C%20and%20classes, (Accessed: 20/06/2022).

Web 6, (2022), https://docs.unity3d.com/Manual/PhysicsSection.html, (Accessed: 20/06/2022).

Web 7, (2021), https://www.agisoft.com/pdf/metashape-pro_1_7_en.pdf, (Accessed: 20/06/2022).

Web 8, (2013), https://web.archive.org/web/20131019122343/http://dictionaryofforestry.org/dict/term/forestry, (Accessed: 01/07/2022).

Web 9, (2022), https://www.blender.org/about/, (Accessed: 18/08/2022).

Web 10, (2022), https://www.unrealengine.com/en-US, (Accessed: 18/08/2022).

Wehr A., Lohr U., (1999), "Airborne laser scanning—an introduction and overview", ISPRS Journal of Photogrammetry and Remote Sensing, 54 (2-3), 68-82.

Weng Q., (2009), "Thermal infrared remote sensing for urban climate and environmental studies: Methods, applications, and trends", ISPRS Journal of Photogrammetry and Remote Sensing, 64 (4), 335-344.

Westoby M. J., Brasington J., Glasser N. F., Hambrey M. J., Reynolds J. M., (2012), "'Structure-from-Motion'photogrammetry: A low-cost, effective tool for geoscience applications", Geomorphology, 179, 300-314.

Wolf P. R., Dewitt B. A., Wilkinson B. E., (2014), "Elements of photogrammetry with applications in GIS", McGraw-Hill Education.

Woodhouse I. H., (2017), "Introduction to microwave remote sensing", CRC press.

Xie F., Lin Z., Gui D., Lin H., (2012), "Study on construction of 3D building based on UAV images", International Archives of the Photogrammetry, Remote Sensing and Spatial Information Sciences, 39, 469-473.

Yastikli N., (2007), “Documentation of cultural heritage using digital photogrammetry and laser scanning”, Journal of Cultural Heritage, 8 (4), 423-427.

Yue J., Lei T., Li C., Zhu J., (2012), “The application of unmanned aerial vehicle remote sensing in quickly monitoring crop pests”, Intelligent Automation & Soft Computing, 18 (8), 1043-1052.

Zang W., Lin J., Wang Y., Tao H., (2012), “Investigating small-scale water pollution with UAV remote sensing technology”, World Automation Congress, 1-4, Puerto Vallarta, Mexico, 24-28 June.

Zhang D., Liu J., Ni W., Sun G., Zhang Z., Liu Q., Wang Q., (2019), “Estimation of forest leaf area index using height and canopy cover information extracted from unmanned aerial vehicle stereo imagery”, IEEE Journal of Selected Topics in Applied Earth Observations and Remote Sensing, 12 (2), 471-481.

Zhang D., Zhou G., (2016), “Estimation of soil moisture from optical and thermal remote sensing: A review”, Sensors, 16 (8), 1308.

Zhang Y., Yue P., Zhang G., Guan T., Lv M., Zhong D., (2019), “Augmented reality mapping of rock mass discontinuities and rockfall susceptibility based on unmanned aerial vehicle photogrammetry”, Remote Sensing, 11 (11), 1311.

Zheng J. M., Chan K. W., Gibson I., (1998), “Virtual reality”, IEEE Potentials, 17 (2), 20-23.

Zhu L., Hyyppä, J., (2014), “Fully-automated power line extraction from airborne laser scanning point clouds in forest areas”, Remote Sensing, 6 (11), 11267-11282.

Zhu W., Fan G., (2016), “Application of computer virtual reality technology in virtual tour”, International Journal of Advanced Media and Communication, 6 (2-4), 273-282.

BIOGRAPHY

Mertcan NAZAR earned his bachelor's degree in Geomatics Engineering from Istanbul Technical University, in 2020. He continued his education with master's degree at the Department of Geomatics Engineering, Graduate School of Natural and Applied Sciences, Gebze Technical University. In 2021, he joined the Department of Geomatics Engineering, Faculty of Engineering, Gebze Technical University. He is currently working as a Research Assistant in Geomatics Engineering Department.

APPENDICES

Appendix A: Publications Within the Scope of Thesis Study

Sefercik U. G., Kavzoglu T., Nazar M., Atalay C., Madak M., (2022), "Creation of a virtual tour .exe utilizing very high-resolution RGB UAV data", International Journal of Environment and Geoinformatics, (Accepted).

Sefercik U. G., Kavzoglu T., Nazar M., Atalay C., Madak M., (2021), "UAV-based 3D virtual tour creation", Int. Arch. Photogramm. Remote Sens. Spatial Inf. Sci., XLVI-4/W5-2021, 493-499.

Sefercik U. G., Kavzoglu T., Nazar M., Atalay C., Madak M., (2021), "Integration of high resolution UAV data into the virtual environment", International Symposium on Applied Geoinformatics, Riga, Latvia, 2-3 December.

Sefercik U. G., Kavzoglu T., Nazar M., Atalay C., Madak M., (2021), "Virtual campus tour generation using UAV data: Case study Gebze Technical University", The 42nd Asian Conference on Remote Sensing, Can Tho, Vietnam, 22-24 November.

Appendix B: Publication List

Sefercik U. G., Kavzoglu T., Nazar M., Atalay C., Madak M., (2022), "Creation of a virtual tour .exe utilizing very high-resolution RGB UAV data", International Journal of Environment and Geoinformatics, (Accepted).

Sefercik U. G., Kavzoglu T., Colkesen I., Nazar M., Ozturk M. Y., Adali S., Dinc S., (2022), "3D positioning accuracy and land cover classification performance of multispectral RTK UAVs", International Journal of Engineering and Geosciences, (Publishing phase).

Sefercik U. G., Nazar M., (2022), "Coherence analysis of DSMs generated by multispectral RTK and RGB non-RTK UAVs' simultaneous data", International Geoscience and Remote Sensing Symposium (IGARSS'2022), Kuala Lumpur, Malaysia, 17-22 July.

Yildirim E., Nazar M., Sefercik U. G., Kavzoglu T., (2022), "Stone pine (*Pinus Pinea L.*) detection from high-resolution UAV imagery using deep learning model", International Geoscience and Remote Sensing Symposium (IGARSS'2022), Kuala Lumpur, Malaysia, 17-22 July.

Sefercik U. G., Kavzoglu T., Colkesen I., Adali S., Dinc S., Nazar M., Ozturk M. Y., (2021), "Land cover classification performance of multispectral RTK UAVs", Int. Arch. Photogramm. Remote Sens. Spatial Inf. Sci., XLVI-4/W5-2021, 489–492.

Sefercik U. G., Kavzoglu T., Nazar M., Atalay C., Madak M., (2021), "UAV-based 3D virtual tour creation", Int. Arch. Photogramm. Remote Sens. Spatial Inf. Sci., XLVI-4/W5-2021, 493-499.

Sefercik U. G., Kavzoglu T., Colkesen I., Nazar M., Ozturk M. Y., Adali S., Dinc S., (2021), "Geolocation and land cover classification performance of multispectral RTK UAVs", International Symposium on Applied Geoinformatics, Riga, Latvia, 2-3 December.

Sefercik U. G., Kavzoglu T., Nazar M., Atalay C., Madak M., (2021), "Integration of high resolution UAV data into the virtual environment", International Symposium on Applied Geoinformatics, Riga, Latvia, 2-3 December.

Sefercik U. G., Kavzoglu T., Colkesen I., Adali S., Dinc S., Nazar M., Ozturk M. Y., (2021), "3D positioning accuracy and land cover classification performance of the UAVs: Case study of DJI Phantom IV Multispectral RTK", The 42nd Asian Conference on Remote Sensing, Can Tho, Vietnam, 22-24 November.

Sefercik U. G., Kavzoglu T., Nazar M., Atalay C., Madak M., (2021), "Virtual campus tour generation using UAV data: Case study Gebze Technical University", The 42nd Asian Conference on Remote Sensing, Can Tho, Vietnam, 22-24 November.